Abstract

Using Texture Analysis on

Biometric Technology for Personal Identification

Using texture analysis as a tool to extract biometric features for personal identification is the main goal of this thesis. In this study, three biometrics, the iris, palmprint and ear are investigated. Each of them shows a different level of achievement.

As far as iris recognition is concerned, we propose a new noise detection model for accurate segmentation of an iris. Eyelashes, the eyelids and reflection are the three main sources of noise. The eyelid issue has been solved by the traditional eye model; however, eyelashes and reflection have yet to be addressed. To determinate a pixel belonging to an eyelash, our model follows three criteria: 1) separable eyelash condition, 2) non-informative condition and 3) connective criterion. For reflection, strong reflection points are detected by a threshold and the weak reflection areas around the strong points are determined by a connective criterion and a statistical test. Using Boles's [47-49] texture-based iris recognition approach to evaluate the accuracy and usefulness of our detection model, we find the experimental results encouraging.

For palmprint identification, we develop a novel textured feature extraction technique, in which a 2-D Gabor filter is used to obtain the texture information and two palmprint images are compared by their hamming distance. The experiments give impressive results and show that our method is effective and comparable with fingerprint (FingerCode), iris (IrisCode) and 3-D hand geometry.

For ear recognition, we consider two issues: 1) image acquisition and 2) textured feature extraction technique. We have developed a special device for image acquisition. We also propose a novel feature extraction for ear recognition that measures two ear features by a simple vector norm. The experimental results show that ear recognition can provide middle level security.

Acknowledgement

First of all, I would like to express my gratitude to my supervisor, Prof. David Zhang. In the course of my MPhil study, he has provided me with helpful guidance, comments and criticisms, which drive me to the success of my research.

Many thanks to Prof. Zhaoqi Bian, Prof. Chengshui Zhang, professors at Tsinghua University and Qingyun Dai, associate professor in GuangDong University of Technology. They opened useful discussion on my research.

I also thank biometric research students, Wenxin Li, Lisheng Xu, Pang Bo, Yu Li, Guangming Lu, Yanlai, Li and Li Bin who are working at the Biometrics Research Centres of Harbin Institute of Technology and The Hong Kong Polytechnic University. They held concrete discussion on various biometrics technologies. In addition, I should thank all my friends in the Department of Computing for providing me with a warm and comfortable environment for research.

Finally, I would like to express my greatest gratitude to my parents and my girl friend, Lan for their endless support, patience and love.

CONTENTS

Chapter 1.

Introduction to Biometric Technology

1.1   Weakness of traditional personal identification methods

In recent years, biometric technology is one of the hottest research topics the in IT field because there is more critical demand for accurate personal identification or verification in security systems of various applications such as e-commence, Internet banking, access control, immigration, attendance control, and law enforcement.

Although we have widely applied traditional tools including password, physical key and smart card in security systems, high level security standard and requirements in our sophisticated society still cannot be fulfilled because these tools are subject to easy loss, duplication, high cost and low accuracy. In current Internet-based applications, the password is the most common tool to identify a person; nevertheless, its reliability is very limited. Generally, since users cannot remember long, complex, meaningless passwords, their passwords should be some meaningful text or numbers, such as their name, telephone number and birthday. This lets hackers easily guess or obtain their passwords. Besides, users tend to write the passwords down if web managers or administrators force them to use very complicated passwords. Thus, the password is subject to the same limitations as the physical key. Another problem is that Internet-based applications are supported by numerous service providers and companies, which have their own authentication systems. If users receive unique passwords from each of the companies, they will probably forget their own passwords. Therefore, they tend to solve this problem by writing down all their passwords or by using a particular password for all applications. This greatly reduces the reliability of the security systems.

Thorough discussions on the weaknesses of the password are mentioned in [1]. Some security systems are supported by smart card or physical key, which can be easily stolen, lost or duplicated. On the other hand, an authorized user can share his/her access right with unauthorized users. For the above reasons, biometric technology has become one of the hottest topics in the IT field in recent years.

1.2 Overview of Biometrics

Computer-based personal identification, also known as biometric computing, attempts to recognize a person by his/her body or behavioral characteristics. It has more than 30 years of history. The first commercial system, called Identimat, which measured the shape of the hand and the lengths of the fingers, was developed in 1970s. At the same time, fingerprint-based automatic checking systems were widely used in law enforcement. Rapid development of hardware, particularly in the speed of computers and in capture devices drives, the iris, retina, face, voice, palmprint, signature and DNA to join the biometric family [2-3].

1.2.1 Biometric Classification

Based on features, biometric technology is divided into two categories: physiological and behavioral technologies. The physiological technology verifies or identifies a person by means of his/her physical features, such as fingerprints, iris, hand geometry, face and retina. The behavioral technology relies on our customs like signature, keyboard typing and voice.

The two technologies have their own advantages and disadvantages so they have different applications. In general, physiological recognition systems are more stable and accurate than behavioral recognition systems. However, the capture devices for behavioral technology, such as voice and keyboard typing, are cheaper than those for physiological technology. However, many physiological recognition systems, e.g., fingerprint, hand and retina recognition systems, require users to touch the equipment. This may make some users feel psychologically uncomfortable. Nevertheless, physiological biometric technology still shared about 90% of the total sales volume in the biometric industry [27] in 1999.

Based on applications, biometric technologies can be classified into personal identification and automatic diagnosis. In this thesis, we only concentrate on personal

identification using iris, palmprint and ear. Fingerprint recognition systems deployed in various applications including law enforcement, computer securities, network securities are the most mature personal identification technology. Automatic diagnosis observes the changes in human bodies, similar to Traditional Chinese Medicine, iridology and palmprint diagnosis [2-4, 7]. Recently, Traditional Chinese Medicine is the most active member. It includes two main parts, tongue and blood pulse diagnoses. Iridology is a subject that studies the iris pattern to identify the weaknesses of the body. Palmprint diagnosis is implemented by observing the change in or the appearance of the lines in our palms. In fact, it is a new research area in medicine and computer science so we do not get any international papers on this. One of the active researchers is a medical doctor named Chenxia Wang, who has published a number of Chinese books and papers to explore her research results.

1.3 Biometric System Architecture

A biometric system for personal identification consists of five main parts: Signal Acquisition, Preprocessing, Feature Extraction, Pattern Matching and Feature Storage. The functions of each part are described as follows:

1) Signal Acquisition — Collects biometric signal such as an iris' image, voice and signature motion. It is an important part in the whole process. If the signal is contaminated by noise or is blur, the overall performance of the system will be affected.

2) Preprocessing — Serves several purposes including segmentation, noise reduction, rotational normalization and translation normalization.

3) Feature Extraction — Extracts a set of stable and unique features for personal identification.

4) Pattern Matching— A classifier to make a final decision whether two features belonged to the same person or not.

5) Data Storage — Stores the features extracted from registered signals possibly in smart cards or hard disks for later comparisons.

A biometric recognition system runs on three modes — enrollment, identification and verification. In the enrollment mode, a new user's biometric feature is extracted and then stored in a database for later comparisons. In the identification mode, an input biometric must

pass through Image Acquisition, Preprocessing and Feature Extraction. The feature extracted is compared with all records in a given database. The difference between the identification and verification modes is that in the verification mode, each user must have a user ID and his/her biometric feature can only be compared with all the features belonging to the same user ID. Fig. 1.1 summarizes the information about these three modes.
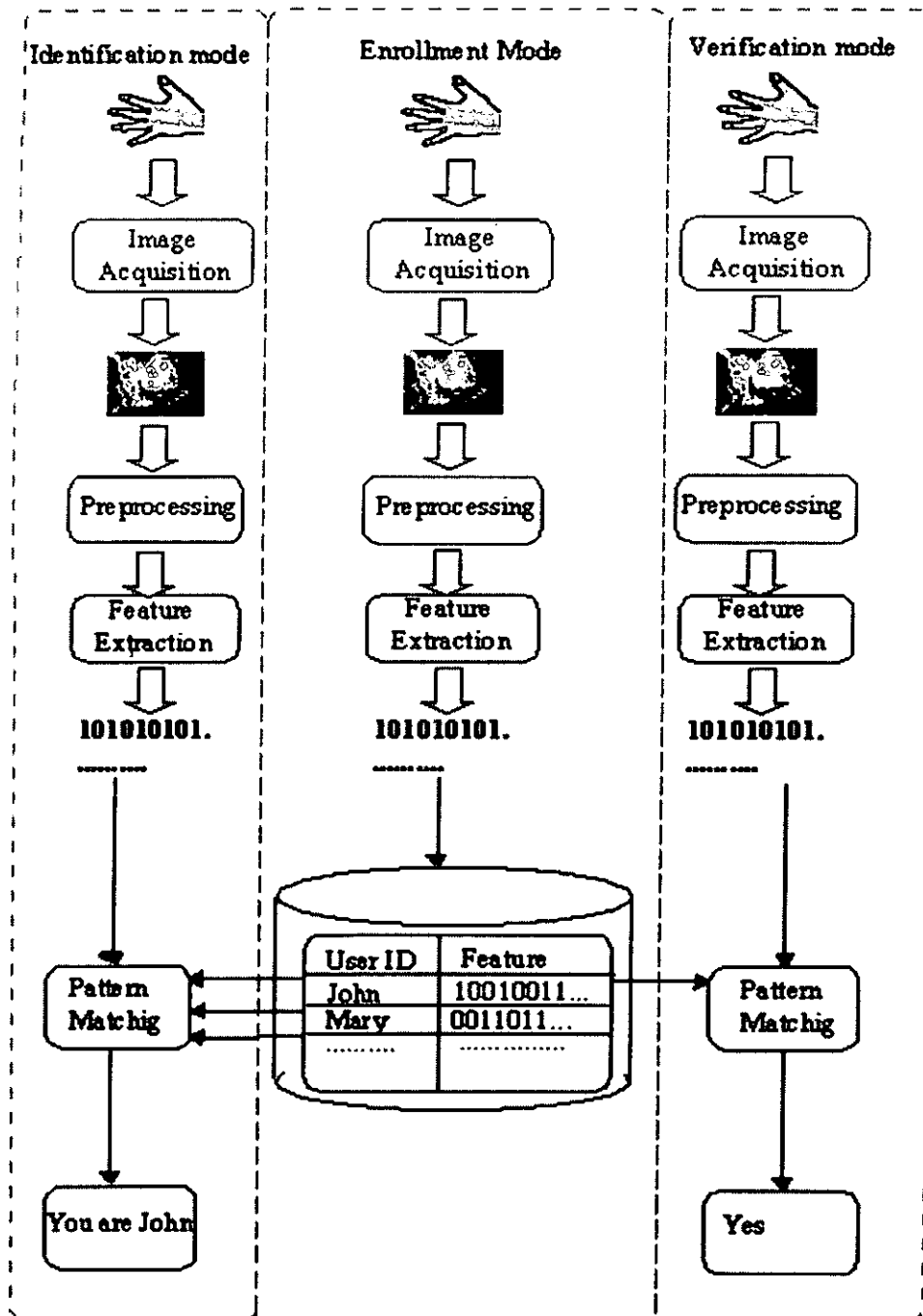
Fig. 1.1 Process of identification, enrollment and verification

1.4   Evaluation of Biometrics and Biometric System

A good biometric and a good biometric system should have a high degree of universality, uniqueness, permanence, collectability, performance and acceptability [2-3].

1) **Universality** — A biometric is a set of features extracted from the human body or behavior. Some people do not have certain biometrics. A worker may have lost his/her fingerprint in accident. A dumb person does not have voice print. Universality points out the ratio of people possessing a particular biometric.

2) **Uniqueness** — If a biometric is unique to a person, it can be used to distinguish him/her from another person in the world. Twins with the same genetic genotype contribute an important case to the test for uniqueness. Observing the similarity of any 2 biometric records in a large database is also a useful indicator for uniqueness.

3) **Permanence** — Permanence implies the stability of a biometric. Iris and fingerprint are relatively permanent biometrics because of their stability over time. However, many biometrics will change over time, for example, voice print and face.

4) **Collectability** — Although some biometrics have high permanence, uniqueness and universality, they cannot be used for the public because of collectability. If the data collection process is too complex or requires high cost input devices, the collectability of that biometric is low. DNA and retina suffer from this problem.

5) **Performance** — "Performance" implies accuracy. It is measured by two rates, 1) False Acceptance Rate (FAR) and 2) False Rejection Rate (FRR), which are controlled by a threshold. Reducing FAR (FRR) means increasing FRR (FAR). Equal Error Rate (EER) or crossover rate also implies accuracy. A system with 1% EER or crossover rate means that this system has 1% FRR and 1% FAR [8].

6) **Acceptability** — To be computer scientists, we should try our best to produce a user-friendly biometric system. In fact, almost all the current biometric systems are not physically intrusive to users although some of them, such as retina-based recognition system, are psychologically invasive systems.

Retina-based recognition system requires a user to put his/her eye very close to the equipment and then have infrared light passing through his/her eye in order to illuminate his/her retina for capturing an image [9-12].

1.5 Different Biometrics

In this section, we introduce different biometrics including fingerprint, dental, 3-D hand geometry and retina.

1) Fingerprint — It is one of the most mature biometric technologies. Automatic fingerprint identification began in the early 1970s. At that time, fingerprint verification was used for law enforcement. In the 1980s, with rapid development of personal computer and fingerprint scanner; fingerprint identification started to be used for non-criminal applications [14]. Current fingerprint systems utilize minutiae and singular points as the features [15-20]. Fingerprint has high performance, uniqueness and user acceptance. However, some people's fingerprints are not easy to be clearly captured. Fig 1.2 illustrates fingerprint images with different quality.
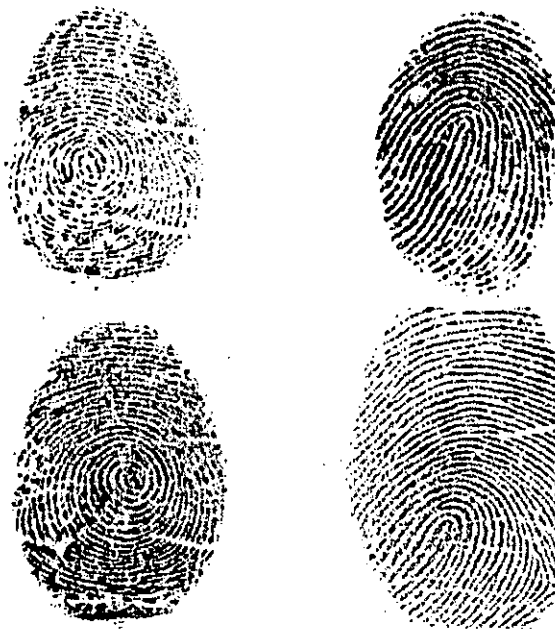
Fig 1.2 Fingerprint images with different quality

2)   Dental — Dental recognition mainly takes place when a disaster happens in which many fatalities have occurred in a hectic environment. High-energy disasters such as bombings and plane crashes are often accompanied by massive destruction and fire. This may result in the destruction of identifiable biometrics such as facial features, fingerprints and ID tags. Consequently, we can only rely on dental characteristics as a "hard fingerprint" to identify the victims. Fig. 1.3 shows several dental images. For more information about this, please refer to [99-101].
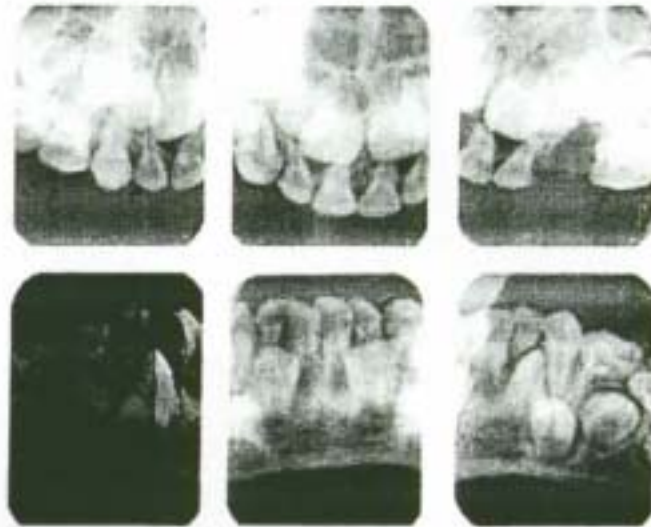
Fig. 1.3 Radiographs of skull

3)   Hand geometry — Hand geometry measures on the length and width of the finger and the width and thickness of the hand. Compared with other biometrics, hand geometry has several advantages including small feature size, low-cost computational algorithm and using low-resolution image [102-103]. Nevertheless, the current hand geometry system suffers from high cost and low accuracy [26]. Due to the low accuracy of hand geometry, current systems normally combine smart cards or passwords with hand geometry recognition to provide tighter security. Fig 1.4 shows one of the current systems called Hand Key II from Recognition System Inc.

Fig 1.4 A hand geometry recognition system, Hand Key II

4)   Retina — The blood vessel pattern in the retina is the feature for retinal
recognition technology. This technology requires a user's eye to be aligned
with the camera target. This is a very intrusive procedure. An infrared light
source illuminates the retina of the eye. Infrared light is applied due to the
fact that the blood vessels on the retina absorb infrared energy faster than the
surrounding eye tissue(s). The infrared light with the retinal pattern will then
be reflected to the camera, which then captures the retinal pattern and
converts it into a digital signal. Currently, there are two major representations
of the retina; the original representation consists of 40 bytes of contrast
information encoded as real and imaginary coordinates in the frequency
domain. This is generated by the Fast Fourier Transform. The second
representation with 48 bytes is the contrast data in the time domain. The
primary advantage of the time domain representation of the retinal signature
is computational efficiency [9-12]. Figs. 1.5(a) and (b) show a retinal image
and a retinal recognition system produced by EyeDentify, respectively.

8
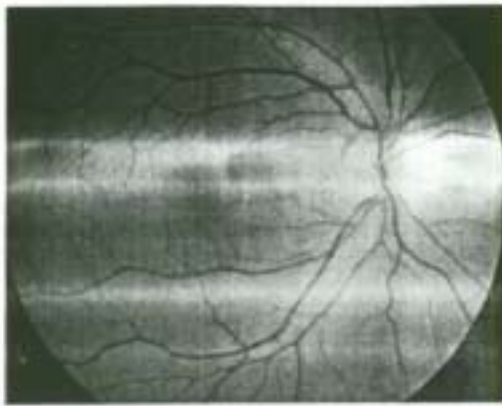
(a)
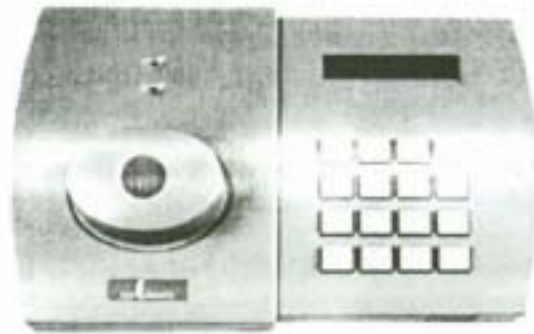
(b)

Fig 1.5 Retinal image and current retinal capture device. (a) A retinal image with the blood vessel pattern and (b) a current product from EyeDentify.

1.6 Sale of Different Biometric Products

Different biometric products have different applications, cost and performance. As a result, they get different shares in the biometric technology market. Fig. 1.6 shows the revenue of different biometric technologies in 1999. The data comes from the International Biometrics Group [27].
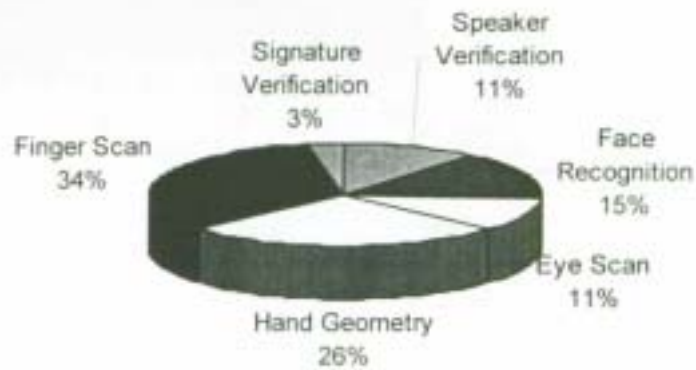
Fig 1.6 Revenue of different biometric technologies in 1999.

(Source: International Biometrics Group.)

9

Total revenue in 1999 was US$ 58.4 million and the projected revenue in 2003 is $594.0 million. Finger Scan (fingerprint recognition) obtained the highest revenue because it was the most mature technology in the industry. Hand geometry suffers from high-cost and low recognition rate; however, it still got about a quarter of the total revenue because of high end-users acceptance. Face recognition also gets high acceptance from end-users and only needs low-cost input devices, but it suffers from low accuracy. Nevertheless, it took up 15% in 1999. Although speaker verification and eye-scan shared the same amount of revenue, their target markets are different. Speaker verification is for the market that accepts low recognition rates using low cost products. On the other hand, eye-scan including iris recognition and retina recognition focuses on high-security markets such as nuclear power station security and automatic teller machines (ATMs) [2-3].

1.7   Organization of this Thesis

This thesis is organized as follows: Chapter 1 provides an introduction to biometric technologies. Chapter 2 describes some mathematical tools for texture analysis. A novel noise detection model for iris recognition is given in Chapter 3. Chapter 4 explains a new biometrics, palmprint and Chapter 5 discusses a palmprint identification system. The explanation of another new biometric, the ear, is given in Chapter 6. Finally, conclusions and suggestions for further research are made in Chapter 7.

Chapter 2

The Mathematical Tools for Texture Analysis

Objective — In this Chapter, we introduce some mathematical tools for texture analysis, including statistical and wavelet approaches. Various statistical approaches for texture analysis such as co-occurrence, gradient analysis and the autocorrelation function, are given. Then several 1-D wavelet approaches will be discussed. Some wavelets and Gabor functions are discussed thoroughly towards in the end of this Chapter since they will be utilized in the following chapters.

2.1   Definition of Texture

Texture is a term that is widely used in image processing and computer vision fields but it does not have a universal definition. Some researchers have given their own definitions. Their main ideas are that texture is a spatial self-similar or spatial repetitive object. Julesz thinks that texture is constituted by a set of basic elements called textons [79]; Haralick and Shapiro have similar idea but they name the basic elements texels [80]. Fig. 2.1 shows 12 typical texture images illustrating the properties of spatial self-similarity and repetitiveness. The term, texture, is extended in this thesis. It represents an image with some basic elements that may not be spatial-similar and repetitive throughout the whole piece of texture. Taking a palmprint image as an example, we find that line is the basic element but a patch in the image may not be similar to another patch in the same image. Fig. 2.2 gives three palmprint images illustrating our definition. Since the application of our research is personal identification, we do not expect images with severe spatial repetitiveness, which would reduce information in the images.
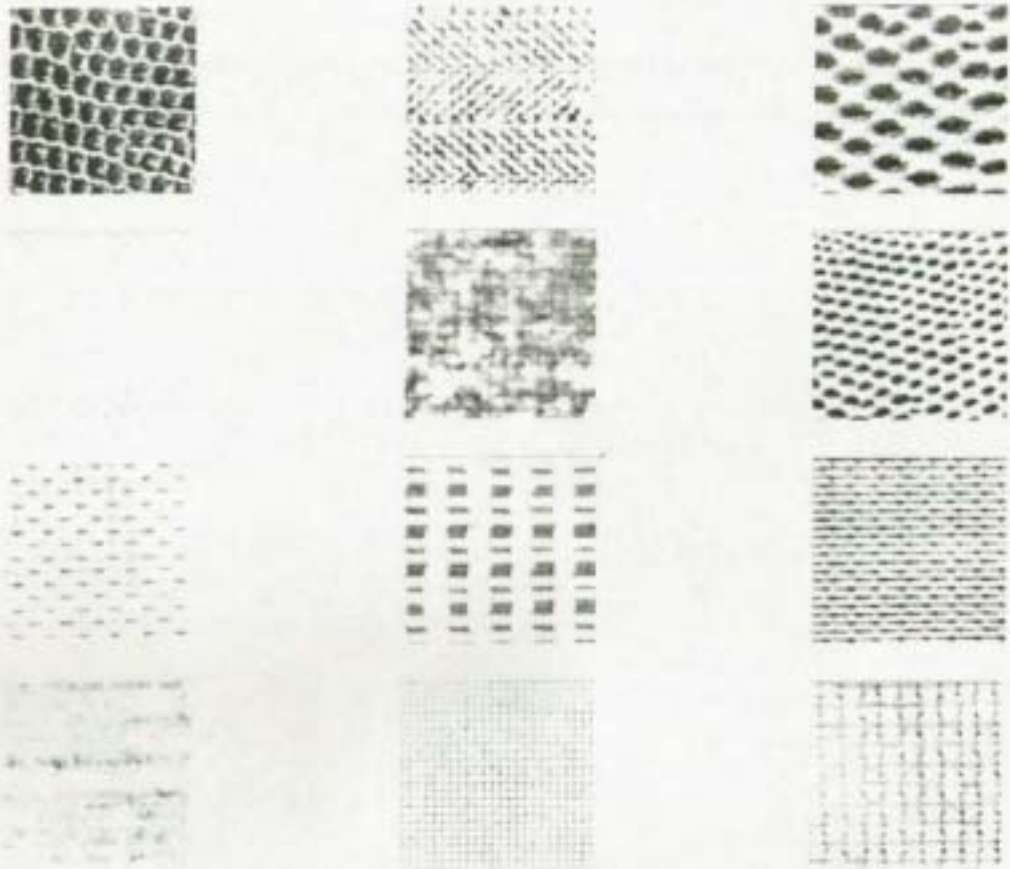
Fig. 2.1 Typical texture images that are collected from [81].
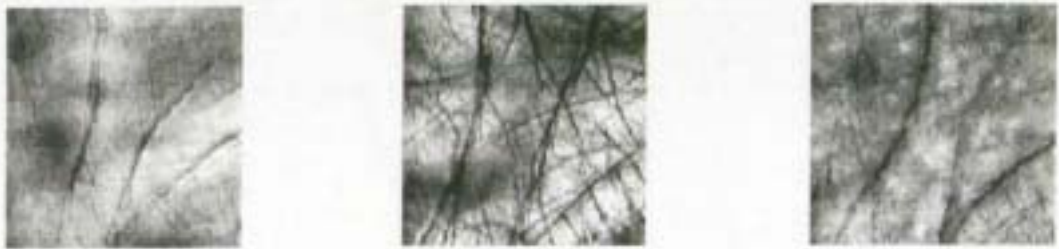
Fig. 2.2 Three palmprint images illustrate our definition of texture.

2.2 Statistical Features for Texture Analysis

In this section, we will introduce some basic statistical methods for texture analysis including autocorrelation, gradient analysis, relative extrema density, co-occurrence, moments of the gray-level histogram and gray-tone co-occurrence. They have been applied to texture classification and texture segmentation. Although these tools will not be used in the following chapters, it is worth giving their background knowledge here.

2.2.1 Autocorrelation

Autocorrelation is a function measuring the size of the tonal primitives (textons). Large and small textons are indicative of coarser and fine textures, respectively. The autocorrelation function is,

$$A(x,y) = \frac{\frac{1}{(L_x - |x|)(L_y - |y|)} \int_{-\infty}^{\infty} \int_{-\infty}^{\infty} I(u,v)I(u+x,v+y)dudv}{\frac{1}{L_x L_y} \int_{-\infty}^{\infty} \int_{-\infty}^{\infty} I^2(x,y)dudv}, \qquad (2-1)$$

where I is a texture image; L_x and L_y are the width and length of the image, respectively. Here, we are assuming the image with mean zero. If a texton is small, then the response of the autocorrelation function will decay quickly and then rise. On the other hand, provided that a texton is large, the response of the autocorrelation function will drop slowly [82].

2.2.2 Gradient Analysis

Gradient analysis is an edge-based approach proposed by Rosenfeld, Troy, Rosenfeld and Thurston [83-84]. According to their idea, texture is regarded as the amount of "edge" per unit area. The edge operators, such as Roberts and Laplacian operators extract the edge information of the texture in a small window. Then, it takes the mean of the results as a texture feature.

2.2.3 Relative Extrema Density

Rosenfeld and Troy also proposed an extrema-based approach — the number of extrema per unit image area for texture measure [83]. Besides, several other researchers including Ledlely

13

and Rotola [86-87] had similar ideas. They suggested implementing this technique on smoothed images so as to eliminate extrema caused by noise.

2.2.4 Moments of the Gray-Level Histogram

In this approach, texture feature is described by the texture moment of the gray-level histogram in an image [85]. Let z be a random variable representing discrete image intensity and let $p(z_i)$, $i=1, 2, ...L$ be the corresponding histogram, where L is the number of intensity levels. The mth order moment can be computed by the following equation,

$$\mu_m = \sum_{i=1}^{L}(z_i - \mu)^m p(z_i),$$ (2-2)

where μ is the mean of the histogram. However, this approach does not consider the relative positions amongst pixels so some researchers proposed to use gray-tone co-occurrence.

2.2.5 Gray-Tone Co-Occurrence

Gray-tone Co-occurrence is represented by an occurrence matrix C whose element is,

$$c_{ij} = \frac{a_{ij}}{\sum_{i=1}^{k}\sum_{j=1}^{k}a_{ij}},$$ (2-3)

where a_{ij} is the number of times that points with gray level z_i and points with gray level z_j occur under a specified relative position, where $1 \le i, j \le k$ [82, 85]. From the co-occurrence matrix, several descriptors are computed to represent different texture including:

1)   maximum probability

$$\max_{i,j}(c_{ij}),$$ (2-4)

2)   element different moment of order k

$$\sum_i\sum_j(i-j)^k c_{ij},$$ (2-5)

3)   inverse element different moment of order k,

$$\sum_i\sum_j\frac{c_{ij}}{(i-j)^k},$$ (2-6)

4)   entropy,

$$-\sum_i \sum_j c_{ij} \log c_{ij}, \tag{2-7}$$

5)   energy,

$$\sum_i \sum_j c_{ij}^2. \tag{2-8}$$

2.3   Wavelets and Gabor Functions

Wavelets and Gabor functions are powerful multiresolution analysis techniques widely implemented in the fields of image processing, computer vision and compression. Because of their multi-resolution property, they have been applied to different areas in texture analysis, namely texture classification and texture segmentation [95-98]. In this section, we briefly give a review of wavelets. Several 1-D wavelets and 2-D Gabor functions will be discussed. Details of their theory can be referred to in [88-89].

2.3.1   Wavelet Transform

Wavelet decomposes an image by dilating and translating its mother wavelet. It is an effective tool to analyze an image at different scales. A wavelet is a function, $\psi \in L^2(\Re)$ with a zero mean and its norm $\|\psi\| = 1$. A set of time-frequency atoms is generated by scaling ψ by s and translating by u:

$$\psi_{u,s}(t) = \frac{1}{\sqrt{s}} \psi\left(\frac{t-u}{s}\right). \tag{2-9}$$

The wavelet transform of f at the time u and scale s is

$$Wf(u,s) = \int_{-\infty}^{\infty} f(t) \frac{1}{\sqrt{s}} \overline{\psi_{u,s}(t)} dt. \tag{2-10}$$

In fact, wavelet transform can be regarded as a convolution:

$$Wf(u,s) = \int_{-\infty}^{\infty} f(t) \frac{1}{\sqrt{s}} \overline{\psi_{u,s}(t)} dt = f * \psi'_{u,s}(t), \tag{2-11}$$

with

$$\psi'_{,s}(t) = \frac{1}{\sqrt{s}} \overline{\psi\left(\frac{-t}{s}\right)}, \tag{2-12}$$

where ⁻denotes complex conjugate. When s and u are set to power of 2, the wavelet transform is called dyadic wavelet.

2.3.2 1-D Wavelets

In this sub-section, we introduce several 1-D wavelets, which will be used in Chapter 3 to test our noise segmentation model. The wavelets include normalized Mexican hat, Shannon and Haar. Their formulas are mentioned in Eq. 2-13 to Eq. 2-15. The Mexican hat wavelets are second derivatives of a Gaussian. They have been applied to an multi-scale edge detection [90]. The Shannon wavelets are generated by Shannon multi-resolution approximation [89]. Haar wavelet is the simplest wavelet, which is generated by a box function and it has been implemented on many areas, such as segmentation, clustering, and image coding [91-94].

Normalized Mexican hat:

$$w_M(t,\sigma) = \frac{2}{\pi^{1/4}\sqrt{3\sigma}}\left(\frac{t^2}{\sigma^2}-1\right)\exp\left(-\frac{t^2}{2\sigma^2}\right), \qquad (2\text{-}13)$$

Shannon:

$$w_s(t) = \frac{\sin(2\pi(t-\frac{1}{2}))}{2\pi(t-\frac{1}{2})} - \frac{\sin(\pi(t-\frac{1}{2}))}{\sin(\pi(t-\frac{1}{2}))}, \qquad (2\text{-}14)$$

Haar:

$$w_h(t) = \begin{cases} 1 & \text{if } 0 \le t < 0.5 \\ 2 & \text{if } 0.5 \le t < 1 \\ 0 & \text{otherwise} \end{cases} . \qquad (2\text{-}15)$$

2.3.3 Gabor Functions

Gabor filters, Gabor filter banks, Gabor transform and Gabor wavelets are widely applied to image processing, compute vision and pattern recognition fields. The Gabor function was first investigated by Gabor in 1946 [64]. This function can provide accurate time-frequency location, which is governed by the "Uncertainty Principle" [65]. Originally, Gabor only investigated 1-D case:

$$w_g(t,\sigma,\eta) = \frac{1}{\sqrt[4]{\sigma^2\pi}}\exp\left(\frac{-t^2}{2\sigma^2}\right)\exp(i2\pi\eta t). \qquad (2\text{-}17)$$

The Gabor function was extended to 2-D case by Daugman in 1980 [66-67]. A 2-D circular Gabor filter in the spatial domain has the following general form,

$$G(x,y,\theta,u,\sigma) = \frac{1}{2\pi\sigma^2}\exp\left\{-\frac{x^2+y^2}{2\sigma^2}\right\}\exp\{2\pi i(ux\cos\theta + uy\sin\theta)\}, \qquad (2\text{-}18)$$

where u is the frequency of the sinusoidal wave; θ controls the orientation of the function; σ is the standard deviation of the Gaussian envelope and i is defined as $i^2=1$. Fig. 2.3 gives a graphic representation of the Gabor function. Gabor filters have several important characteristics so many researchers utilize them to solve problems in computer vision and biometric technology. Firstly, it can capture local information, which is governed by the "Uncertainty Principle". It also provides robustness against varying brightness and contrast in images. Moreover, it can model the receptive fields of a simple cell in the primary visual cortex. The above features motivate many researchers to apply Gabor filters to many areas [68-70]. In biometric research, Gabor filters have been applied to iris, face and fingerprint recognition [30, 71-76].
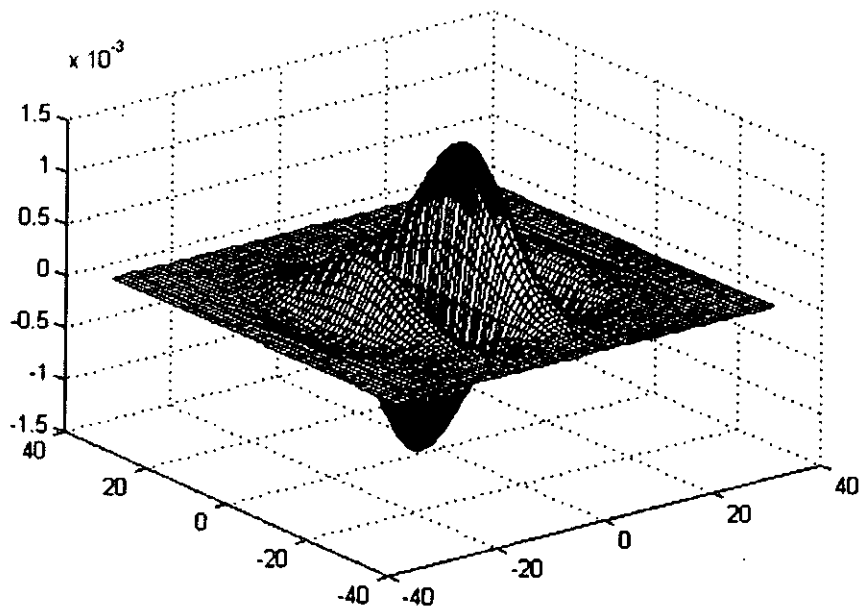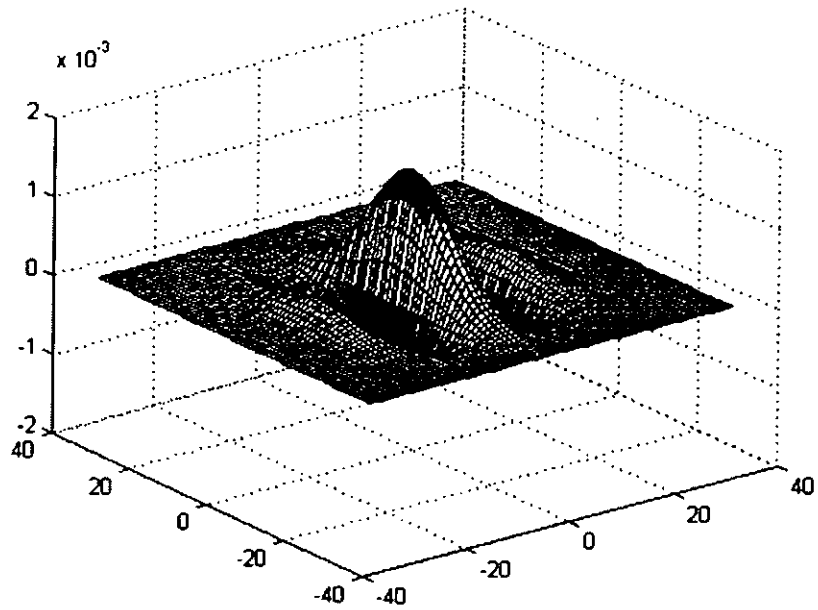
Fig.2.3 A graphical representation of a Gabor function (u=0.05, θ=90 and σ=100), (a) Real part of a Gabor function and (b) Imaginary part of a Gabor function

Chapter 3

Accurate Iris Segmentation Based on Novel Reflection and Eyelash Detection Model for Iris Recognition

Objective — In this chapter, we propose a novel noise detection model for accurate segmentation of an iris from an image. Eyelashes, eyelid and reflection are the three main sources of noise. The eyelid has been detected by the traditional eye model; however, eyelash and reflection have not been regarded. To determinate a pixel belonging to an eyelash, our model follows three criteria: 1) separable eyelash condition, 2) non-informative condition and 3) connective criterion. The first condition handles separable eyelash and the second one manages multiple eyelashes. The last criterion avoids misclassifying strong iris texture as a single and separable eyelash. For reflection, strong reflection points are detected by a pre-defined threshold and the weak reflection areas around the strong points are determined by a connective criterion and a statistical test. A number of images are selected to evaluate the accuracy and usefulness of the proposed model and the experimental results are encouraging.

In addition, Boles' approach [48-49] using 1-D wavelet is evaluated in this chapter. Since it was only tested on a small database, the accuracy of this approach cannot be proved.

3.1   Iris Recognition History

In 1987, two ophthalmologists, Flom and Safir, proposed that the iris can be used as a biometric signature. They discovered that every iris has highly complex and unique texture,

which remains unchanged over a decade. They obtained a US patent for their discoveries; nevertheless, they did not develop an automatic recognition algorithm.

In 1989, Ophthalmoloy Associate of Connecticut cooperated with Daugman to setup a photographic iris database. Then, a frame grabber board, a video camera and lens constituted an iris capture device. From 1992 to 1995, Daugman published several papers to prove the accuracy and effectiveness of his iris recognition method [29-33]. The most important paper was published in 1993 [30], which deeply discussed his algorithm and results. In his papers, he claimed that his algorithm got very high recognition rate and it only needed very short computation time. In 1994, he obtained a US patent for his algorithm[31].

At the same time, Flom, Safir and Daugman established a company called Iriscan. From 1993 to now, several reports have proved the accuracy of his method [34-39]. Nowadays, many companies apply Daugman's algorithm to producing various iris recognition systems. They focus on hardware development in order to get high user acceptance [40-42].

Another research team also developed an iris recognition system, which also got very high recognition rate [43-46]. They put a lot of effort to control the light source so as to capture high quality images and to ensure that users feel comfortable. Same as Daugman, they got a US patent [46].

The third research team proposed a new recognition algorithm based on wavelet transformation [47-48]. However, their testing database is very small. Thus, their experimental results cannot show the reliability and accuracy of their algorithm. Nowadays, some Chinese researchers are working on iris recognition but they are still working on a small database [50].

3.2 Advantages of Recognizing a Person by Iris Pattern

The iris possesses many good characteristics for personal identification. According to Flom and Safir research results, every iris has highly complex and unique texture. Fig. 3.1 displays the detailed texture of nine irises, which were captured by a special device and were downloaded from http://www.cl.cam.ac.uk/users/jgd1000/. Based on the unique characteristics of the pattern, Flom and Safir proposed that iris can be used for personal

identification. Even left and right irises of the same person or irises from two twins also contain a lot of distinguishable features. Fig. 3.2 shows two irises from the same person. Observable features include contraction furrows, striations, pits, collagenous fibers, filaments, crypts, serpentine vasculature, rings and freckles. Among the visible features in the iris, some of them can be observed in Fig. 3.2. Also, the iris is an internal organ, which is protected by the cornea so it cannot be surgically modified without unacceptable risk to vision. Besides, it responds to light, which can be utilized as a natural test against artifice.
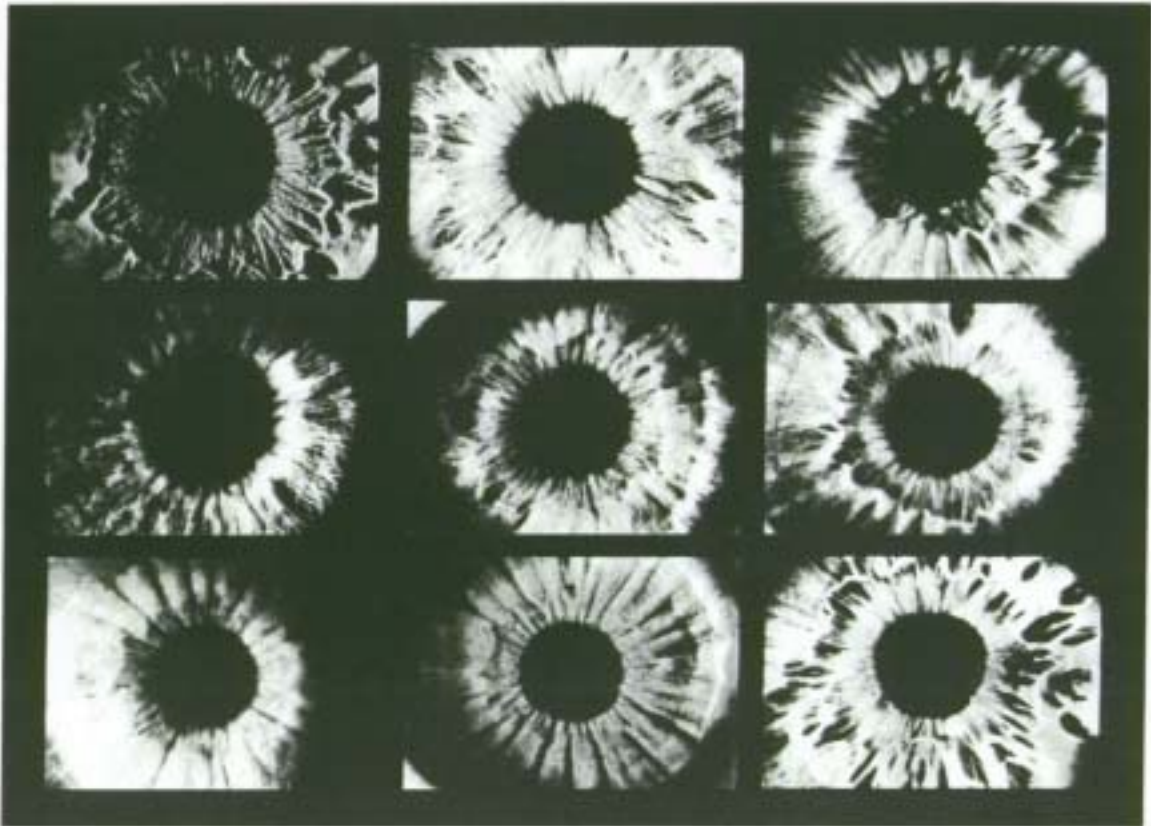
Fig. 3.1 Irises with highly complex and unique texture
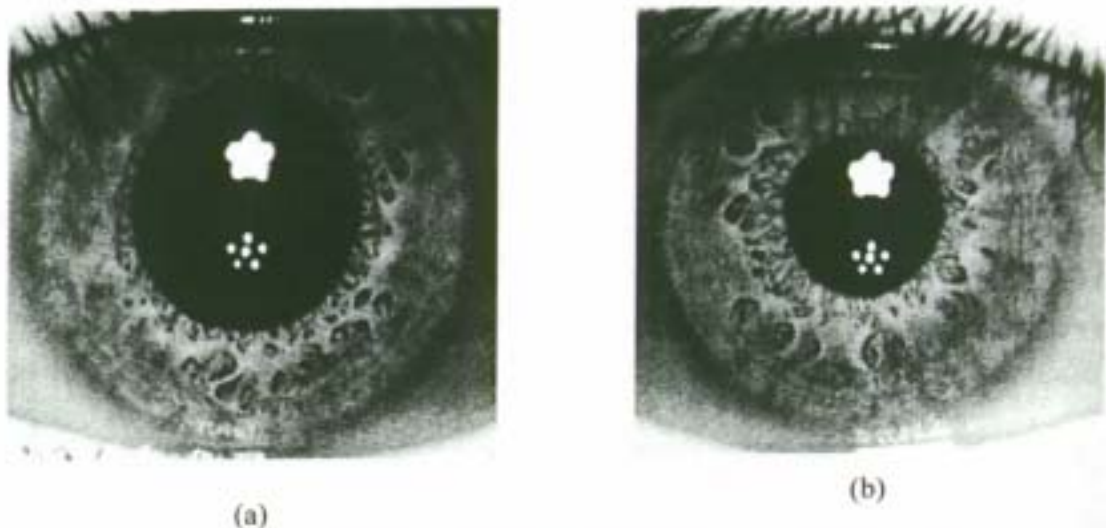
Fig. 3.2 Left and right eyes of the same person have different iris pattern;

(a) left eye and (b) right eye

3.3 Difficulties of Using Iris Pattern for Personal Identification

Although the iris has many good features, using the iris for personal identification still has many difficulties. First of all, the cornea may cause serious reflection. Some parts of the iris may be covered by eyelids and eyelashes. Furthermore, a user's contact lens cannot easily be removed when using an iris recognition system. Everyone tends to protect his or her eyes against flash and close objects such as capture devices. So flash and short distance between the equipment and the user are not suitable. The size of the iris will change under different lighting conditions. However, we generally cannot control the conditions of lighting. Therefore, if an iris recognition system cannot handle this property, it cannot be used to test against artifice or dead iris.

3.4 Features Inside Our Iris

Our iris can be divided into two parts, pupillary zone and cillary zone. These two zones are separated by collarette. In the cillary zone, we have mole, crypt and peripheral crypt [51]. These features are shown in Fig. 3.3. The texture in the pupillary zone is clearer than that in Cillary zone

People of different nationalities have different classes of irises. According to [51], the surface of an iris has rich texture information (refer to Fig. 3.4). A darker iris has more

pigment so the surface is smoother. Fig. 3.5 shows three irises from three people of different nationalities.
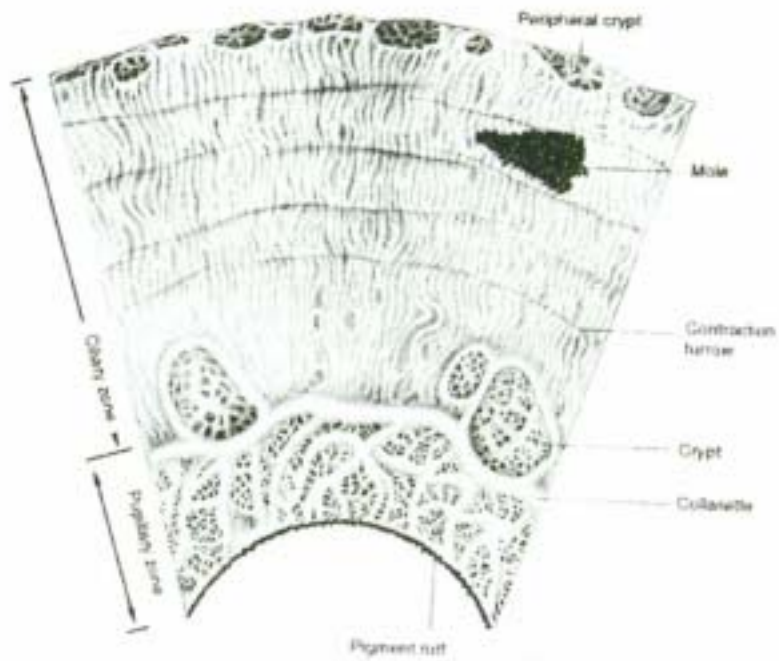
Fig. 3.3 Fundamental feature in our iris. From [51]
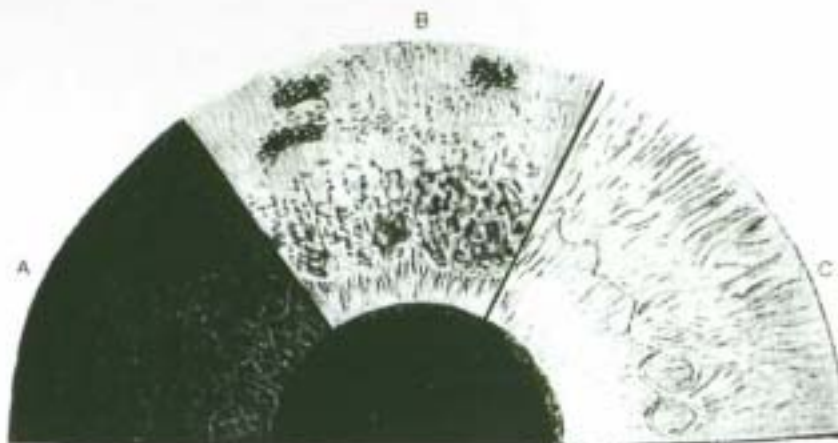
Fig. 3.4 Varieties of human iris A) deeply pigmented;
B) Medium European; C) Blonde European. From[51]
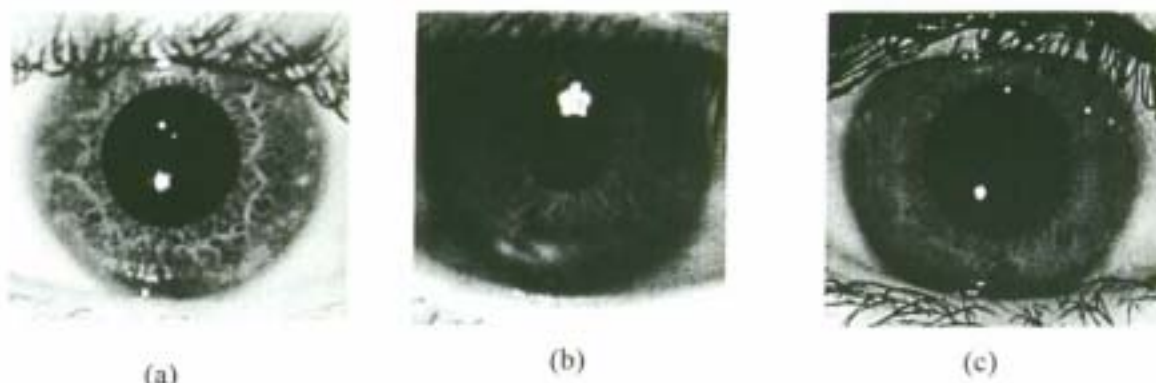
Fig. 3.5 People of different countries have different classes of texture

(a) Western iris; (b) Chinese iris; (c) Korean iris

3.5. Literature Review

3.5.1 Iris System Architecture

Basically, existing iris recognition approaches [30-34,43-48] have similar architectures including the five steps described as follows:

1) *Image Acquisition* is to yield a high quality image containing a clear iris.

2) *Iris Localization* points out the position of the iris in the acquired image.

3) *Iris Normalization* standardizes the variation of iris size.

4) *Feature Extraction* is to extract the texture information by a set of filters or wavelet.

5) *Comparison* makes a final decision whether two iris features belong to the same person or not, based on a classifier.

3.5.2 Daugman's Approach

This method can be divided into four parts: 1) Iris Localization, 2) Doubly Dimensionless Projection, 3) Iris Code and 4) Comparison. Details of this approach are mentioned in [30-34]. His experimental results were obtained from the images with 480×640 pixels and the outer diameters of the irises were greater than 60 pixels. They were usually between 100 and 200 pixels.

1) Iris Localization

Daugman designed a special integrodiffererntial operator to search the pupil and limbus boundaries over the image domain. In order to accurately locate

the boundary of the limbus, the operator only searches the left and right parts of the limbus boundary. Besides, he applies a non-linear enhancement technique to detect the boundary of the pupil.

2)   Doubly Dimensionless Projection

The optical size of an iris in an image would change because of pupillary constriction, variation of distance between the camera and the eye, and different video zoom factors. Thus, Daugman proposed a doubly dimensionless non-concentric polar coordinate system to normalize all the effects. Under this transformation, the optical sizes of the irises are standardized.

3)   IrisCode

Texture information in transformed iris images is extracted by a 2-D Gabor filter. The phase information in the filtered image is coded by a set of inequalities, producing IrisCodes. Fig. 3.6 shows an iris image and its IrisCode.

4)   Comparison

The similarity between two IrisCodes is measured by their normalized hamming distance.
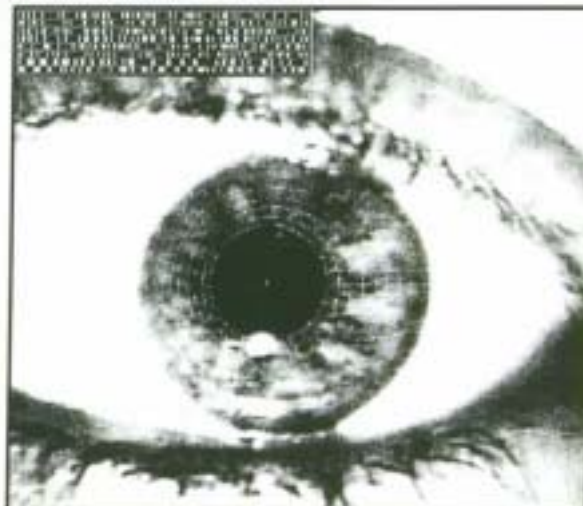
Fig. 3.6 shows an iris image and its IrisCode

3.5.3 Wildes's Approach

In this subsection, we would mention the key ideas of Wildes's approaches [43-46]. Wildes's approach has very good performance. After an image is captured, Hough Transform is applied to locate the boundaries of the iris [52]. Then, an image-registration technique is used to align two images [53]. Afterwards, the Wildes's system employs an isotropic band-pass decomposition derived from the application of Laplacian of Gaussian filters in order to get four different frequency bands [54]. Each frequency band is cut down into a lot of small blocks. The size of a small block is 8×8 pixels. The similarity between two small blocks is measured by normalized correlation. At the end, a Fister's linear discriminant makes the final decision [55].

3.5.4 Boles' Approach

Boles' approach uses Wavelet Transform to extract iris features [47-48]. Same as Daugman and Wildes's approaches, his approach models the iris as a circular object. The circular part of the iris is cut down and considered as a one dimension period signal. Then, he applies 1-D Wavelet Transform to this signal to decompose it into several levels. At the end, two dissimilarity functions are defined for making the final decision. The database is very small so the experiment cannot demonstrate the accuracy of his approach.

3.6　Usefulness of Accurate Iris Segmentation

Automatic personal identification using iris, iris diagnosis (iridology) and determination of human ocular torsion are three different applications that require accurate iris segmentation [29-34, 43-48, 56]. It is widely accepted that the boundaries of an iris in an image are modeled by two circles for the pupil and limbus (the outer boundary of the iris), and two parabolas for the upper and lower eyelids. This model has been used in several areas, including iris recognition, eye tracking and animation [29-34, 43-48, 59-60]. However, eyelashes and reflection detection are not considered. If the eyelashes or reflection are considered as a part of the iris, the accuracy for automatic personal identification is reduced. This problem is especially serious for people with small eyes and dense eyelashes because the percentage of eyelashes classified as the iris is large. In the following sub-sections, we propose a noise detection model for accurate iris segmentation. The model is divided into two parts, eyelash detectionl and reflection detection.

3.7 Traditional Iris Segmentation Model

In general, an eye is modeled by two circles, the pupil and limbus, and two parabolas, the upper and lower eyelids. The circles are defined as

$$(x-x_i)^2 + (y-y_i)^2 = r_i^2,\tag{3-1}$$

where (x_i, y_i) is its center and r_i is its radius ($i = p, l$; p – pupil and l – limbus). The two parabolas have the following general form,

$$(-(x-h_j)\sin\theta_j + (y-k_j)\cos\theta_j)^2 = a_j((x-h_j)\cos\theta_j + (y-k_j)\sin\theta_j),\tag{3-2}$$

where a_j (< 0) is used to control the curvature of the parabola, (h_j, k_j) is the vertex of the parabola and θ_j is an angle between the x-axis and the principal axis of the parabola ($j = m, n$; m – upper eyelids and n – lower eyelids).

Fitting the contours of both the pupil and the limbus can be divided into two steps. To remove the noise, an image would be convoluted by a lowpass filter, such as a two-dimensional Gaussian. Then, a gradient operator, ($\nabla = (\partial / \partial x \; \partial / \partial y)$, is imposed to select the edge points. Mathematically, it can be represented by $|\nabla G(x, y) \bullet f(x, y)|$, where $G(x, y)$ is a two-dimensional lowpass filter and $f(x, y)$ is a raw image. If any point with the magnitude of the intensity gradient image is greater than a certain threshold, it is considered as an edge point. Hough Transform is applied to find out the three parameters, (x_p, y_p, r_p) [52]. Fig. 3.7 shows an image that is implemented by this traditional segmentation method. Similar techniques are able to determine the parameters of the parabolas.
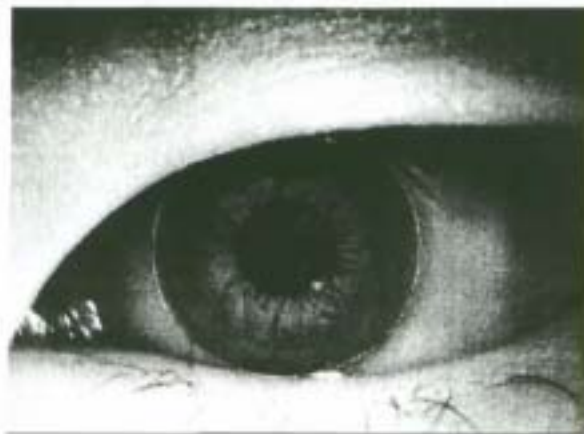
Fig. 3.7 Illustration of traditional iris segmentation technique

3.8   Eyelash Detection

There are two types of eyelashes defined in our eyelash detection model (see Fig. 3.8). One is separable eyelashes that are able to be distinguished from other eyelashes. Another one is multiple eyelashes of which the eyelashes will overlap one another in a small area so they are impossible to be separated.
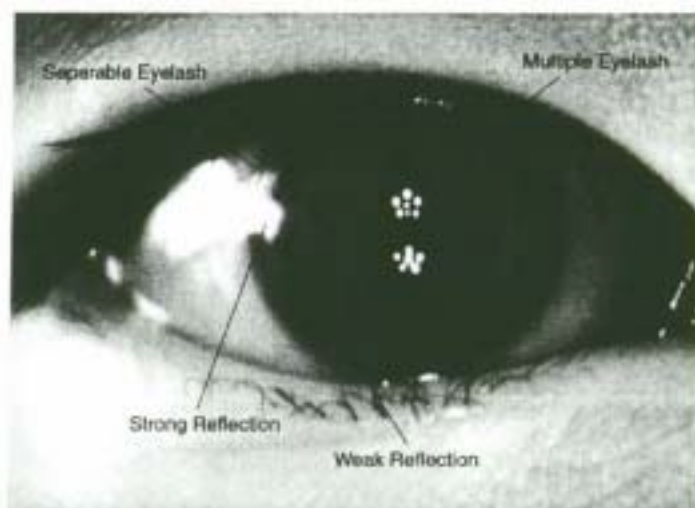
Fig. 3.8 Two types of eyelashes and reflections

3.8.1   Separable Eyelash Condition

A real part of a Gabor filter captures the separable eyelashes such that a 1-D Gabor filter in the spatial domain has the following general form,

$$G(x,u,\sigma) = \exp\{x^2/2\sigma^2\}\cos(2\pi ux),$$
(3-3)

where u is the frequency of the sinusoidal wave, and σ is the standard deviation of the Gaussian envelope. The convolution of a separable eyelash with $G(x,u,\sigma)$ would be very small. In fact, the Gabor filter serves as an edge detector. Thus, if a resultant value of a point is smaller than a threshold, it is noted that this point belongs to an eyelash. Mathematically, it can be represented by

$$f(x) * G(x,u,\sigma) < K_1,$$
(3-4)

where K_1 is a pre-defined threshold that is $-$ 45 for the following experiments and "$*$" represents an operator of convolution.

3.8.2. Non-Informative Condition

Non-Informative Condition manages multiple eyelashes. When many eyelashes overlap in a small area, the pixels in the small area have similar intensity values. Thus, if the variance of intensity in a small window is smaller than a threshold, the center of the window is considered as a point in an eyelash. This criterion is described by,

$$\frac{\sum\limits_{i=-N}^{N} \sum\limits_{j=-N}^{N} (f(x+i, y+j) - M)^2}{(2N+1)^2 - 1} < K_2 , \tag{3-5}$$

where M is the mean of intensity in the small window, $(2N+1)$ is the size of the window and K_2 is a threshold. In our following experiments, K_2 and $(2N+1)^2$ are defined as 6 and 5x5, respectively.

3.8.3. Connective Criterion

In order to provide more robust and high accuracy detection methods, the connective property of an eyelash is utilized to avoid misclassification from the previous criteria. Each point in an eyelash should connect to another point in the eyelash or in the eyelid. If any point fulfills one of the two previous criteria, its neighbor pixels are required to check whether they belong to the eyelash or eyelid. If none of the neighbor pixels has been classified as a point in an eyelid or an eyelash, it is not classified as a pixel in an eyelash.

3.9.   Reflection Detection Model

We also give two definitions for strong and weak reflection (see Fig. 3.8). A pixel belongs to strong reflection if its intensity is larger than a certain threshold. Weak reflection is a transition region from strong reflection to the iris. Mathematically, strong reflection is recognized by the following equation,

$$I(x,y) > K_3, \tag{3-6}$$

where $I(x,y)$ is the intensity value of an image at point (x,y) and K_3 is a threshold which is taken as 180 in the following experiments.

According to our discovery, the intensity of the iris pixel close to a normal distribution. In order to prove the statement, we have selected 50 iris images to build Fig 3.9, where the black line and the gray line represent a standard normal cumulative distribution and

an empirical cumulative distribution, respectively. The empirical cumulative distribution is generated by the normalized intensity pixels which are computed by the following equation,

$$d(x,y) = \frac{I(x,y) - \bar{x}}{S}, \tag{3-7}$$

where $\bar{x}$ and S are the sample mean and sample standard derivation of an iris intensity, respectively. Strictly speaking, according to Kolmogorov – Smirnov goodness of test, intensity of the iris pixels does not follow normal distribution [61]
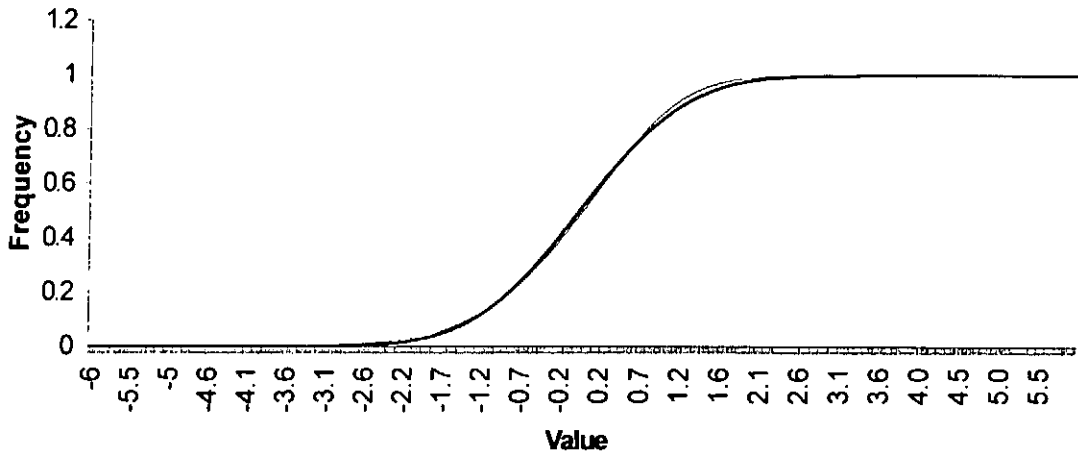
Fig. 3.9 Comparison between cumulative distribution of a normal distribution and a cumulative distribution of intensity of an iris image. The black and gray curves represent the normal and iris distribution respectively. Their means and standard deviations are the same.

Since the iris distribution is close to a normal distribution, we propose to impose a statistical test to determinate the weak reflection points. This test is based on the following equation,

$$\mu + \alpha\sigma < I(x,y), \tag{3-8}$$

where μ and σ are the mean and standard deviation of the intensity distribution of the iris pixels, respectively; α is a parameter to control type I and type II errors. If any point around the strong reflection points satisfies Eq. 3-8, it will be noted as a weak reflection point. According to this equation, we need to estimate μ and σ. Generally μ and σ are approximated by sample mean, $\bar{X}$, and sample standard deviation, S, respectively. They can be obtained by the following equations,

$$\overline{X} = \frac{\sum\limits_{k \in P} I_k}{N_p},$$ (3-9)

$$S = \sqrt{\frac{\sum\limits_{k \in P} I_k^2 - N_p \overline{X}^2}{N_p - 1}},$$ (3-10)

where P represents a set of pixels that only belongs to the iris and N_p is the number of pixels in P and I_k is the intensity value of pixel, k.

Originally, we want to detect the weak reflection points, which are formulated to a statistical test. The test requires estimating the mean μ and standard deviation σ by $\overline{X}$ and S, respectively. However, in order to compute $\overline{X}$ and S, we should construct a set P, which is the original goal in our detection mode. Our formulation forms a close loop that can be solved by an iterative approach. The steps are briefly described as below:

1) Set $P=P_j$ and $j=0$. P_j is a set of pixels which does not belong to the eyelash, strong reflection and the eyelid; N_j is defined as the number of pixels in P_j. Compute $\overline{x_j}$ and S_j by Eq. 3-9 and Eq. 3-10, respectively. Let Q_j be a set of pixels that belongs to strong reflection.

2) According to Eq. 3-8, test all pixels in P_j which connect to any pixel in set Q_j. If a pixel with intensity x satisfies Eq. 3-8, it is removed from set P_j and inserted into Q_j. Update $\overline{X}_j$, S_j and N_j by the following equations,

$$N_{jnew} = N_j - 1,$$ (3-11)

$$\overline{X}_{jnew} = \frac{N_j \overline{X}_j - x}{N_{jnew}},$$ (3-12)

$$S_{jnew}^2 = \frac{N_{jnew}(S_j^2 - \overline{X}_{jnew}^2) + N_j \overline{X}_j^2 - x^2}{N_{jnew} - 1}.$$ (3-13)

3) If none of the pixels is removed from P_j in Step 2, set $P=P_j$ and exit the loop. Otherwise, repeat Step 2.

3.10   Experimental Results

Many different iris images have been selected to test the proposed model. Some typical examples are shown in Fig. 3.10. Figs. 3.10(a) and (c) give the segmentation results using the traditional model and Figs. 3.10(b) and (d) show the detection results using the proposed model. The white regions in Figs. 3.10(b) and (d) are marked as the eyelashes and reflection by our detection model. Comparing these two types of the results mentioned above, we can see that many eyelashes and large reflection area still remain in the segmented part in Figs. 3.10(a) and (c) but in Figs. 3.10(d) and (d), almost all the eyelashes and reflection areas are recognized by the proposed model. The resultant images demonstrate the effectiveness and accuracy of our model.

(a)   (b)

(c)   (d)
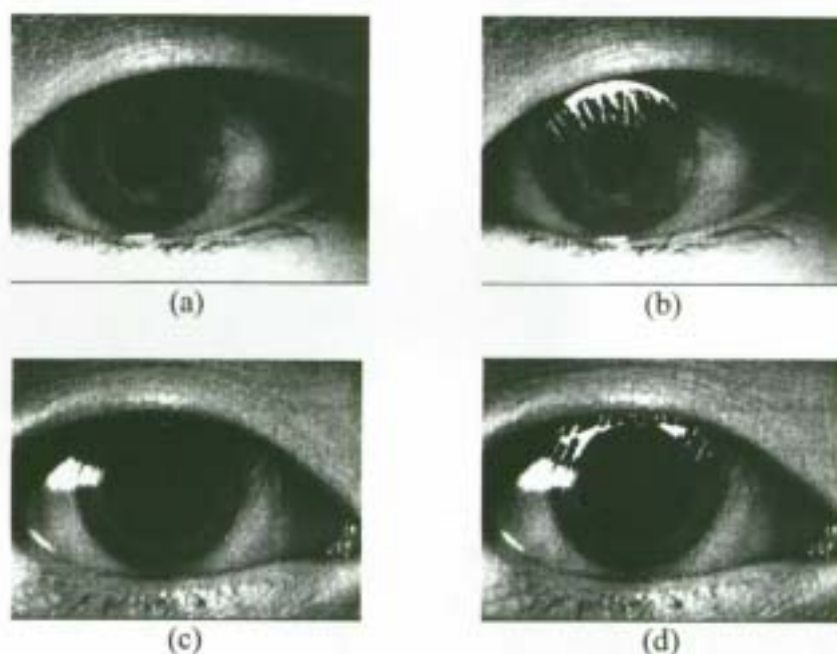
Fig. 3.10 Different segmentation results from the traditional model with and without the proposed model. (a) and (c) are the results using the traditional model, (b) and (d) are the results using the proposed model.

3.10.1 Identification Test

The purpose of this test is to investigate the effect of the proposed model to iris recognition. Boles' recognition engine can be modified to test our model. His approach assumes that the eyelids do not cover the iris so his approach can use the periodic property of the iris. However,

this assumption does not always hold and the size of the images in Boles' database is different from that of our images. Therefore, some parameters in his approaches should be adjusted. The functions of each part are briefly described as follows:

3.10.1.1 Modified Boles' Approach

1) Segmentation

Firstly, the traditional model, which detects the boundaries of the pupil, limbus, upper and lower eyelids, is applied to the input image. The second step is to recognize the eyelashes and reflection by the proposed method. The computational details have been discussed in the previous sections.

2) Normalization

There are two functions in this part. One is to select the region of an iris which will be utilized for feature extraction in the next section. This region is decomposed into eight rings and each ring is normalized to a standard size. Fig. 3.11 demonstrates the region and rings that are separated by the white circles. The centers and radii are obtained by linear interpolation of the centers and radii of the pupil and limbus. Mathematically, they can be described by,

$$x_j = x_0 + j\frac{x_8 - x_0}{8}, \tag{3-14}$$

$$y_j = y_0 + j\frac{y_8 - y_0}{8}, \tag{3-15}$$

$$r_j = r_0 + j\frac{r_8 - r_0}{8}, \tag{3-16}$$

where $j=1$ $2,..$, 7 and $(x_j,\ y_j)$ and r_j are the center and radius of the white circles, respectively. The outmost and inmost circles are the limbus $(x_8,\ y_8,\ r_8)$ and the pupil $(x_0,\ y_0,\ r_0)$, respectively, and are obtained from the previous section. Then each ring is normalized to a 1-D signal with a fixed length. Fig. 3.12 illustrates the four 1-D signals, which are generated by the first four inmost rings from Fig. 3.11
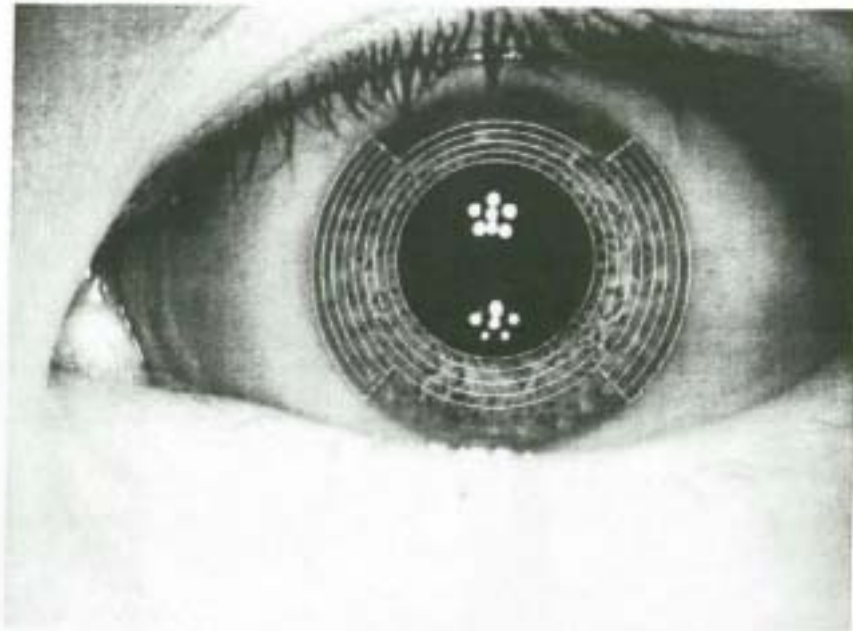
Fig 3.11 Demonstration of the region for feature extraction in the test method

and the corresponding rings
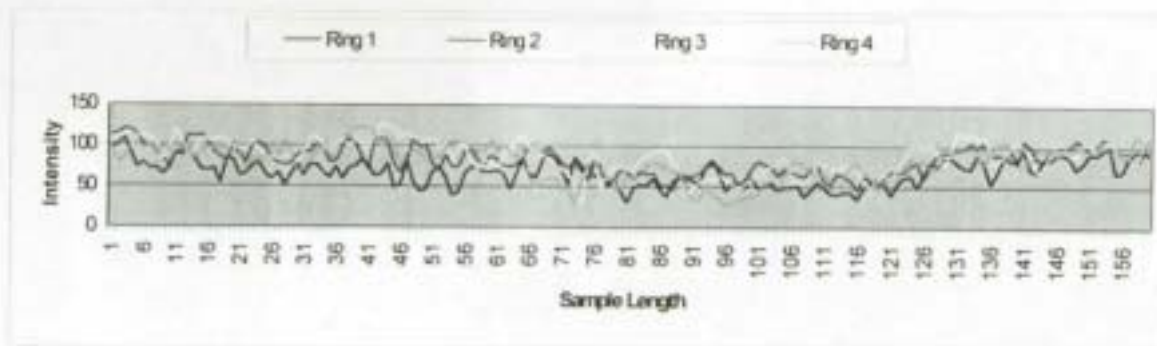
Fig 3.12 Illustration of the four 1-D signals that are generated by the four inmost rings

in Fig 3.11

3)   Wavelet-based feature extraction

Same as Boles' approaches, 1-D wavelet is applied to each ring. Four different wavelets with different parameters are implemented on the normalized 1-D signals. However, we cannot use the circular property of the iris so we do not apply circular convolution to the wavelet transformation.

4)   Matching

The matching process relies on a vector norm. Let the p_j and q_j be tha sets of normalized 1-D signals from the two irises, where $j=1,2, \ldots. 8$ represent different rings in the irises. The $w_k(p_j, n)$ denotes a function value of a wavelet transform at the ring j in the iris p at the level k in the position n. Each normalized 1-D signals associates with a mask M_{pj} which is generated by the two different segmentation models discussed in the previous sections. In the traditional iris segmentation model, the mask only denotes the eyelids. In the proposed segmentation technique, the mask points out the areas of the eyelids, eyelashes and reflection. The matching score of two irises at level k is computed by,

$$S(p,q,k) = \sum_{j=1}^{8} \frac{\displaystyle\sum_{n \in M_{pj} \cup M_{qj}} \left| w_k(p_j,n) - w_k(q_j,n) \right|}{\displaystyle\sum_{n \in Mpj \cup Mqj} 1}. \qquad (3\text{-}17)$$

In order to provide rotational invariant matching, the above matching equation is improved to be,

$$D(p,q,k) = \min_{|m|<4} \sum_{j=1}^{8} \frac{\displaystyle\sum_{n \in M_{pj} \,\&\, m+n \in M_{qj}} \left| w_k(p_j,n) - w_k(q_j,n+m) \right|}{\displaystyle\sum_{n \in M_{pj} \,\&\, m+n \in M_{qj}} 1}. \qquad (3\text{-}18)$$

3.10.1.2   Experimental Results

Our testing database has 238 images from 48 persons. All the irises are lighted up by infrared light and captured by a CCD camera. Fig. 3.13 shows eight iris images in our database. In the experiment, four different wavelets, Haar, Gabor, Shannon and Mexican hat, are tested. This has been discussed in Chapter 2. Gabor and Mexican hat wavelets are tested under 3 and 6 sets of parameters, respectively. All the wavelets and their parameters are mentioned in Table 3.1. The equal error rates of different wavelets at different levels prove the usefulness of the proposed segmentation model, as shown in Table 3. The numbers in the brackets are the

percentages of improvements in terms of equal error rates using our method. The equal error rates using our proposed segmentation technique are smaller than or equal to the corresponding equal error rates without using our model. Some wavelets at some levels are not sensitive to eyelashes and reflection; however, they only provide relative low recognition rates. For example, the smallest equal rate that was not improved by the proposed model is 21%. The best equal error rate is 11%, which also obtains the greatest improvement (3% equal error rate) using our method.

For comparing the wavelets, we list the best equal error rates in Table 3.3. From this table, we can see that Shannon wavelet was not improved by our segmentation technique and different levels do not affect the recognition results. Besides, all the best recognition results appear in Level 3 or 4, which conform to Boles' research result. In addition, except Shannon, all the best results reply on our model. The imaginery part of Gabor wavelets provide the best result, at 11% equal error rate; however, it is still far away from Daugman's result.

3.11 Conclusions

A new eyelash and reflection detection model has been developed and reported in this chapter. Three conditions, separable eyelash, non-informative condition and connective condition provide accurate iris segmentation. A number of images are selected to evaluate the accuracy segmentation model and the results are encouraging. Based on the modified Boles' recognition engine using several wavelets with different parameters, the usefulness of our segmentation technique is ascertained and our proposed model can reduce equal error rate by 3%.
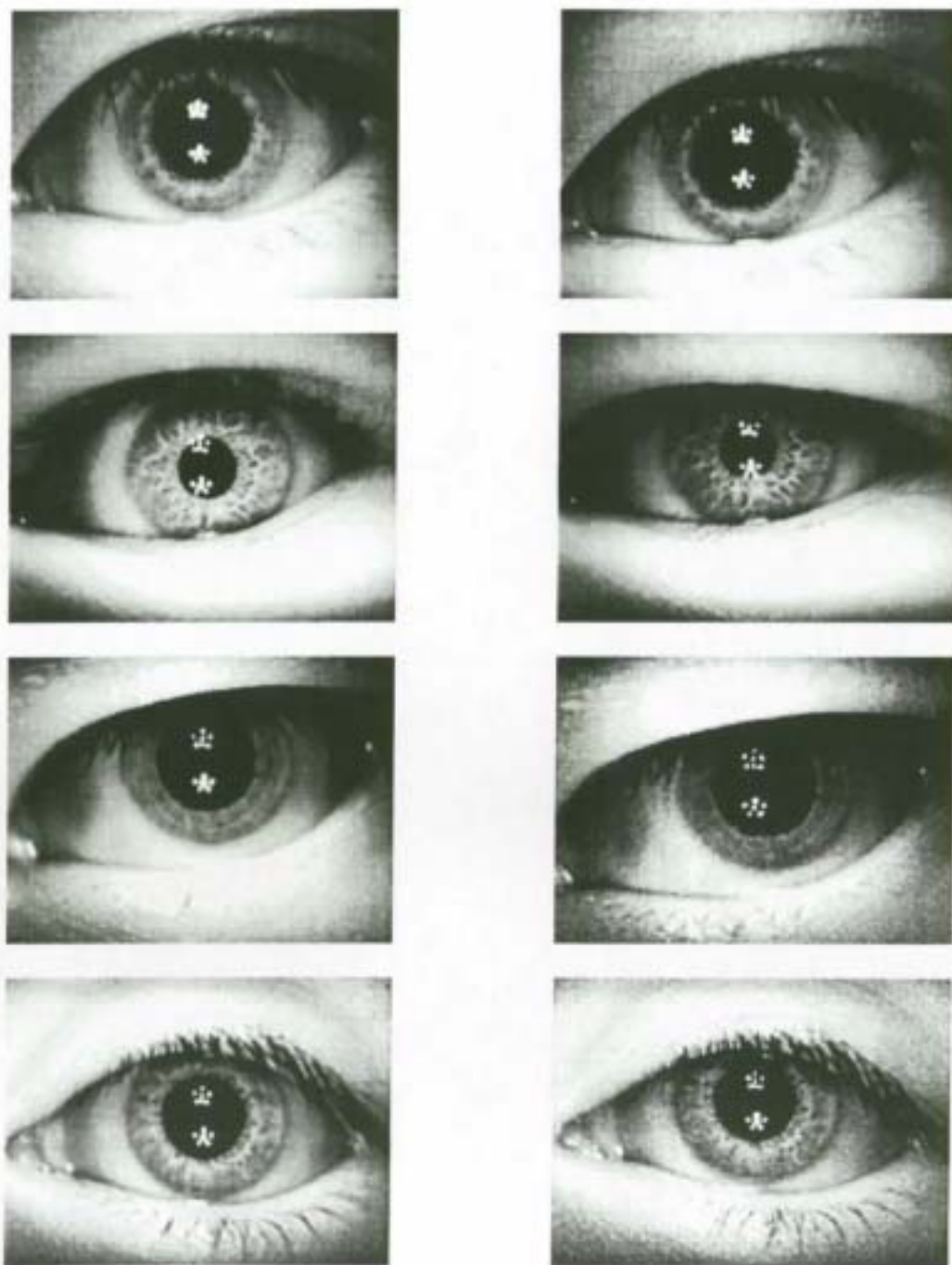
Fig 3.14 Eight typical iris images from
four persons in our iris database.

Table 3.1 Different wavelets and parameters used in the identification test

Symbol	Wavelets	Parameters
w_{M1}	Mexican Hat	$w_M(x, 0.2)$, $\sigma=0.2$
w_{M2}	Mexican Hat	$w_M(x, 0.3)$, $\sigma=0.3$
w_{M3}	Mexican Hat	$w_M(x, 0.4)$, $\sigma=0.4$
w_{M4}	Mexican Hat	$w_M(x, 0.75)$, $\sigma=0.75$
w_{M5}	Mexican Hat	$w_M(x, 2)$, $\sigma=2.0$
w_h	Haar Wavelet	$w_h(x)$
w_s	Shannon	$w_s(x)$
w_{g1}	Gabor	$w_g(x, 0.3512, 1.4663)$, $\sigma=0.3512$, $\eta=1.4663$
w_{g2}	Gabor	$w_g(x, 0.7023, 0.7332)$, $\sigma=0.7023$, $\eta=0.7332$
w_{g3}	Gabor	$w_g(x, 1.4046, 0.3666)$, $\sigma=1.4046$, $\eta=0.3666$

Table 3.2 The equal error rates are generated from wavelets at different levels. Each wavelet at one certain level produces two equal error rates. One imposes our proposed model and one does not. The numbers in the brackets are the percentages of improvement in equal error rates using our method

Wavelets	Equal Error Rate (%)							
	Level 1		Level 2		Level 3		Level 4	
	Without Using our Model	Using Our Model	Without Using our Model	Using Our Model	Without Using our Model	Using Our Model	Without Using our Model	Using Our Model
w_{M1}	23	23 (0)	22	22 (0)	30	29 (1)	21	19 (2)
w_{M2}	23	23 (0)	31	31 (0)	24	22 (2)	16	13 (3)
w_{M3}	22	22 (0)	30	29 (1)	21	19 (2)	18	16 (2)
w_{M4}	31	30 (1)	22	20 (2)	16	14 (2)	24	24 (0)
w_{M5}	18	16 (2)	21	21 (0)	24	24 (0)	24	24 (0)
w_h	28	27 (1)	21	21 (0)	19	18 (1)	15	12 (3)
w_s	23	23 (0)	23	23 (0)	23	23 (0)	23	23 (0)
$Re(w_{g1})$	23	23 (0)	23	23 (0)	36	34 (2)	24	23 (1)
$Re(w_{g2})$	23	23 (0)	36	34 (2)	24	23 (1)	18	16 (2)
$Re(w_{g3})$	36	34 (2)	24	23 (1)	18	16 (2)	23	23 (0)
$Im(w_{g1})$	21	20 (1)	21	20 (1)	35	34 (1)	26	24 (2)
$Im(w_{g2})$	21	20 (1)	35	34 (1)	26	24 (2)	14	11 (3)
$Im(w_{g3})$	35	34 (1)	26	24 (2)	14	11 (3)	13	11 (2)

Table 3.3 Summary the best results from different wavelets and levels

Wavelets	Levels	Equal Error Rates (%)	Improvement (%)
w_{Ml}	4	13	3
w_h	4	13	3
w_s	1,2,3,4	23	0,0,0,0
$Re(w_{g2})$, $Re(w_{g3})$	4,3	16	2,2
$Im(w_{g2})$, $Im(w_{g3})$, $Im(w_{g3})$	4,3,4	11	3,3,2

Chapter 4

Palmprint Feature Extraction Using a 2-D Gabor Filter

Objective — A branch of biometric technology, palmprint recognition, whereby the lines and points can be extracted from our palms for personal identification has been proposed several years ago. In this chapter, we develop a novel textured feature extraction technique for palmprint identification — a 2-D Gabor filter is used to obtain the texture information and two palmprint images are compared in terms of their hamming distance. The experimental results show that our method is effective and comparable with fingerprint (FingerCode), iris (IrisCode) and 3-D hand geometry.

4.1   Introduction

Computer-based personal identification, also known as biometric computing, which to recognize a person by his/her body or behavioral characteristics, has more than 30 years of history. The first commercial system called *Identimat*, which measured the shape of the hand and the length of fingers, was developed in the 1970s. At the same time, fingerprint-based automatic checking systems were widely used in law enforcement. Because of the rapid development of hardware, including computation speed and capture devices, iris, retina, face, voice, signature and DNA have joined the biometrics family [2-3].

Fingerprint identification has drawn considerable attention over the last 25 years. However, some people do not have clear fingerprint because of physical work or problematic

skin. Iris and retina recognition can provide a very high accuracy but suffer from high costs of input devices or intrusion into users. Recently, many researchers focus on face and voice identification systems; nevertheless, their performance is still far from satisfaction [26]. The accuracy and uniqueness of 3-D hand geometry are still open questions [2, 102, 26]. Compared with other physical characteristics, palmprint has several advantages: 1) low-resolution imaging; 2) low cost capture device; 3) low intrusiveness; 4) stable line feature and 5) high user acceptance.

Palmprint identification can be divided into two categories, off-line and on-line. For off-line identification, all palmprint samples are inked, which are then transmitted into a computer with a scanner. For on-line identification, the samples are captured with a palmprint scanner which directly connects to a computer. Off-line palmprint recognition was the main focus in past palmprint researches [3, 62-63]. Recently, a CCD camera-based palmprint capture device has been developed [3]. Fig. 4.1 shows an image captured with the device. Real-time applications of this on-line palmprint recognition device are possible. Because of the relative high-resolution of off-line palmprint image (400 dpi), some techniques applied to fingerprint recognition can be used for the off-line palmprint recognition, where lines, datum points and singular points are extracted [62-63]. In this chapter, we use low-resolution on-line images (65 dpi), so we attempt a new approach to extract texture features from palmprint images.
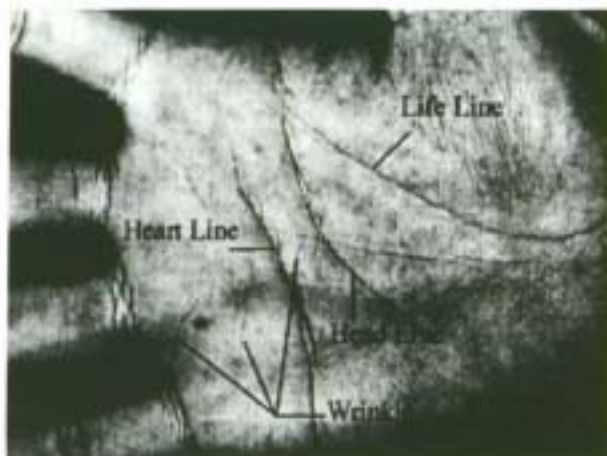
Fig. 4.1 A palmprint image with line definition.

An on-line palmprint identification system can be examined under the five functions area summarized below:

1) Image Acquisition — Capture a palmprint by a palmprint scanner [3].

2) Preprocessing — Determine a coordinate system and extract the central part of the palmprint image.

3) Feature Extraction — Extract some stable and unique features.

4) Pattern Matching — Decide whether two palmprints belong to the same person.

5) Data Storage — Store the features from the registered images for later comparisons.

This chapter is organized as follows: a preprocessing part is mentioned in Section 4.2. Palmprint feature extraction by texture analysis is explained in Section 4.3. Section 4.4 discusses Gabor filters selection and parameter tests. Experimental results and the analysis of our palmprint feature (PalmCode) are given in Section 4.5 and Section 4.6, respectively. In Section 4.7, we compare the proposed PalmCode with other biometrics, including off-line palmprint, on-line palmprint, iris, fingerprint and other hand-based biometrics. Finally, our conclusions are given in Section 4.8.

4.2. Palmprint Image Preprocessing

The goal of preprocessing is to obtain a sub-palmprint image for feature extraction and to eliminate the variation caused by rotation and translation. This preprocessing method is improved from [107], which was proposed by W. Li and D. Zhang. In fact, the two preprocessing methods are very similar. Five main steps are given below (see Fig. 4.2):

Step 1: Apply a lowpass filter to the original image. Then, use a threshold, T_p, to convert this original image to a binary image as shown in Fig. 4.2(b). Mathematically, this transformation can be represented as

$$B(x, y)=1 \text{ if } O(x,y) * L(x,y) \geq T_p, \qquad (4\text{-}1)$$

$$B(x, y)=0 \text{ if } O(x,y) * L(x,y) < T_p, \qquad (4\text{-}2)$$

where $B(x,y)$ and $O(x,y)$ are the binary image and the original image, respectively; $L(x,y)$ is a lowpass filter such as Gaussian, and "$*$" represents an operator of convolution.

Step 2: Extract the boundaries of the holes, $(F_i x_j \; F_i y_j)$, (i=1,2,3), between fingers using a boundary tracking algorithm. The start points, $(Sx_i \; Sy_i)$, and end points, $(Ex_i \; Ey_i)$, of the holes are then marked in the process (see Fig. 4.2(c)).

Step 3: Compute the center of gravity, $(Cx_i \; Cy_i)$, of each hole with the following equations:

$$Cx_i = \frac{\sum\limits_{j=1}^{M(i)} F_i x_j}{M(i)} , \qquad (4\text{-}3)$$

$$Cy_i = \frac{\sum\limits_{j=1}^{M(i)} F_i y_j}{M(i)} , \qquad (4\text{-}4)$$

where $M(i)$ represents the number of boundary points of the hole, i. Then, construct a line that passes through $(Cx_i \; Cy_i)$ and the midpoint of $(Sx_i \; Sy_i)$ and $(Ex_i \; Ey_i)$. The line equation is defined as

$$y = x\frac{(Cy_i - My_i)}{(Cx_i - Mx_i)} + \frac{My_i Cx_i - Mx_i Cy_i}{Cx_i - Mx_i} , \qquad (4\text{-}5)$$

where $(Mx_i \; My_i)$ is the midpoint of $(Sx_i \; Sy_i)$ and $(Ex_i \; Ey_i)$. Based on these lines, three key points, $(k_1, \; k_2, \; k_3)$, can easily be detected (see Fig. 4.2(d)).

Step 4: Line up k_1 and k_3 to get the Y-axis of the palmprint coordinate system, and make a line through k_2, which is perpendicular to the Y-axis to determine the origin of the palmprint coordinate system (see Fig. 4.2(e)). This coordinate system can align different palmprint images.

Step 5: Extract a sub image with a fixed size on the basis of the coordinate system, which is located at a certain part of the palmprint for feature extraction (see Fig. 4.2(f)).
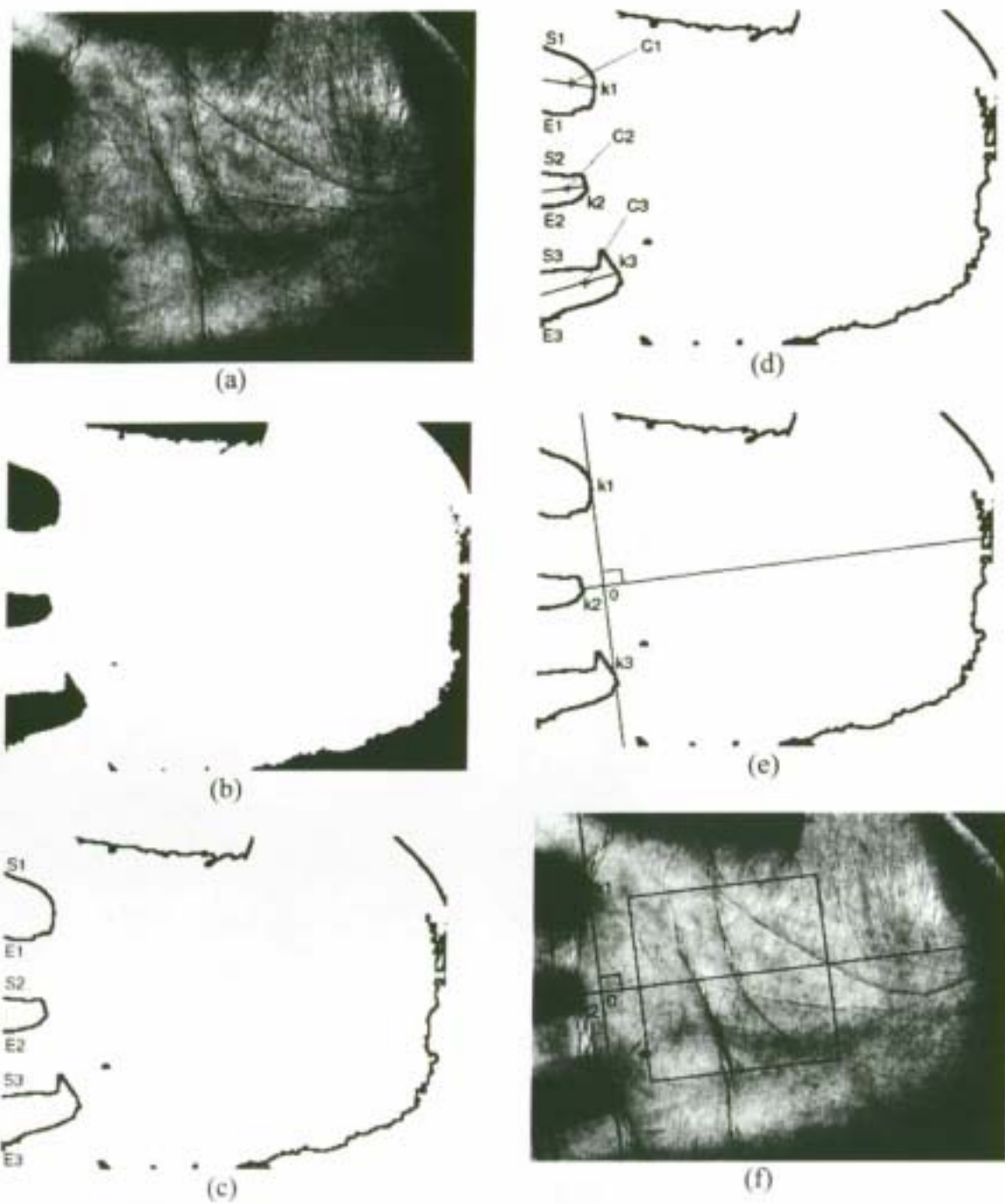
Fig. 4.2 The main steps of our preprocessing. (a) Original image, (b) Binary image,
(c) Boundary tracking, (d) Key points (k_1, k_2 and k_3) detecting,
(e) Coordinate system, and (f) Central part of a palmprint.

4.3 Palmprint Feature Extraction By Texture Analysis

This section defines our palmprint feature extraction method, which includes filtering and matching. The motivation for using a Gabor filter on our palmprint research is discussed in Chapter 2.

4.3.1 Filtering and Feature Extraction

Generally, a palmprint has some principal lines, wrinkles and ridges (see Fig. 4.1). Some algorithms such as the stack filter [107] can extract the principal lines. However, these principal lines do not contribute adequately to high accuracy because of their similarity amongst different people. Wrinkles play an important role in palmprint identification but accurately extracting them is a difficult task. This motivates us to apply texture analysis to palmprint recognition.

In fact, a Gabor function, $G(x, y, \theta, u, \sigma)$ with a special set of parameters (σ, θ, u), is transformed to a discrete Gabor filter, $G[x, y, \theta, u, \sigma]$. The parameters will be chosen from 12 sets of parameters based on an accuracy test in the next section. In order to provide more robustness to brightness, the Gabor filter is turned to zero DC with the application of the following formula:

$$\tilde{G}[x, y, \theta, u, \sigma] = G[x, y, \theta, u, \sigma] - \frac{\sum_{i=-n}^{n} \sum_{j=-n}^{n} G[i, j, \theta, u, \sigma]}{(2n+1)^2}, \qquad (4\text{-}6)$$

where $(2n+1)^2$ is the size of the filter. In fact, the imaginary part of the Gabor filter automatically has zero DC because of odd symmetry. This adjusted Gabor filter will convolute with the central part of a palmprint. Each point in the filtered image is coded to two bits, (b_r, b_i), by the following inequalities,

$$b_r = 1 \text{ if } \mathrm{Re}[\tilde{G}[x, y, \theta, u, \sigma] * I] \geq 0, \qquad (4\text{-}7)$$

$$b_r = 0 \text{ if } \mathrm{Re}[\tilde{G}[x, y, \theta, u, \sigma] * I] < 0, \qquad (4\text{-}8)$$

$$b_i = 1 \text{ if } \mathrm{Im}[\tilde{G}[x, y, \theta, u, \sigma] * I] \geq 0, \qquad (4\text{-}9)$$

$$b_i = 0 \text{ if } \mathrm{Im}[\tilde{G}[x, y, \theta, u, \sigma] * I] < 0, \qquad (4\text{-}10)$$

where I is the central part of a palmprint. Using this coding method, only the phase information in palmprint images is stored in the feature vector.

4.3.2 Palmprint Matching

In order to describe clearly the matching process, each feature vector is considered as two 2-D feature matrixes, real and imaginary. Palmprint matching is based on a normalized hamming distance. Let P and Q be two palmprint feature matrixes. The normalized hamming distance can be described as,

$$D_o = \frac{\sum_{i=1}^{N}\sum_{j=1}^{N}\left(P_R(i,j)\otimes Q_R(i,j) + P_I(i,j)\otimes Q_I(i,j)\right)}{2N^2}, \qquad (4\text{-}11)$$

where $P_R(Q_R)$ and $P_I(Q_I)$ are the real part and the imaginary part of P (Q), respectively; the Boolean operator, "$\otimes$", is equal to zero if and only if the two bits, $P_{R(I)}(i,j)$ and $Q_{R(I)}(i,j)$ are equal and the size of the feature matrixes is $N{\times}N$. It is noted that D_o is between 1 and 0. The matching score for perfect matching is zero. In order to provide translation invariance matching, Eq. 4-12 can be improved as

$$D_{min} = \min_{|s|<S,|t|<T} \frac{\sum_{i=\max(1,1+s)}^{\min(N,N+s)}\sum_{j=\max(1,1+t)}^{\min(N,N+t)}\left(P_R(i+s,j+t)\otimes Q_R(i,j) + P_I(i+s,j+t)\otimes Q_I(i,j)\right)}{2H(s)H(t)}, \qquad (4\text{-}12)$$

where S and T control the range of horizontal and vertical translation of a feature in the matching process, respectively and,

$$H(s) = \min(N, N+s) - \max(1, 1+s). \qquad (4\text{-}13)$$

The matching score, D_{min}, can support translation matching; nevertheless, it is not a rotational invariant matching. Therefore, all registered images are rotated with some degrees. Their features will then be extracted and stored. Finally, combining the effect of preprocessing and rotated images, Eq. 4-13 can provide rotational and translation invariance matching. How to choose the degrees will rely on rotational robustness of the filter. The following sections will answer this question.

4.4   Parameter Selection and Rotational Test

The above section solely gives the architecture of the proposed method. In this section, parameter selection and rotational robustness are two main issues. Twelve filters with different parameters are selected to test their robustness. Gabor filters with these sets of

46

parameters constitute a filter band and their real parts could be applied to texture analysis [68]. The parameters of all the filters are shown in Table 4.1. For presentation convenience, Filters 1-4 are marked as Level 1; Filters 5-8 and 9-12 are noted as Level 2 and Level 3, respectively. In order to investigate the relationship between feature size and accurate rate, two sets of images will be tested. The size of the first set is defined as 128 by 128 (Database I) and the size of the second set is defined as 64 by 64 (Database II), which is resized from the first ones. The parameters, S and T, are 12 for Database I and 6 for Database II. The databases for testing contain 425 images from 95 persons. Fig. 4.3 shows nine typical images in our database with various texture features. Fig. 4.4 illustrates the real and imaginary parts of our features (PalmCode) described in Eq. 4-12. Those features are generated by the best filter, Filter 7 (will be proved in the following sub-sections) and the corresponding preprocessed images.

Table 4.1: The filter's parameters and their definitions.

Levels	No	Sizes	θ	u	σ
1	1	9 by 9	-45	0.3666	1.4045
	2	9 by 9	0	0.3666	1.4045
	3	9 by 9	45	0.3666	1.4045
	4	9 by 9	90	0.3666	1.4045
2	5	17 by 17	-45	0.1833	2.8090
	6	17 by 17	0	0.1833	2.8090
	7	17 by 17	45	0.1833	2.8090
	8	17 by 17	90	0.1833	2.8090
3	9	35 by 35	-45	0.0916	5.6179
	10	35 by 35	0	0.0916	5.6179
	11	35 by 35	45	0.0916	5.6179
	12	35 by 35	90	0.0916	5.6179
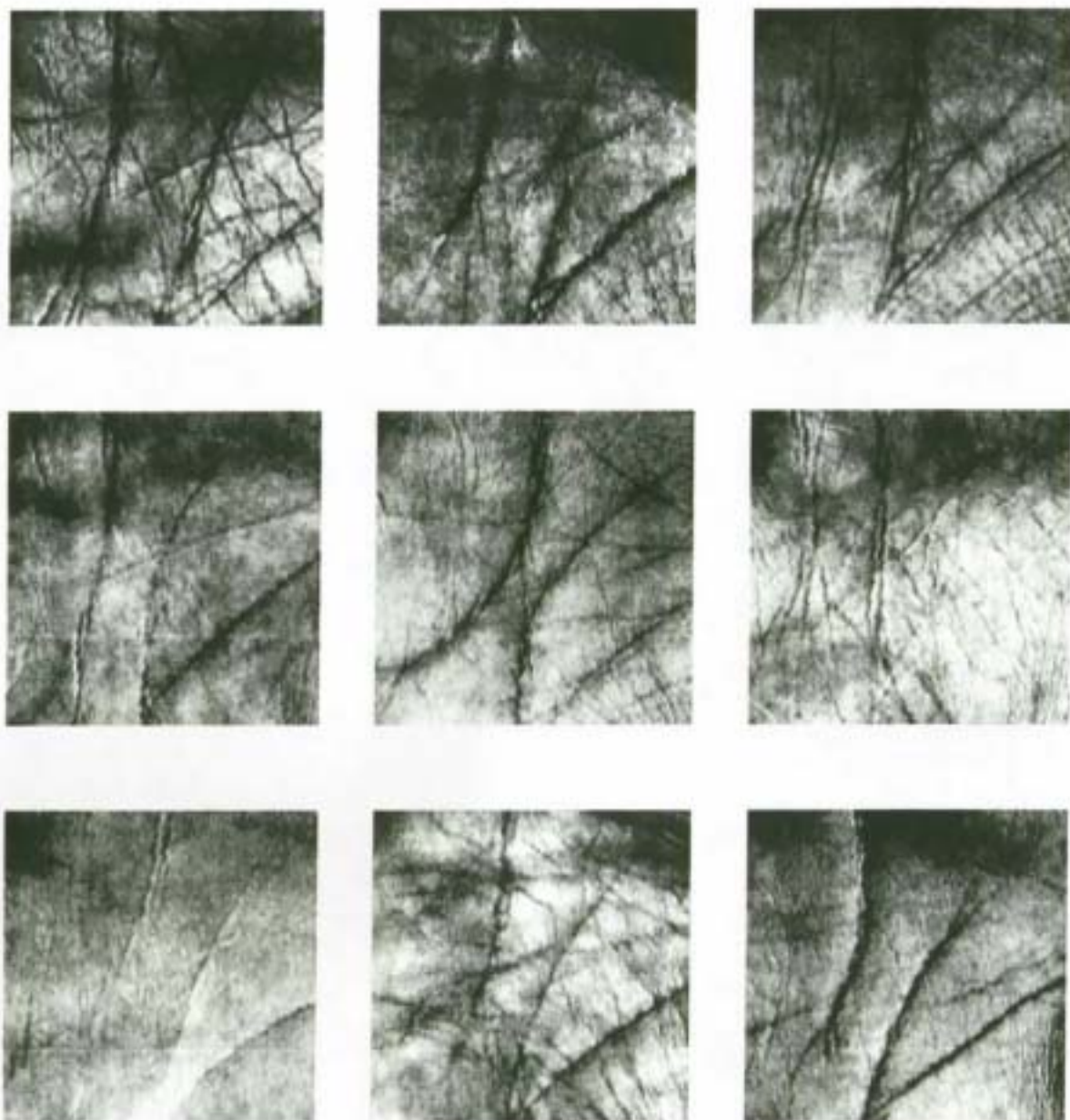
Fig. 4.3 Typical images from our databases.
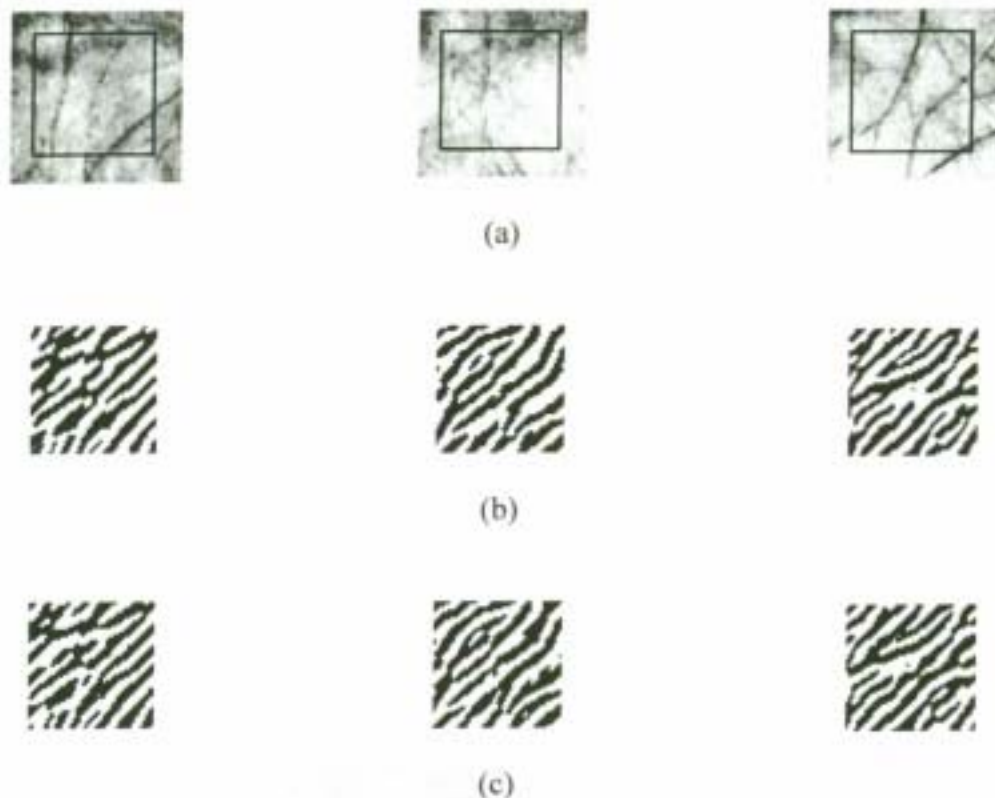
Fig. 4.4 Original images and their features captured by Filter 7 in the given rectangle. (a) Original images with the effective area, (b) Features from the real part of Filter 7 and (c) Features from the imaginary part of Filter 7.

4.4.1 Accuracy Test

We apply the twelve filters to the two databases to observe the relationship between parameters and accuracy. Each imposter distribution and genuine distribution are generated by 1,083 and 769 comparisons, respectively. When σ increases and u decreases, we can obtain several properties from Fig. 4.5, which shows the means of the imposter and genuine distributions on the two databases. The standard deviations of both imposter and genuine distributions on Databases I and II are given in Fig. 4.6. It is noted that the means of the imposter and genuine distributions decrease when σ increases and u decreases. As a result, the similarity between two palmprints increases no matter the two palmprints come from the same subject or not. According to Fig. 4.6, it is clear that the standard deviation of the

imposter distributions becomes larger. Intuitively, the number of the degree-of-freedom reduces because of the large size of the Gaussian envelope in the Gabor filter. The recognition rates of this test are shown in Table 4.2; the recognition rates using the Level 3 filters on Database I are similar to using the Level 2 filters on Database II. This is because the ratios of the length (width) of the images in Database I to σ in Level 3 filters and those in Database II to σ in Level 2 filters are the same. For Database I, in Table 4.2, the false reject rate decreases when the size of filter and σ increase. However, this statement is not true for Database II. In the optimal case, using Filter 7 on Database II, the false reject rate is 2.5% with 0% false accept rate. Different filters produce different sizes of feature, as mentioned in Table 4.3. The sizes of features are between 210 and 3,540 bytes.
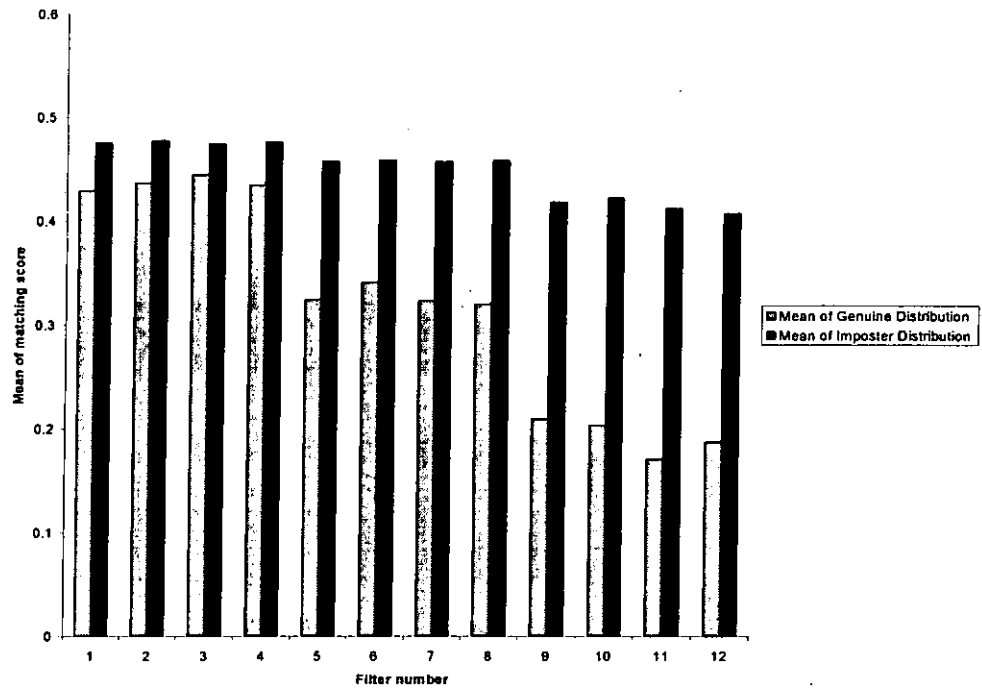
(a)
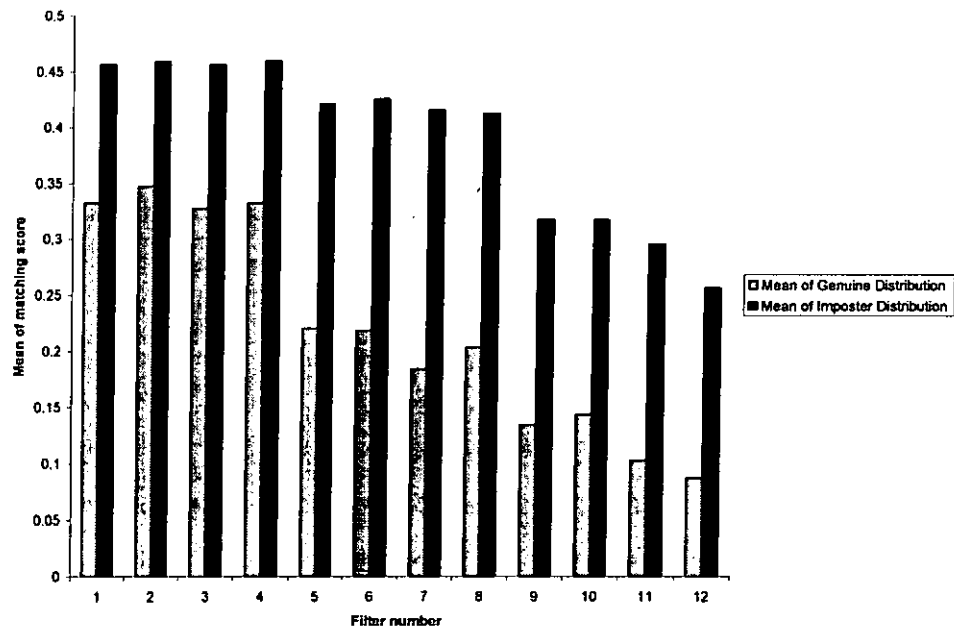
(b)

Fig. 4.5 Mean of genuine and imposter distribution generated by the filters.

(a) Results from Database I and (b) Results from Database II.
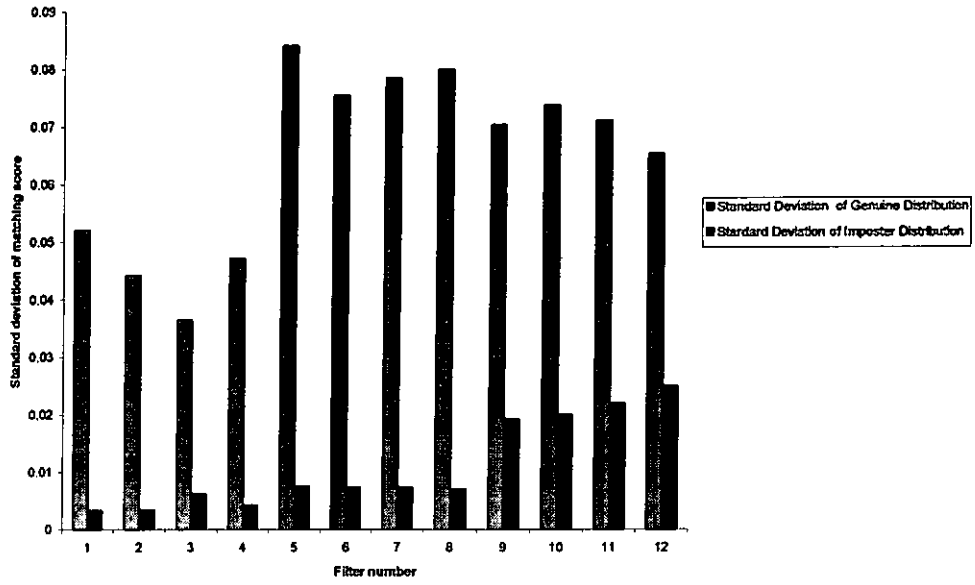
(a)
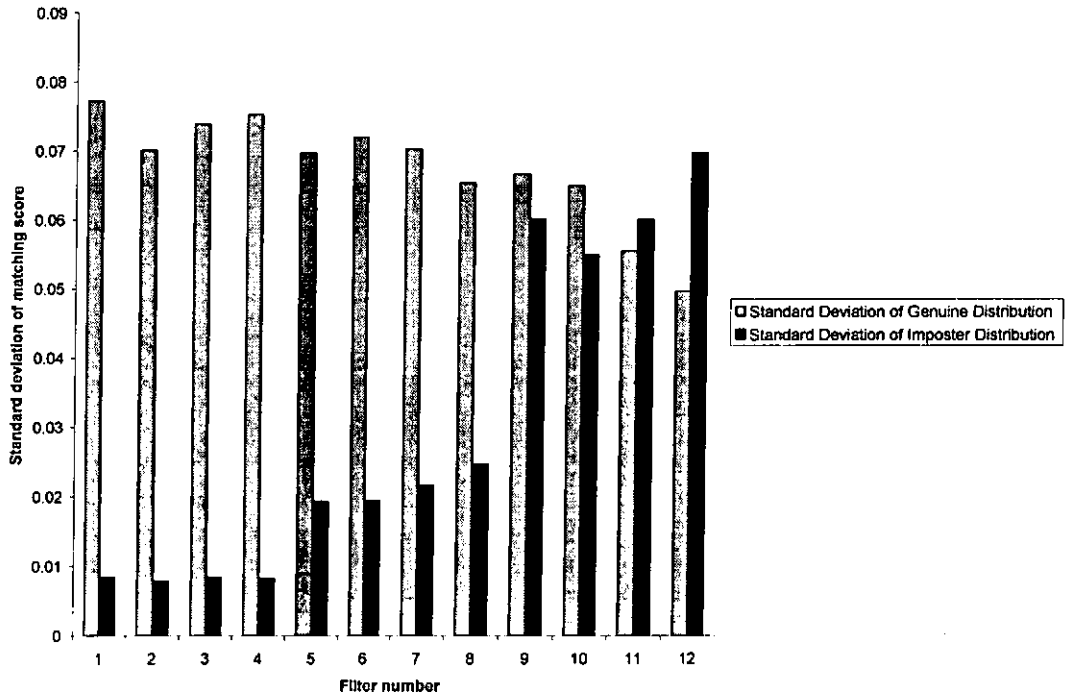
(b)

Fig. 4.6 Standard deviation of genuine and imposter distribution generated by the filters. (a) Results from Database I and (b) Results from Database II.

Table 4.2: Summary of accuracy rate for the different filters on two databases.

Filter No.	Database I		Database II	
	False accept rate (%)	False reject rate (%)	False accept rate (%)	False reject rate (%)
1	0	42.4	0	15.8
2	0	41.4	0	17.9
3	0	41.1	0	15.0
4	0	68.8	0	12.4
5	0	46.4	0	5.9
6	0	17.7	0	5.0
7	0	19.2	0	2.5
8	0	13.9	0	7.2
9	0	6.4	0	29.3
10	0	5.6	0	28.2
11	0	2.9	0	18.7
12	0	7.3	0	36.0

Table 4.3: Size of the defined features for the different filters and the databases.

Filter Level	Feature size in bytes	
	Database I	Database II
1	3540	756
2	3080	552
3	2162	210

4.4.2 Rotational Test

The rotational robustness of our method is investigated in this test. In each database, fifty images with different rotation degrees are selected and each of them will match with its original image. Same as the previous experiments, the twelve filters will be applied to the original images and the rotated images. The means of matching scores are illustrated in Fig. 4.7. Obviously, the means of matching scores increase if the degree of rotation increases. Besides, according to Fig. 4.7, a small image is more robust to rotation than a large one using the same filter. Level 3 filters are very robust to rotation for Database II; nevertheless, their recognition rates are very low.

As a summary of parameter selections and rotational tests mentioned above, Filter 7 is the best one in terms of accuracy in Database II, and it provides a certain level of robustness to rotation. On Database II, its feature size is also only 552 bytes. From the experimental results, using Filter 7 on Database II yields the best results in the experiments. Thus, we only apply Filter 7 to Database II in the following sections.
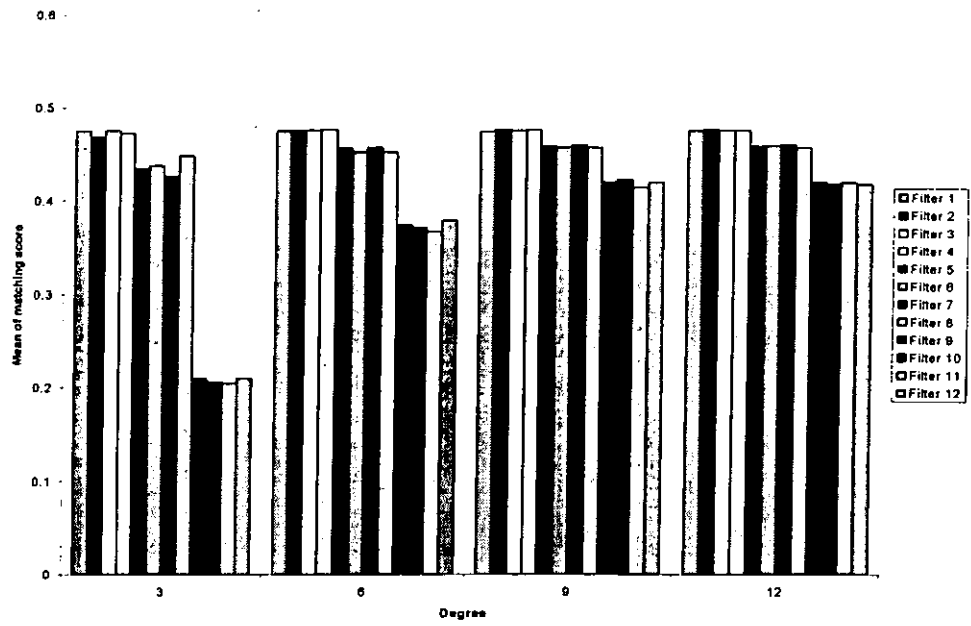
(a)
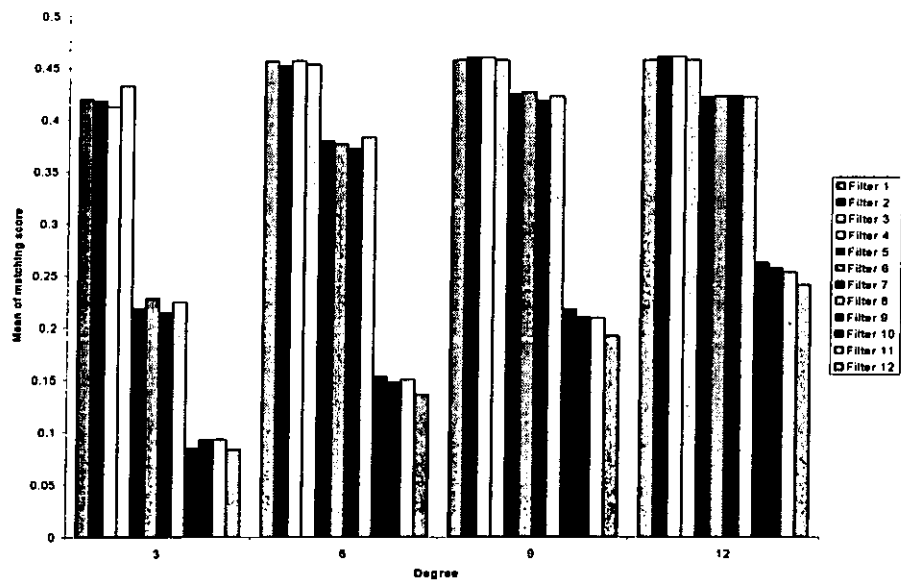
(b)

Fig. 4.7 Comparisons of rotational robustness for different filters.

(a) Mean of matching scores from Database I and

(b) Mean of matching scores from Database II.

4.5 Experimental Results

Database II is used to test the overall performance of our method. From the rotational test, we can see that Filter 7 cannot accept more than $3°$ as angular intervals because the genuine matching score would be greatly increased if it is larger than $3°$. Despite providing small genuine matching scores by smaller angular intervals, at the same time, the imposter matching score also becomes smaller and the computation time will increase for each decision. To balance all the above issues, we take $2°$ as angular intervals. Combined with assistance of hardware with preprocessing, the maximum rotational range is set between $-6°$ to $6°$ which is enough to bound all possible rotations in the central part of a palmprint. This means that all registered images are rotated with $-6°$, $-4°$, $-2°$, $0°$, $2°$, $4°$ and $6°$ degrees. At each angle, the features are extracted and stored. After combining the effect of the preprocessing with robustness of the filter, these rotated images can provide rotational invariance matching. Let Q^0 be a feature extracted from a registered image. The features from the rotated images are denoted by $Q^1, Q^2, \dots Q^6$. The whole matching process can be described by,

$$\tilde{D}_{min} = \min_{\substack{|s|<S, |t|<T, \\ n=0,1,\dots 6}} \frac{\sum_{i=\max(1,1+s)}^{\min(N,N+s)} \sum_{j=\max(1,1+t)}^{\min(N,N+t)} \left(P_R(i+s, j+t) \otimes Q_R^n(i,j) + P_I(i+s, j+t) \otimes Q_I^n(i,j) \right)}{2H(s)H(t)} \quad .(4\text{-}15)$$

Using Eq. 4-15 in the matching process, we show the distribution of imposter and genuine in Fig. 4.8(a), but Fig. 4.8(b) is generated by Eq. 4-13. In fact, Eqs. 4-13 and 4-15 are modified from Eq. 4-12. Let Eq. 4-12 be a unit of matchings. The number of matching units of Eq. 4-15 is seven times of Eq. 4-13. As a result, the distribution of imposter shifts to the left in Fig. 4.8(a). Compared with the two genuine distributions, it has almost the same shape but right tail of the genuine distribution in Fig. 4.8(a) is thinner than that of the genuine distribution in Fig. 4.8(b). It is reflected that some previous matchings have been improved. Their important statistics are summarized in Table 4.4.

Table 4.4: Comparisons of mean and standard deviation of

both imposter and genuine distributions.

Statistics	Generated by Eq. 4-13		Generated by Eq. 4-15	
	Imposter	Genuine	Imposter	Genuine
Mean	0.416	0.184	0.414	0.155
Standard deviation	0.021	0.067	0.022	0.052

The performance of the proposed method under different thresholds to control the false accept rate and false reject rate is shown in Table 4.5. When the threshold is 0.335, the false reject rate is 0.9% with 0% false accept rate. The false reject rate is 1% less than the method using Eq. 4-13 in the matching process. Some images are still not recognized by the proposed method because of the non-linear distortion.

Table 4.5: False acceptance and false reject rates with different threshold values

Threshold value	False acceptance rate (%)	False reject rate (%)
0.325	0.00	1.56
0.335	0.00	0.91
0.345	0.37	0.65
0.355	0.92	0.65
0.365	2.50	0.39
0.375	5.36	0.13
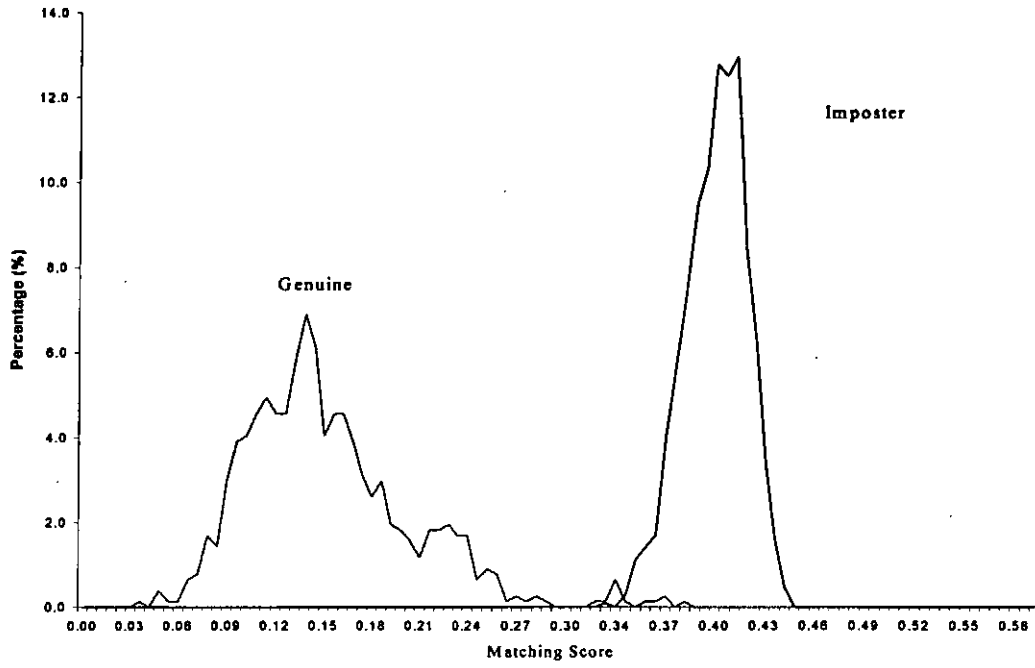
(a)
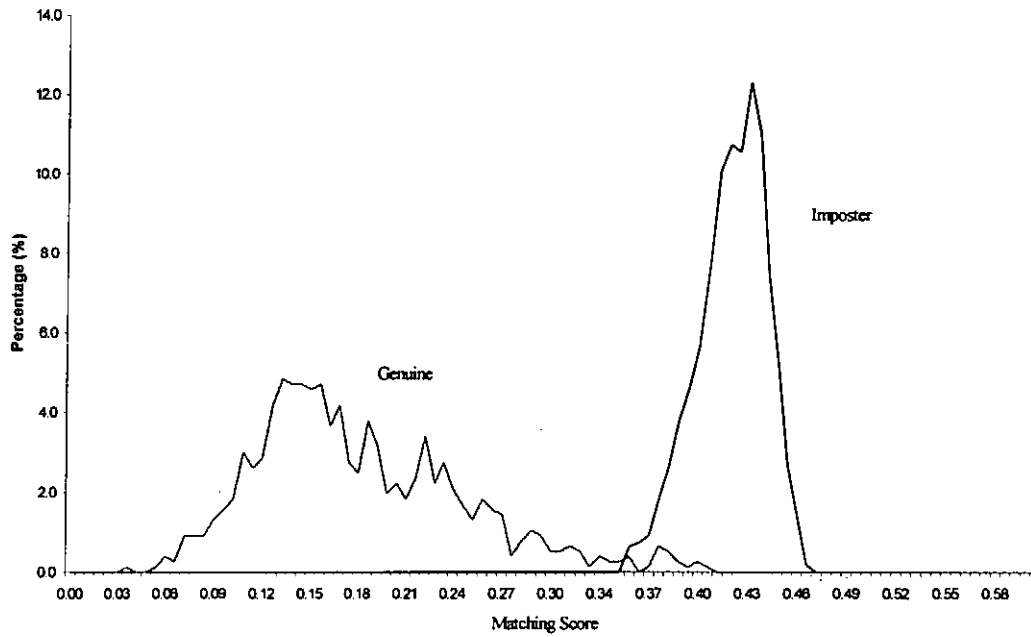
(b)

Fig. 4.8 Imposter and genuine distribution using Filter 7, (a) considering rotational problem and (b) without considering rotational problem.

4.6. A Study of Correlation, Capacity and Performance of PalmCode

In this section, we want to investigate the correlation between PalmCodes across the population, the capability and the performance of PalmCode. The capacity of PalmCodes, which can reflect the uniqueness of a PalmCode, is defined as the maximum number of palmprints a PalmCode can represent. To investigate the correlation between PalmCodes across the population, we need to study information entropy at different positions of the PalmCodes, as well as the degrees-of-freedom of the imposter and genuine to understand the statistical independence of PalmCode. Based on the degrees-of-freedom, the capability can be estimated. At the end of this section, we will evaluate the performance of PalmCode.

4.6.1 Information Entropy and Correlation across the Population

Using Shannon entropy measure [105], information in a bit of PalmCode can be computed by,

$$E_i = p_i \log(p_i) + (1 - p_i)\log(1 - p_i), \tag{4-15}$$

where p_i is the probability of its value in a bit equal to 1 at the position, i. When E_i reaches the maximum, all p_i should be equal to 0.5. Figs. 4.9(a) and (b) illustrate the p_i values of the first 100 bits of PalmCode in the real part and the imaginary part, respectively. Fig. 4.9 is generated by 95 independent PalmCodes from different persons. All the p_i's are around 0.5. It means that a bit of a code is close to the maximum information entropy. It also reflects that there is no systemic correlation across the population.
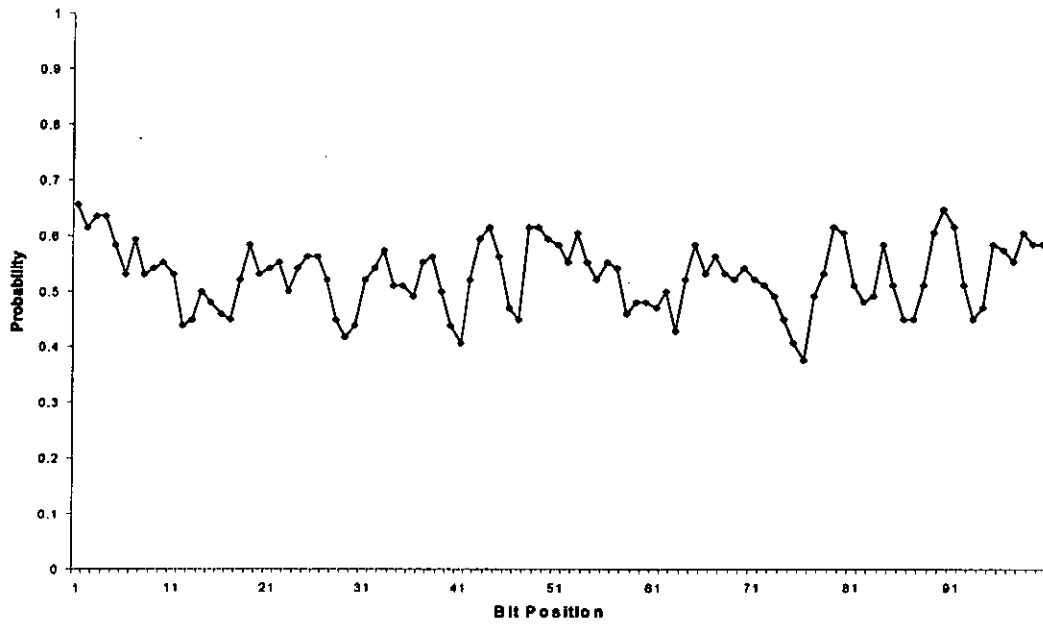
(a)
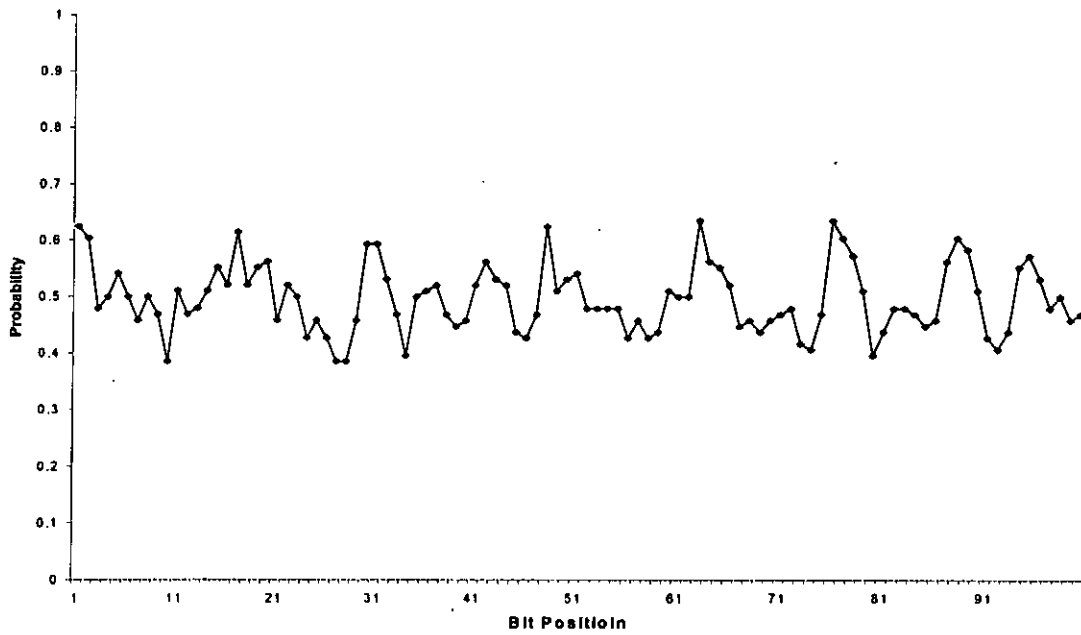
(b)

Fig. 4.9 Bit probability from (a) real part of PalmCode and

(b) imaginary part of PalmCode.

4.6.2 Statistical Independence and Capacity of PalmCodes

A palmprint can generate different PalmCodes. Also, we know that the bits in a PalmCode are not completely independent because of the intrinsic correlation from systemic line features in a palmprint. The statistical independence and capacity can be estimated by the degrees-of-freedom of a Binomial Distribution.

Each bit of PalmCode is zero or one and the bits are compared by the Boolean operator, $\otimes$, so each comparison of bit can be modeled by the Bernoulli trial. Then, the matching processing can be modeled by a Binomial Distribution [77]. A matching score and a Binomial Distribution follow,

$$s = \frac{Z}{N},$$

(4-17)

$$f(Z) = \frac{Z!}{N!(N-Z)!} p^Z (1-p)^{N-Z}.$$

(4-18)

The mean and variance of a Binomial Distribution can be described as

$$\mu = Np,$$

(4-19)

and

$$\sigma_b = \sqrt{Np(1-p)}.$$

(4-20)

Using the same database as in the previous experiments, we generate an imposter distribution which does not consider translation and rotation. Its mean and standard deviation are 0.495 and 0.039, respectively. According to the Eqs. 4-17 to 4-20, the degrees-of-freedom, N, should be 164. The empirical and theoretical distributions of the imposter are shown in Fig. 4.10. This means that the probability of completely matching two independent (from different subjects) PalmCodes is 1 over $2^{164} (\approx 2.3 \times 10^{49})$. Thus, the capacity of PalmCode is 2^{164}, which is totally enough to store all palmprints in the world. Since the theoretical distribution of the genuine part will be analyzed by understanding the performance of PalmCode in the next section, the corresponding degree-of-freedom and the probability, p, are given at the end of this sub-section. Based on Table 4.4, the mean and standard deviation of the genuine distribution are 0.155 and 0.052, respectively. Similarly, the corresponding degree-of-freedom and the probability, p, are 48 and 0.155, respectively. The empirical and theoretical distributions of the genuine part also are shown in Fig. 4.10.

4.6.3 Performance of PalmCode

Because of translation and rotation problems, PalmCodes are required to be shifted, rotated and matched. The number of matching unit in one decision depends on the accuracy of the preprocessing. Thus, analysis of the original performance of PalmCode should assume that the central part can be correctly located after the preprocessing; one matching is enough to make the final decision. Based on this assumption, the imposter and genuine distributions in Fig. 4.10 are imposed to investigate the discrimination power. Table 4.6 lists the theoretical and empirical performance of PalmCode under different thresholds. The equal error rates of the empirical and theoretical performance are 0.00% and 0.03%, respectively. The results show that our PalmCode is powerful.
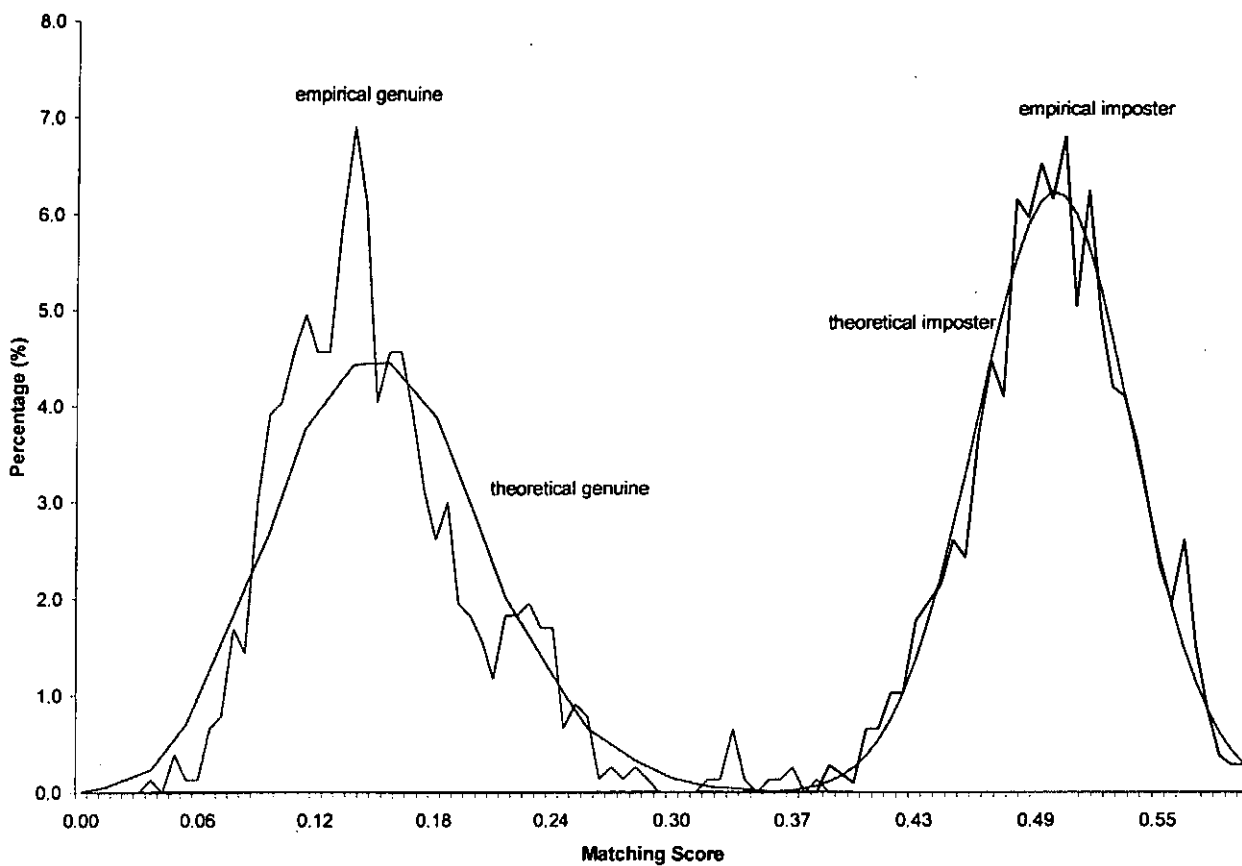
Fig. 4.10 Empirical and theoretical genuine and imposter distributions. The smooth curve on the left-hand side and the smooth curve on the right-hand side are the theoretical genuine and imposter distributions, respectively. The other two are empirical distributions. The imposter distributions do not consider rotation and translation problems.

Table 4.6: Performance of PalmCode proposed in this chapter.

Threshold	Empirical result		Theoretical result	
	False accept rate (%)	False reject rate (%)	False accept rate (%)	False reject Rate (%)
0.34	0.00	0.78	0.00	0.11
0.35	0.00	0.65	0.01	0.06
0.36	0.00	0.39	0.03	0.03
0.37	0.00	0.13	0.06	0.02
0.38	0.00	0.00	0.17	0.01
0.39	0.28	0.00	0.28	0.01
0.40	0.56	0.00	0.70	0.00

4.7 Comparisons with Other Biometrics

We will first compare our feature extraction method with off-line and on-line palmprint approaches [62, 63]. Then, similar comparisons with iris and fingerprint [29, 71] are discussed. Since hand geometry and palmprint are both hand-based biometric technology so we also give their comparisons at the end of this section.

Off-line palmprint identification uses lines as feature [62, 105-106]. This approach requires high-resolution image (compared with the proposed method), 400 by 400 pixels, for the whole palm. The proposed method only uses 64 by 64 image for the center part of a palm. Besides, the off-line approach requires a set of filters or operations to extract line and point information, but our method only imposes two filters to extract texture information. Based on the above two reasons, feature extraction using our method should be much faster than the off-line approach. The discrimination power of our texture-based method is very high because it can handle palmprint images with unclear lines (see Fig. 4.11) and similar principal lines (see Fig 4.12). Importantly, the accuracy rate of the method is higher than that of the off-line one and our method can support real-time applications.

Compare with the current on-line palmprint approach [107], which considers the local mean of amplitude in frequency domain as the feature, our proposed features extracting method can provide better recognition rate. The frequency-based approach has 5% rank one error. Although two different databases are used to test the two methods, according to current experimental results, the accuracy of our method is higher.

As a comparison, the features extracted by similar methods for the iris and fingerprint are marked as IrisCode and FingerCode, respectively. Table 4.7 summarizes their different performance. In fact, our PalmCode only requires very small image so the computation time for filtering is very short. In terms of accuracy, IrisCode is the best. However, it suffers from high costs of input devices. According to the current experimental results, PalmCode is better than FingerCode but we are still using a relative small database.

Hand and finger(s) geometry shared 26% of the biometric technology market in 1999 [27]. This sales volume is only lower than finger scan (fingerprint) but higher than iris. There are a lot of business reasons to supporting this sales volume. In terms of technology, hand and finger(s) geometry associates with low accuracy approaches [26]. High user acceptance is one of the important technical reasons why the geometry approaches shared 26% of total sales in 1999. Palmprint and the geometry approaches are hand-based biometrics and generally, all of them are not used in law enforcement. As a result, we believe that they obtain the same level of user acceptance. Several biometrics experts have commented on the uniqueness of hand geometry [102]. According to our analysis, the uniqueness of PalmCode is very high. Its capacity is enough to store all the palms in the world. For the above reasons, we think that palmprint and geometry approaches will compete with each other in the market of biometic technology.
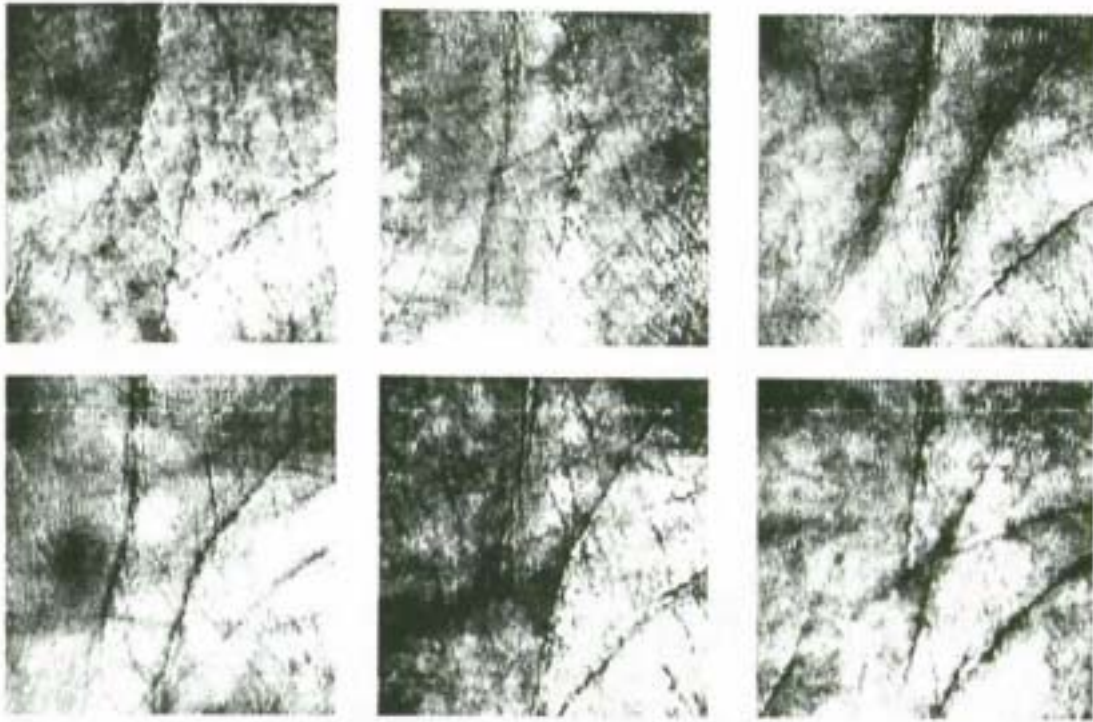
Fig. 4.11 Three typical images with unclear lines.
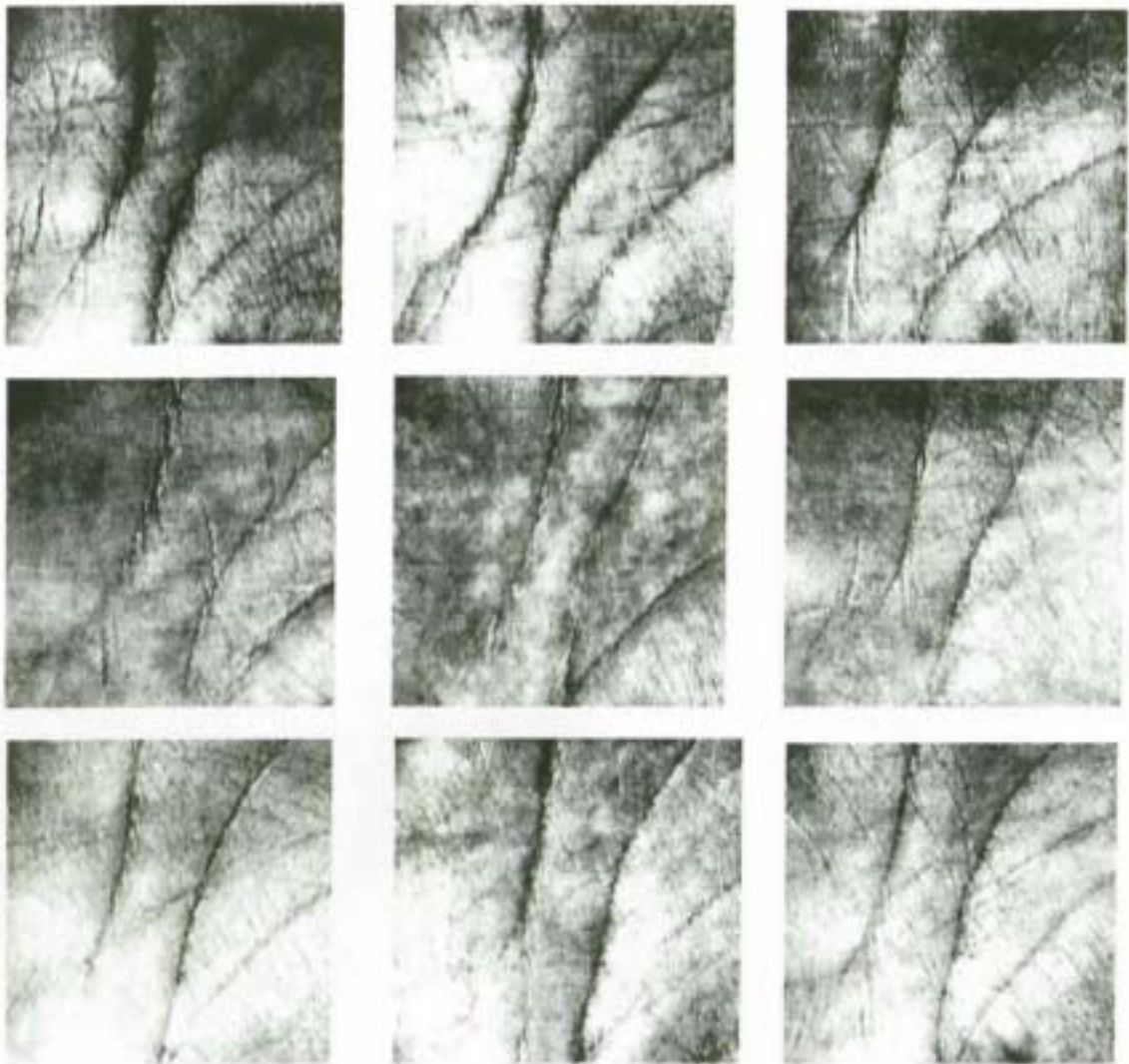
Fig. 4.12 Some palmprints with similar principal lines.

Table 4.7. Comparisons of PalmCode, IrisCode and FingerCode.

	PalmCode	IrisCode [27]	FingerCode [71]
Feature size	552 bytes	256 bytes or 512 bytes [#]	640 bytes or 896 bytes
Number of filter using for feature extraction	2 (real and imaginary)	Multiple	8
Filter size	17 by 17	Unknown	33 by 33
Feature extracted from filtered image	Phase	Phase	Average absolute deviation
Translation invariance	Yes	Yes	Yes
Rotation invariance	Yes	Yes	Approximate
Cost of input equipment	Low	High	Low
User acceptance	High	Depending on capture device	High

Originally, the size of IrisCode is 256. The current products in the market use extra 256 bytes to mark the eyelashes, reflections and boundary artifacts of hand contact lenses.

4.8 Conclusions

This chapter reports a novel feature extraction method for palmprint identification. A palmprint image is considered as a texture image, so an adjusted Gabor filter is imposed to capture the texture information. Proved by our many experiments, Filter 7 is the best one in terms of accuracy. Combined with the effects of preprocessing and rotational robustness of the filter, our matching process is translation and rotational invariance. As shown in the analysis of PalmCode, it has very large capacity, which is enough for all people in the world to be coded; and the uniqueness of PalmCodes and the palmprints is proved. In reference to current experimental results, the accuracy rate of PalmCode is higher than fingerprint using similar approaches [71]. The false reject rate for the optimal cases in our databases is 0.91% , with 0% false accept rate from our databases. Because of low-resolution imaging and easy self-positioning, a capture device at low-cost can be used to overcome the weakness of iris identification. Besides, palmprint and hand geometry approaches have the same user level of acceptance but the uniqueness of palmprint is higher than geometry approaches. In fact, we do believe that iris, fingerprint and palmprint will have different applications. However, palmprint and the geometry approaches will compete with each other.

Chapter 5.

On-Line Palmprint Identification

Objective — Using palmprint recognition as a method for personal identification is a new biometric technology. Previous palmprint researches focused on inked palmprint images; and by now, some companies have developed high-resolution palmprint scanners and identification systems. However, inked palmprint images are not suitable for general applications such as access control and ATM verification. For high-resolution palmprint images, high performance computers are needed for real-time identification. This Chapter describes the design and implementation of an on-line palmprint identification system using low-resolution palmprint images for real-time personal identification. The system consist of two parts: a capture device and recognition algorithm. A novel CCD camera-based palmprint scanner has been developed for capturing high-quality palmprint images. Also, a low-computational cost recognition algorithm is proposed. The verification accuracy is found to be comparable with high-performance automatic fingerprint verification systems. For the 1-against-100 identification accuracy, the system can operate at reasonable genuine acceptance (94%) and low false acceptance rates (0.5%). On an embedded Intel Pentium III processor (500Hz) Pc, the computation time of verification and identification of 1-against-100 are 0.6 and 1.1 seconds, respectively.

5.1. Introduction

Because of the rapid development of electronic banking and e-commerce, and for many security reasons, there has been a great demand for automatic personal identification. Traditional automatic personal identification has been divided into two categories: token-based, such as physical key, ID card, passport, and knowledge-based, such as password. Both

68

approaches have some fundamental problems. For the token-based approach, "the token" is easily stolen and lost; for the knowledge-based approach, "the knowledge" can easily be guessed or forgotten. Thus, biometric technology, identifying a person by his/her physiological characteristics such as iris pattern, retina, palmprint, fingerprint, hand geometry and face or by some aspects of behavior such as voice, signature and gesture [2-3], is an emerging technology for solving personal identification problems. Fingerprint-based personal identification has drawn considerable attention over the last 25 years. Recently, voice, face and iris-based verifications have been studied extensively. As a result, biometric systems for commercial applications have successfully been developed. Compared with other biometric technologies, work reported on palmprint identification and verification has been limited.

A palmprint has different features suitable for personal identification including principal lines, wrinkles, ridges, minutiae points, singular points and texture. Fig. 5.1 illustrates the features. Different features require different image resolutions and have different applications. For minutiae points, ridges and singular points, extracting them requires images with resolution of 400 dpi [111, 113]; for principal lines and wrinkles, they can be obtained from middle-resolution palmprint images, 100 dpi [62-63, 113]. The high-resolution images are suitable for criminal applications since ridges, singular points and minutiae points can be extracted and matched with the features in latent prints. Some companies including NEC and PRINTRAK have developed automatic palmprint identification/verification systems for criminal applications [114, 116]. For civil and commercial applications, low-resolution palmprint images are more suitable than high-resolution images because low-resolution images produce small file size, which results in short computation time for preprocessing and feature extraction and therefore, they are useful for real-time applications. In order to implement a real-time palmprint identification system on low-performance computers, we take advantages of low-resolution images to develop our system. It uses palmprint images with resolution of 75 dpi.

In the literature, an automatic palmprint identification system can be classified into two categories, off-line and on-line. An off-line palmprint identification system uses inked palmprints, which are transmitted into the computer by a digital scanner. An on-line palmprint identification system captures palmprint images by a palmprint capture sensor that is directly connected to a computer. Fig. 5.2 shows the examples of inked and an inkless images. In the past few years, the pioneers of palmprint recognition worked on off-line palmprint images and obtained many useful results. Zhang and Shu proposed to use straight lines to represent a

palmprint [62-63, 111, 113, 115]. Dute et al. and You et al. proposed to use feature points for recognition [105, 106]. You et al. also used texture as features for palmprint retrieval [106]. Chen et al. were interested in using crease for recognition and Wu et al. proposed to use stack filter for extracting the line features [104]. Recently, several researchers have started to work on on-line palmprint images, which are captured by CCD cameras or digital scanners [107, 117]. Besides, several companies, such as NEC, have developed high-resolution on-line palmprint identification/verification systems for criminal applications [114]. Our low-resolution on-line palmprint identification system is designed for civil and commercial applications such as access control. Therefore, the system is different from the current products.

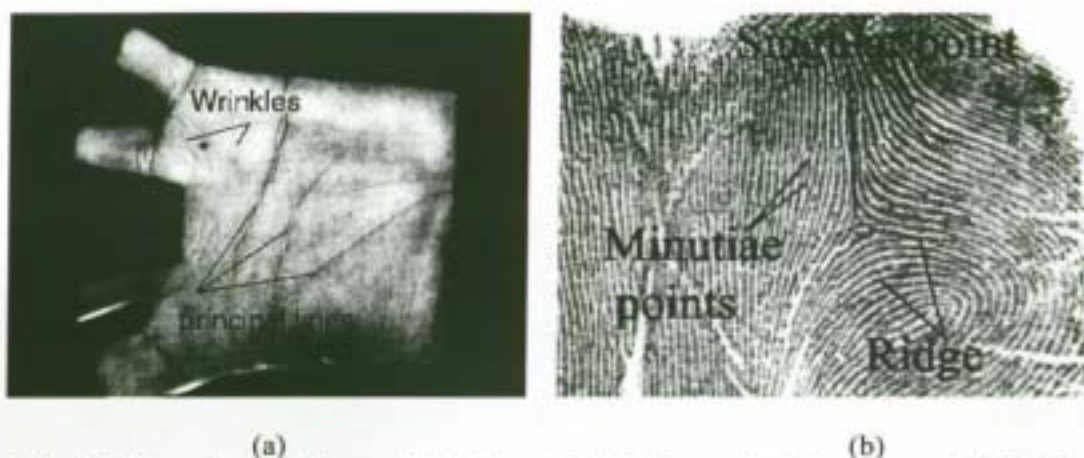(a)   (b)

Fig. 5.1 Palmprint with feature definitions. (a) Wrinkles and principal lines and (b) Ridges, minutiae points and singular points

(a)   (b)
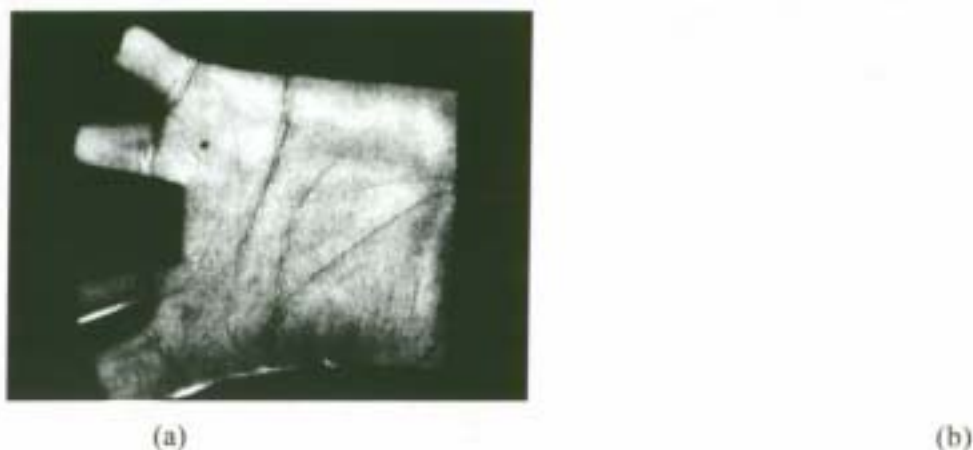
Fig. 5.2 Examples of (a) inkless and (b) inked palmprint.

An on-line palmprint identification system concerns with the following issues:

1)   Palmprint Acquisition: How to acquire a good quality palmprint image in a short time interval such as one second? What kind of devices is suitable for it?

2)   Palmprint Feature Representation: Which features in our palms are suitable for recognition? How to represent them?

3)   Palmprint Identification: How to search for a query palmprint in a given database and obtain a response in limited time?

The goal of palmprint acquisition is to obtain good quality images. Now, several companies have developed special scanners for capturing high-resolution images. Many detailed features that are useful for criminal applications, including minutiae points and singular points can be obtained [114, 116]. Recently, one research team tries to directly capture palmprint images by using a digital scanner [117]. Their capturing process is that a user puts his/her palm on a platform scanner. The hand images of 256 gray levels are acquired from the scanner. Fig. 5.3(a) shows a hand image produced by this capturing process and Fig. 5.3(b) shows the platform scanner. In fact, the platform scanner can only fulfill on-line requirement; however, this approach cannot support real-time applications since it generally takes few seconds to scan a palm. However, without using a special device for inputting a palmprint into a computer to support on-line recognition is an advance of their approach. We are interested in developing a real-time and on-line palmprint identification system; thus, we design a special CCD camera-based palmprint scanner for real-time applications. Fig. 5.4 demonstrates the outlook of our palmprint scanner and a palmprint image captured with this scanner.

(a)   (b)

Fig. 5.3 A palmprint image obtained by a platform scanner.

(a) The palmprint image and (b) a platform scanner.

(a)   (b)
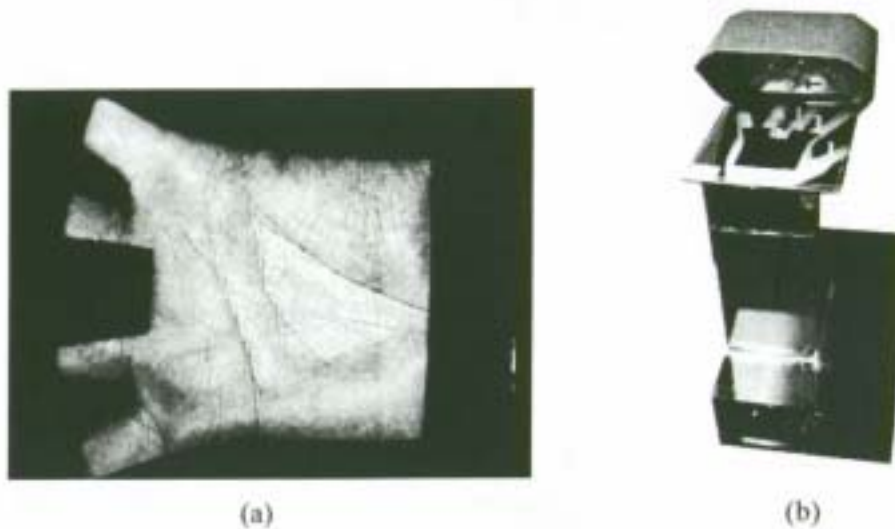
Fig. 5.4 A palmprint image obtained by our palmprint capture device

(a) the palmprint image (b) our capture device.

The goal of palmprint feature representation is to extract some features from our palm to represent a palmprint. Feature representation depends on the image resolution. For high-resolution images (400 dpi), many features can be obtained for representing a palmprint. For low-resolution images (75 dpi), some features, such as ridges, singular points and minutiae points, cannot be observed. However, we can still extract principal lines, wrinkles and texture from them. In the palmprint literature, the line features play an important role. Only, You et al. tried to use texture for coarse-level classification [106]. In fact, texture representations which can produce fixed length feature vectors for fast comparisons in, say, texture-based iris and fingerprint recognition [71, 30, 121] is an effective approach for biometric technologies [30, 71, 117-119]. We will exploit texture to represent a palmprint.

Palmprint identification is a process of matching an input palmprint against a given palmprint database to identify an individual. In fact, this process is a one against N comparison process, where N represents the number of individuals in the given database. It is much more difficult than verification, which is a one against one comparison. For identification, two critical issues must are of concern: 1) accuracy and 2) system computation time. Both issues depend on N. When N increases, generally, system accuracy decreases and computation time increases. For our palmprint identification system, we are interested in $N=50$, 100 and 200. In addition to identification, we will also give the verification accuracy of

our system for comparing with other biometric verification systems. In the palmprint recognition literature, only You et al. [106] consider identification; other researchers are interested in verification. Although You et al.'s paper and this Chapter both consider palmprint identification, their paper and this Chapter greatly differ. Firstly, their interest is in inked palmprint, but we have designed a CCD-based palmprint scanner to capture inkless palmprint for supporting on-line and real-time applications. Moreover, they use points and texture as features for recognition; but we only use texture features throughout the whole identification process.

In this Chapter, we develop an on-line palmprint identification system, whose goal is to use on-line low-resolution palmprint images for real-time personal identification. Fig. 5.5 illustrates the architecture of our on-line palmprint system. The operations of our system are described as follows:

1) *Enrollment*: Our palmprint identification system takes three palmprint images of a person for registration. They are processed by preprocessing and feature extraction modules. Finally, the features are stored as templates in a database for later comparisons.

2) *Identification*: An individual to be identified puts his/her palm on our palmprint scanner. Features are extracted from it. They are then matched against all the templates in the database.

Our on-line identification system has four main components:

1) *Palmprint Acquisition*: transmitting a palmprint to the computer by our CCD-camera-based palmprint scanner.

2) *Preprocessing*: determining a coordinate system for reducing the translational and rotational variations of palmprint image input and then dynamically extracting the central part of the palmprint on basis of the coordinate system. Our preprocessing method is modified from [107].

3) *Texture Feature Extraction*: Obtaining some texture features for recognition. We expect the feature sizes from all palmprint images to be fixed. If the feature sizes vary, matching the features would take much time, just like minutia matching in the fingerprint verification process [16].

4) *Matching*: Deciding whether two palmprints are from the same person. The matching speed is one of our concerns for deciding a classifier for doing this task since our on-line palmprint system needs to do a hundred comparisons within a second.
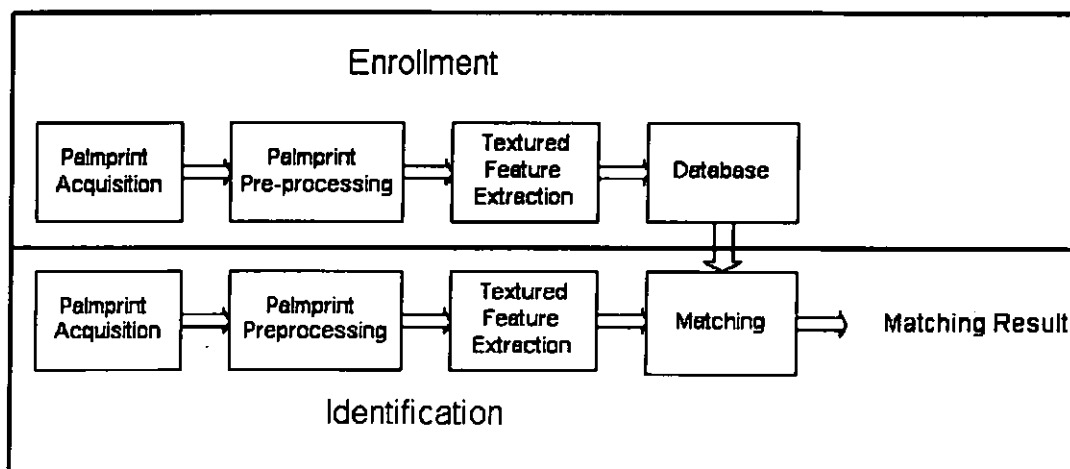
Fig. 5.5 Block diagram of our palmprint identification system.

In the following sections, we will thoroughly describe our on-line palmprint identification system. First of all, we will give the architecture of our CCD camera-based palmprint scanner in Section 5.2. Then we will present the algorithms of palmprint preprocessing, texture feature extraction and matching. Experimental results including verification and identification tests are mentioned in Section 5.3. Finally, Section 5.4 provides our conclusion and summaries.

5.2 Feature Extraction and Matching

5.2.1 Image Capture

Our CCD camera-based palmprint scanner comprises a circular light source, a CCD camera, a lens, a frame grabber, a power supply, a transformer, a platform with six pegs on it, a cover and a case. The frame grabber is connected to a computer so that the images captured by the CCD camera are directly transmitted to the computer by the frame grabber. The case and the cover form a semi-closed environment and the circular light source provides uniform lighting condition for capturing high-quality palmprint. Also, the six pegs on the platform serve as control points for placement of a user's hand. Fig. 5.4(b) has shown the outlook of our CCD camera-based palmprint scanner and Fig. 5.6 depicts the parts of the device. In fact, some

ideas of this device are inspired by the devices for capturing iris and hand images [45, 102, 120]. In the current prototype implementation, two different image sizes, 384×284 and 768×568 can be captured.

Fig. 5.6 The parts of our capture device.

5.2.2   Preprocessing

Our palmprint preprocessing approach uses the holes between fingers as the parameters to build a coordinate system for aligning different palmprint images. This preprocessing dynamically defines the central part for feature extraction. It has six main steps, which are given as follows (see Fig. 5.7):

Step 1: Apply a lowpass filter, $L(u, v)$, such as Gaussian, to an original image, $O(x, y)$. Then, a threshold, T_p, is used to convert the convoluted image to a binary image, $B(x, y)$, as shown in Fig. 5.7(b).

Step 2: Obtain the boundaries of the holes, $(F_i x_j, F_i y_j)$ ($i=1, 2$), between fingers using a boundary tracking algorithm. The boundary of the hole between ring and middle fingers is not extracted since it is not useful for the following processing (see Fig. 5.7(c)).

Step 3: Compute the tangent of the two holes. Let (x_1, y_1) and (x_2, y_2) be any points on $(F_1 x_j, F_1 y_j)$ and $(F_2 x_j, F_2 y_j)$, respectively. If the line ($y=mx+c$) passing though these two points satisfies the inequality, $F_i y_j \leq m F_i x_j + c$, for all i and j (see Fig. 5.7(d)), then the line ($y=mx+c$) is considered as the tangent of the two holes.

Step 4: Line up (x_1, y_1) and (x_2, y_2) to get the Y-axis of the palmprint coordinate system. Construct a line passing through the midpoint of the two points perpendicular to the Y-axis to determine the origin of the system (see Fig. 5.7(d)).

Step 5: Extract a sub-image with a dynamic size on the basis of the coordinate system and compute the Euclidean distance, D, between (x_1, y_1) and (x_2, y_2). The sub-image is located at a certain part of the palmprint image (see Figs. 5.7(d) and 5.7(e)).

Step 6: Normalize the sub-image to a fixed size image by using bilinear interpolation for feature extraction (see Fig. 5.7(f)).
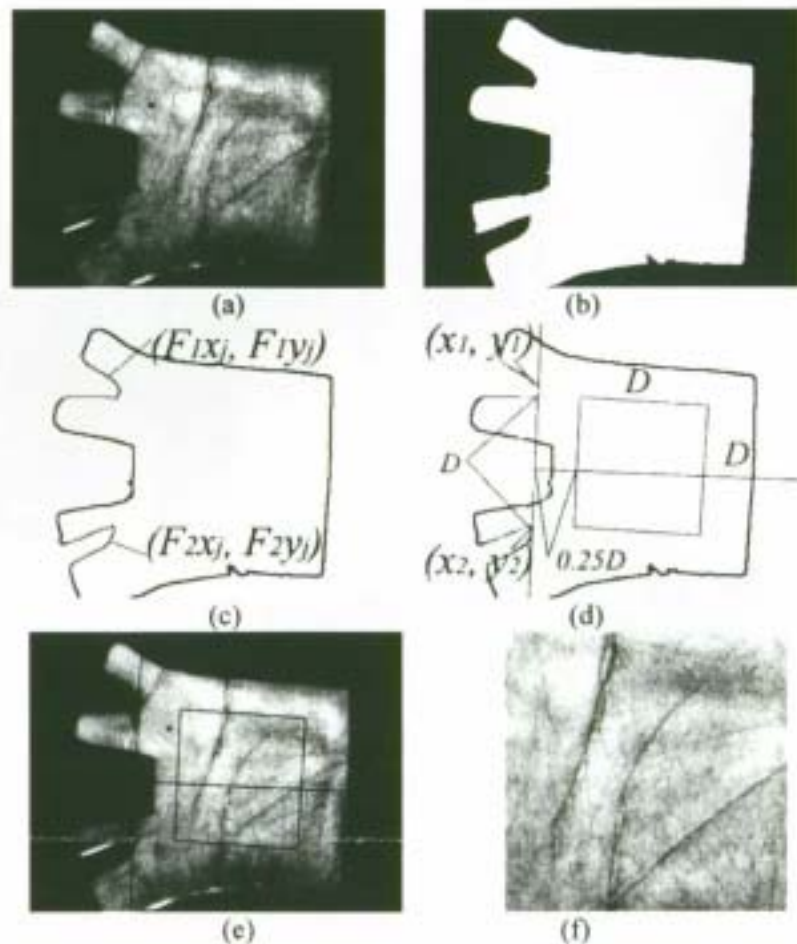
Fig. 5.7 The main steps of preprocessing. (a) Original image, (b) Binary image, (c) Boundary tracking, (d) Building a coordinate system, (e) Central part extraction and (f) Preprocessed result.

5.2.3 Texture Feature Extraction

Generally, a palmprint has some principal lines, wrinkles, singular points and minutiae. Some algorithms such as the stack filter [104] can extract the principal lines. However, these principal lines do not contribute adequately to high accuracy because of their similarity amongst different people. Fig. 5.8 shows 3 preprocessed images with similar principal lines. In our low-resolution palmprint images, singular points and minutiae cannot be observed by human vision. Thus, wrinkles play an important role in palmprint identification. However, in our low-resolution palmprint images, some images do not have clear wrinkles. Fig. 5.9 gives three palmprint images to illustrate this. Thus, it motivates us to apply texture analysis to palmprint recognition. Because of the successful application of the Gabor filter to iris recognition by Daugman [30, 121], we exploit his idea for palmprint recognition.

Fig. 5.8. Three images with the similar principal lines.

Fig. 5.9 Three preprocessed palmprint images without clear wrinkles.

The circular Gabor filter is an effective tool for texture analysis, and has the following general form:

$$G(x,y,\theta,u,\sigma) = \frac{1}{2\pi\sigma^2} \exp\left\{-\frac{x^2+y^2}{2\sigma^2}\right\} \exp\{2\pi i(ux\cos\theta + uy\sin\theta)\}, \qquad (5\text{-}1)$$

where $i = \sqrt{-1}$; u is the frequency of the sinusoidal wave; θ controls the orientation of the function and σ is the standard deviation of the Gaussian envelope. Gabor filters are widely used in texture analysis and biometrics [112-115]. 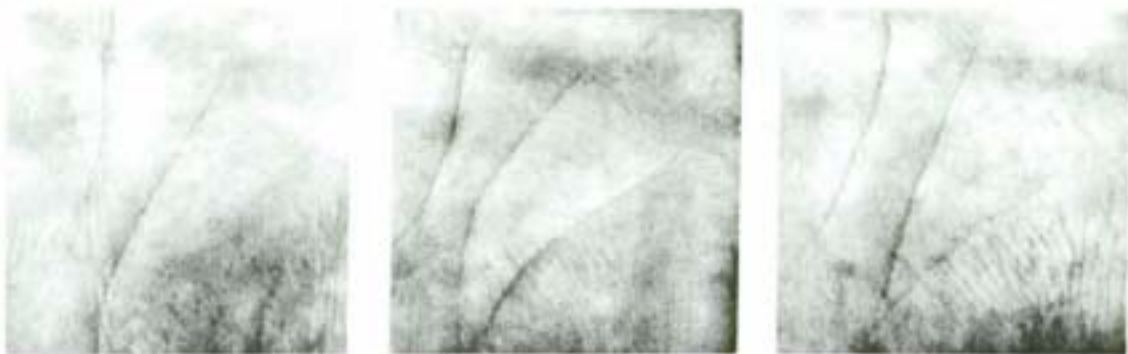In order to provide more robust to brightness, a discrete Gabor filter, $G[x,y,\theta,u,\sigma]$ is turned to zero DC with the application of the following formula:

$$\tilde{G}[x,y,\theta,u,\sigma] = G[x,y,\theta,u,\sigma] - \frac{\sum\limits_{i=-n}^{n}\sum\limits_{j=-n}^{n} G[i,j,\theta,u,\sigma]}{(2n+1)^2}, \qquad (5\text{-}2)$$

where $(2n+1)^2$ is the size of the filter. In fact, the imaginary part of the Gabor filter automatically has zero DC because of odd symmetry. The use of the adjusted Gabor filter is to filter the preprocessed images. Then, the phase information is coded by the following inequalities, which are the same as the Eqs. 14-17 in [30]:

$$b_r = 1 \quad if \quad \text{Re}\left(\sum\limits_{y=-n}^{n}\sum\limits_{x=-n}^{n}\tilde{G}[x,y,\theta,u,\sigma]I(x+x_o,y+y_o)\right) \geq 0, \qquad (5\text{-}3)$$

$$b_r = 0 \quad if \quad \text{Re}\left(\sum\limits_{y=-n}^{n}\sum\limits_{x=-n}^{n}\tilde{G}[x,y,\theta,u,\sigma]I(x+x_o,y+y_o)\right) < 0, \qquad (5\text{-}4)$$

$$b_i = 1 \quad if \quad \text{Im}\left(\sum\limits_{y=-n}^{n}\sum\limits_{x=-n}^{n}\tilde{G}[x,y,\theta,u,\sigma]I(x+x_o,y+y_o)\right) \geq 0, \qquad (5\text{-}5)$$

$$b_i = 0 \quad if \quad \text{Im}\left(\sum\limits_{y=-n}^{n}\sum\limits_{x=-n}^{n}\tilde{G}[x,y,\theta,u,\sigma]I(x+x_o,y+y_o)\right) < 0, \qquad (5\text{-}6)$$

where $I(x, y)$ is a preprocessed image and (x_o, y_o) is center of filtering.

Since some users do not place their hands correctly, the preprocessed images contain some non-palmprint pixels. Fig. 5.10 illustrates an incorrect placement of a user palm and the corresponding preprocessed image. We generate a mask to point out the location of the non-palmprint pixels. Since our palmprint scanner forms a semi-closed environment, the non-palmprint pixels come from the black boundaries of the platform. Thus, we can easily use a threshold to segment the non-palmprint pixels. The feature size including mask and palmprint features is 384 bytes. Fig. 5.11 depicts the preprocessed images, the corresponding texture features and the corresponding masks.

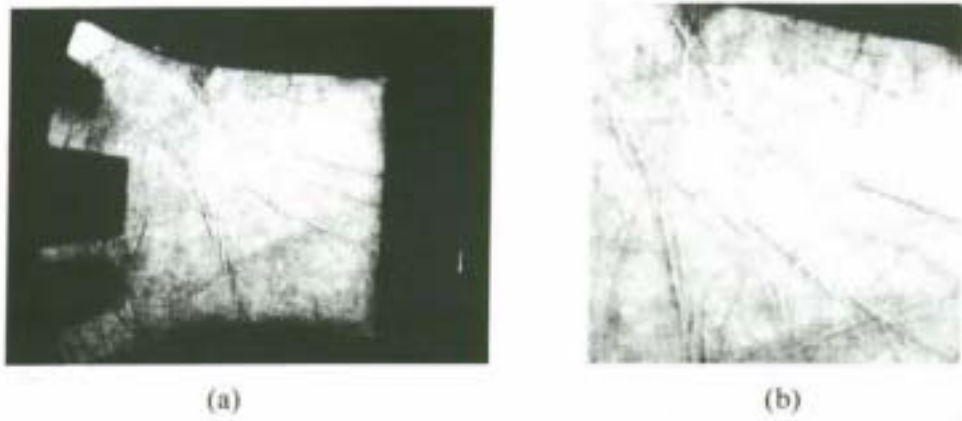(a)   (b)

Fig. 5.10 Incorrect placement of a palm and the corresponding preprocessed image
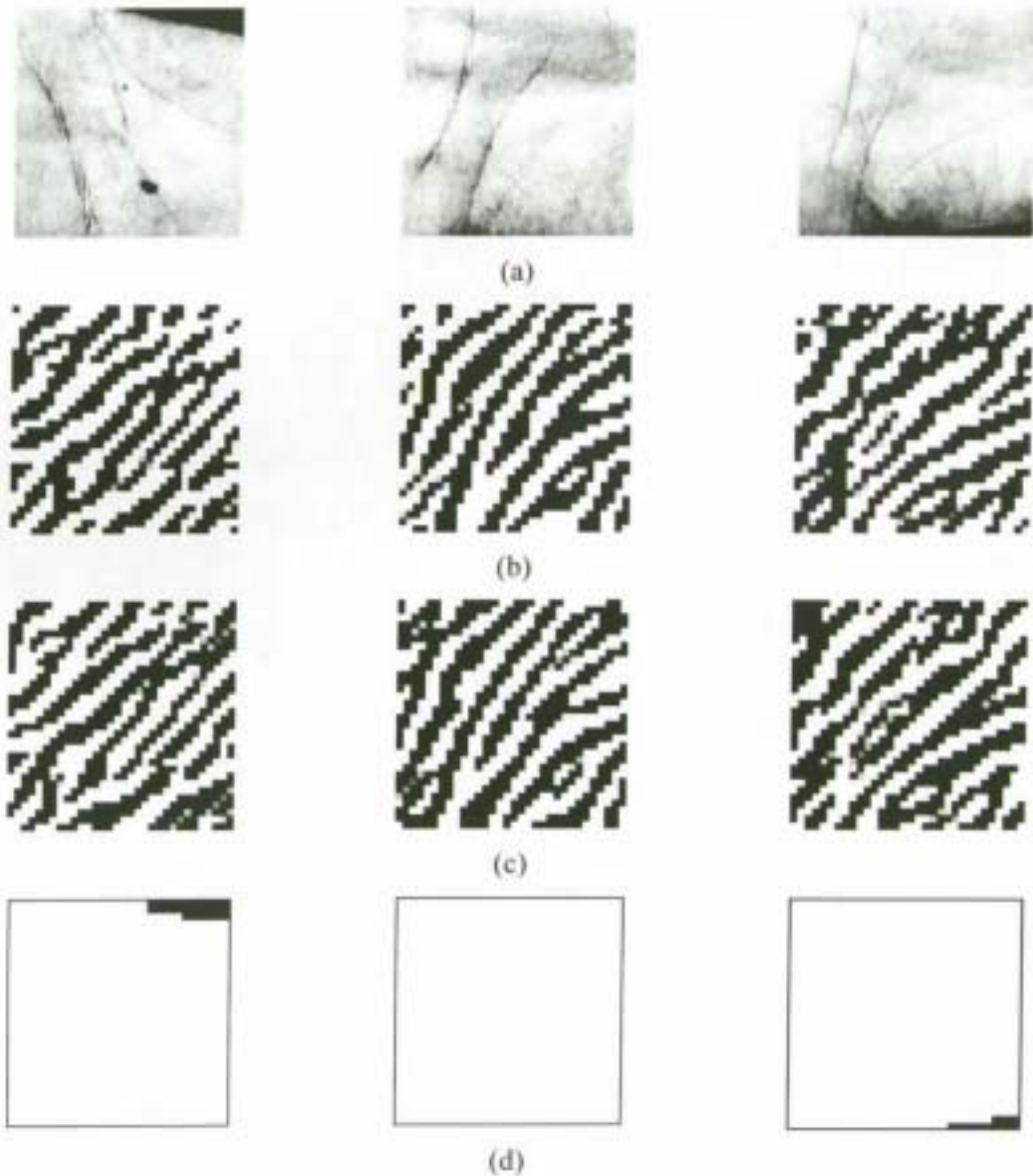

(a)

(b)

(c)

(d)

Fig. 5.11 Preprocessed images, real parts of the features, imaginary parts of the features and the masks. (a) Preprocessed images, (b) real parts of texture features, (c) imaginary parts of the texture features and (d) masks.

5.2.4 Palmprint Matching

In order to describe clearly the matching process, each feature vector will be considered as two feature matrixes, real and imaginary. Palmprint matching is based on a normalized hamming distance. Let P and Q be two palmprint feature matrixes. The normalized hamming distance can be described as,

$$D_o = \frac{\sum_{i=1}^{N}\sum_{j=1}^{N} P_M(i,j)\cap Q_M(i,j)\left((P_R(i,j)\otimes Q_R(i,j)) + P_I(i,j)\otimes Q_I(i,j))\right)}{2\sum_{i=1}^{N}\sum_{j=1}^{N} P_M(i,j)\cap Q_M(i,j)}, \qquad (5\text{-}7)$$

where $P_R (Q_R)$, $P_I (Q_I)$ and $P_M (Q_M)$ are the real part, the imaginary part and mask of P (Q), respectively; the result of Boolean operator, "$\otimes$", is equal to zero if and only if the two bits, $P_{R(I)}(i,j)$, equal to $Q_{R(I)}(i,j)$; $\cap$ represents an AND operator and the size of the feature matrixes is $N \times N$. It is noted that D_o is between 1 and 0. For perfect matching, the matching score is zero. Because of imperfect preprocessing, we need to vertically and horizontally translate one of the features and then match again. Then, the ranges of vertical and horizontal translation are –2 to 2. The minimum of D_0's obtained by translated matchings is considered as the final matching score.

5.3 Experimental Results

5.3.1 Database

We have collected palmprint images from 154 subjects using our palmprint scanner. The subjects mainly consist of students and staff of the Department of Computing, The Hong Kong Polytechnic University and their friends. All are volunteers. 99 of them are male, making up approximately 65% of all subjects. The age distribution of the subjects is shown in Table 1. We collected the palmprint images in two rounds. In each round, the subjects were asked to provide around 10 images of their left palm and 10 images of their right palm. Totally, a person provided about 40 images and our database contains 6191 palmprints of 308 different palms. The average time difference between the first and second collections is 57 days. The maximum and minimum time differences are 90 and 4 days, respectively. After finishing the first collection, we changed the light source and adjusted the focus of the CCD camera to simulate that the first and second collected images were captured by two different palmprint scanners. Fig. 5.12(a) and (b) illustrate preprocessed palmprint images captured at the first and second collections. Since palmprint recognition is new for almost all the subjects,

we provide the subjects with guidance for using the palmprint scanner. Originally, the collected images have two sizes, 384×284 and 768×568. The large images are resized to 384×284; consequently, the size of all the test images is 384×284 with 75dpi resolution.

Table 1. Age distribution of the subjects constituting our database.

Ranges of Ages	Percentage
10-20	2%
21-30	80%
31-40	12%
41-50	3%
51-60	2%
61-70	1%

(a)   (b)
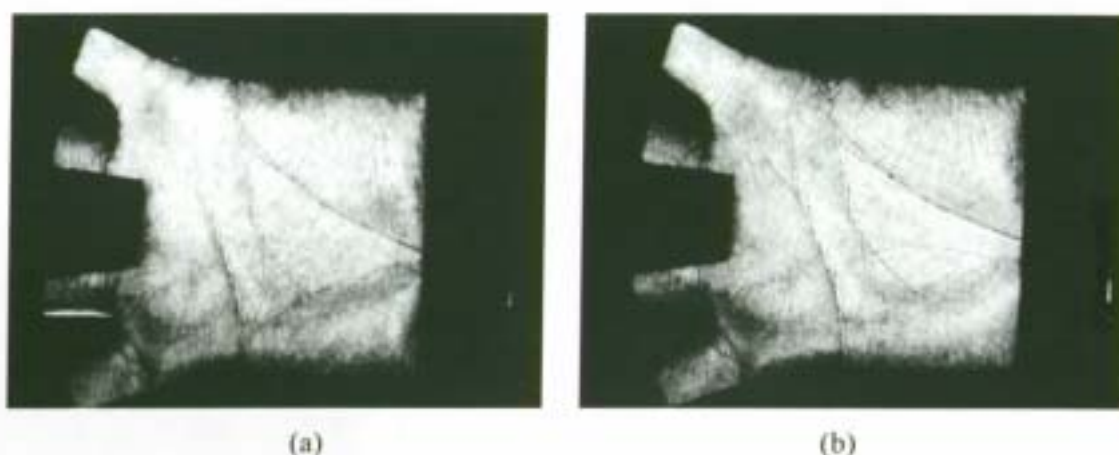
Fig. 5.12 Illustration of the difference in image qualities between the first and second collections. (a) First collected and (b) Second collected images.

5.3.2 Verification

To obtain the verification accuracy of our palmprint system, each palmprint image is matched with all palmprint images in the database. A matching is noted as a correct matching if the two palmprint images are from the same palm and as incorrect if otherwise. The total number of matchings is 19,161,145. None of the matching scores are zero. The number of comparisons with correct matching is 59,176 and the rest of them are incorrect matchings. The probability distributions for the genuine and imposter parts are estimated by the correct and incorrect matchings, respectively, as shown in Fig. 5.13(a). Fig. 5.13(b) depicts the corresponding receiver operating curve (ROC), being a plot of genuine acceptance rate against false acceptance rate for all possible operating points. From Fig. 5.13(b), we can see that our system can operate at 96% genuine acceptance rate and 0.1% false acceptance rate;

the corresponding threshold is 0.35. This result is comparable with previous palmprint approaches and other hand-based biometric technologies including hand geometry and fingerprint verification [6-9, 12, 15, 18, 20, 21, 25].

(a)   (b)

Fig. 5.13 Verification test results. (a) Genuine and imposter distributions for verification test and (b) the receiver operator curve (ROC).

5.3.3 Identification

Identification is a comparison process of one against many, N. To establish the identification accuracy of our palmprint system, we need to specify the N. In the folldwing iden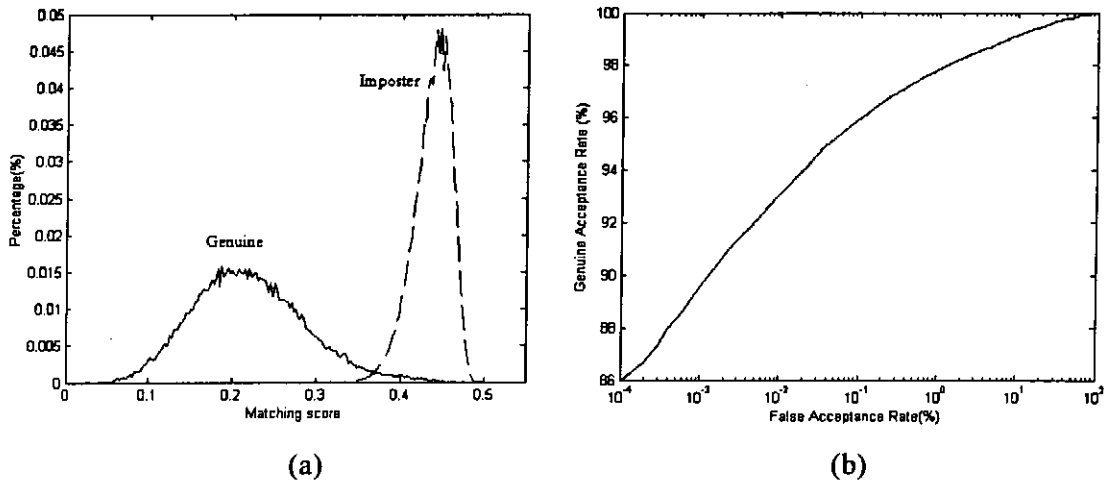tification tests, we are interested in N=(50, 100 and 200) which are similar to the number of employees in small or middle size companies. A practical biometric identification system, generally, stores several users' templates in its database for training the system or for obtaining varied and deformed templates so that the system can recognize the noise or deformed features. In the followings tests, we setup three registration databases for N=50, 100 and 200. The first database contains 150 templates from 50 different palms; each palmprint has three templates. Similarly for N=100 and 200, the second and third registration databases have 300 and 600 templates, respectively. We also set up a testing database with 5591 templates from 308 different palms. None of palmprint images in the testing database are contained in any registration databases. Each palmprint image in the testing database is matched with all the palmprint images in the registration databases for generating incorrect and correct identification matching scores. Since a registered palm has three templates in the registration databases, a palmprint image of a registered palm in the testing database is matched with its three templates in the registration databases to produce three correct matching scores. We take the minimum of them for the correct identification matching score. Similarly, a palmprint image in the testing database is compared with all palmprint images in any registration

database to produce $3N$ incorrect matching scores if the testing palmprint does not have registered images, or $3N$-3 incorrect matching scores if the testing palmprint has registered images. We take the minimum of them for the incorrect identification matching score. All the imposter identification distributions are generated by 5591 incorrect matching identification scores. The genuine identification distributions are established by 864, 1714 and 3420 for N=50, 100 and 200, respectively. Fig. 5.14(a)-(c) illustrate the genuine and imposter distributions and the corresponding receiver operating curves are obtained in Fig. 5.14(d). To compare the imposter distributions of Fig. 5.14(a)-(c), when N increases, the imposter distribution moves to the left. It means that the average of incorrect identification scores reduces. In the experiments, increasing N is equivalent to increasing the number of correct identification matching scores for establishing smoother genuine distributions. Fig. 5.14(d) illustrates that increasing N is equivalent to decreasing the accuracy of the system.

5.3.4 Speed

Using Visual C++ 6.0 on an embedded Intel Pentium III processor (500MHz) PC, we obtain the execution time for the preprocessing, feature extraction and matching, as shown in Table 2. The total execution time is about 0.6 second, which is fast enough for real-time verification. For identification, if the database contains 100 persons and each person registers 3 palmprint images, the total identification time is about 1.1s. In fact, we have not optimized the code so further reduction in the computation time is possible.

Table 2. Execution time for palmprint identification system.

Operation	Execution Time
Preprocessing	538ms
Feature Extraction	64ms
Matching	1.7ms
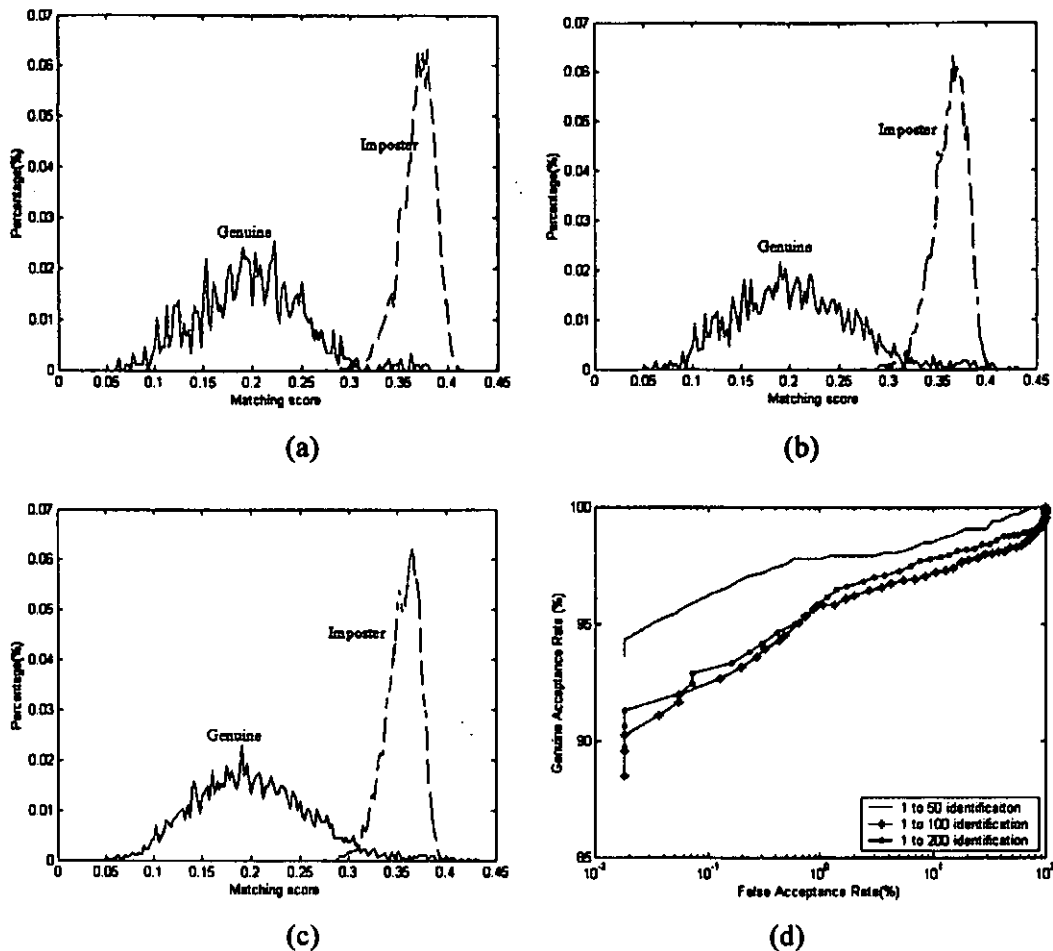
Fig. 5.14 Identification test results. Genuine and imposter distributions for (a) N=50, (b) N=100 and (c) N=200. (d) Their receiver operating curves

5.4　Conclusion

We have developed an on-line palmprint identification system for real-time personal identification. We have designed a novel CCD camera-based palmprint scanner that is directly connected to a computer for capturing palmpint images for on-line recognition support. A preprocessing algorithm dynamically extracts the central part of a palmprint for feature extraction. To represent a low-resolution palmprint image and match different palmprint images, we exploit Daugman's idea [30, 121] to represent a palmprint image by texture feature and use the normalized hamming distance as a distance measure. Using this representation, we manage to confine the total size of a palmprint feature and its mask to only 384 bytes. On our palmprint database containing 6191 palmpint images from 308 different palms, we can achieve high genuine (98%) and low false acceptance (1%) verification rates.

These result are comparable with those of all other palmprint recognition approaches and other hand-based biometrics such as hand geometry and fingerprint verification [16, 71, 102, 120, 122, 123]. For identification, our system can still operate at low false acceptance and reasonably high genuine rates. Using Visual C++ 6.0 on an embedded Intel Pentium III processor (500MHz) PC, the 1-against-100 identification time including preprocessing, feature extraction and matching is about 1.1 second.

From the experimental results, we observe that our palmprint identification system can achieve a reasonable performance in speed and accuracy. However, it still needs some improvements: 1) Our CCD-based palmprint scanner is relatively large; to reduce the size is an advance for some applications. 2) To improve the accuracy of the system, we need to combine the texture energy or other texture features for coarse-level classification and the proposed texture representation.

Chapter 6

An Idea of Ear Recognition

Objective — A branch of biometric technology that measures the shape of our ear for personal identification was proposed about ten years ago. However, research and discussion in this biometric feature are very limited; only several conference papers are related to this technology. In this chapter, we consider two issues 1) image acquisition and 2) textured feature extraction technique for ear recognition. We have developed a special device for image acquisition. We use a 2-D Gabor filter to extract the texture information and two features are measured by a vector norm. The experimental results show that ear recognition can provide middle level security.

6.1   Introduction to Ear Recognition

Iannarelli is the first researcher who proposed to use ear for personal identification. Based on two studies reported in 1989, he claimed that ear shape is a unique object, which can be used for authentication. The first study compared over 10,000 ears drawn from randomly selected samples in California. The similarity of ears from fraternal or identical twins was observed in the second [78]. In addition, Iannarelli reported that ear growth after the first four months of birth is proportional. Although the ear grows proportionally, the ear stretches in the vertical direction because of gravity. This non-linear stretching is most pronounced in the lobe of the ear.

6.2 Recent Ear Recognition Approaches

There were two ear recognition approaches from Iannarelli, Burge and Hurley [21-24, 78]. However, they did not test their approaches in a large database; also they did not give the false acceptance rate and false rejection rate of their approaches. As a result, our method cannot be compared with these two approaches.

6.2.1 Iannarelli's Approach

Iannarelli's approach, which requires the exact alignment and normalization of the ear photos, is based on the 12 measurements illustrated in Fig. 6.1. Besides, the feature displayed in Fig 6.1 is measured in a unit of 3mm and assigned an integer value. Since the feature space is too small, this approach only provides limited classification power. Another flaw of this approach is that all the measurements are dependent on the origin so this approach requires the origin to be accurately located. In fact, Iannarelli was also aware of this weakness of his approach.
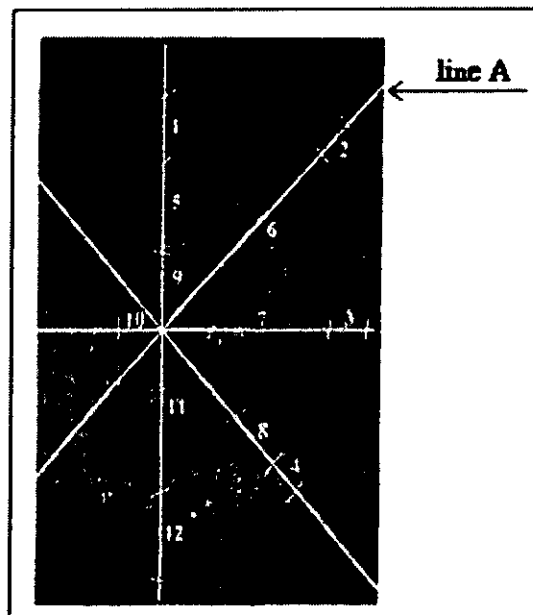
Fig. 6.1 The locations of the measurements used in the "Iannarelli System". From [2].

6.2.2 Burge's Approach

This approach, containing six main steps, uses a Voronoi diagram to represent the shape of the ear.

1. Acquisition: A 300 by 500 grayscale ear image is taken from the subject's head by using a CCD camera.

2. Segmentation: An active contour is used to locate the ear boundary

3. Edge extraction: Edges are extracted by Canny operator.

4. Curve extraction: Edge relaxation is used to form larger curve segments, and the remaining small curve segments will be removed (Fig. 6.2b). After that, a Voronoi neighborhood graph of the curves will be formed.

5. Graph model: A generalized Voronoi diagram of the curves is built and a neighborhood graph is then extracted (Fig. 6.2c).

6. Matching: It is based on the topological relation between two features.
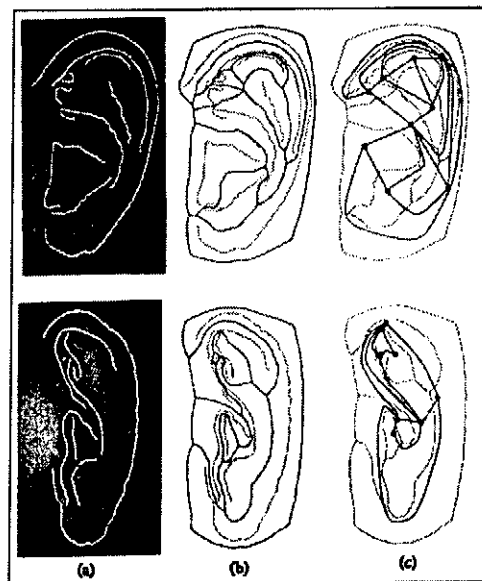
Fig. 6.2 Defining Voronoi diagram and extracting neighborhood graph. From [23]

6.3 Overview of The Proposed Ear Recognition Model

In our proposed method, there are has five main parts. The function of each part is described below:

1) Acquisition: A sequence of images is captured.

2) Image selection: One of the images in the sequence is used for identification.

3) Normalization: Translation and rotation of the ear in the image are normalized in this step.

4) Feature extraction: The filter bank approach used in fingerprint is imposed to capture the shape information of the ear [71].

5) Matching: Two feature vectors are measured by a vector norm.

6.4 Image Acquisition

Different people have different angles between the head and the ears so we design a special device to capture the image. It can provide flexibility to obtain ear image from different directions. Fig. 6.3 shows two ears with different shapes and directions. Fig 6.3(a) shows an ear whose inner parts are covered by its outer parts.

(a)   (b)

Fig. 6.3 Two different ears with different shapes.

Thus, we propose to capture a sequence of images and then select the best of them for recognition. Since the head-to-ear angle is different among individuals (see Fig. 6.4), we design a device with a digital camera rotating around the user's ear horizontally. The outlook and draft of the device are shown in Figs. 6.5(a) and 6.5(b), respectively.
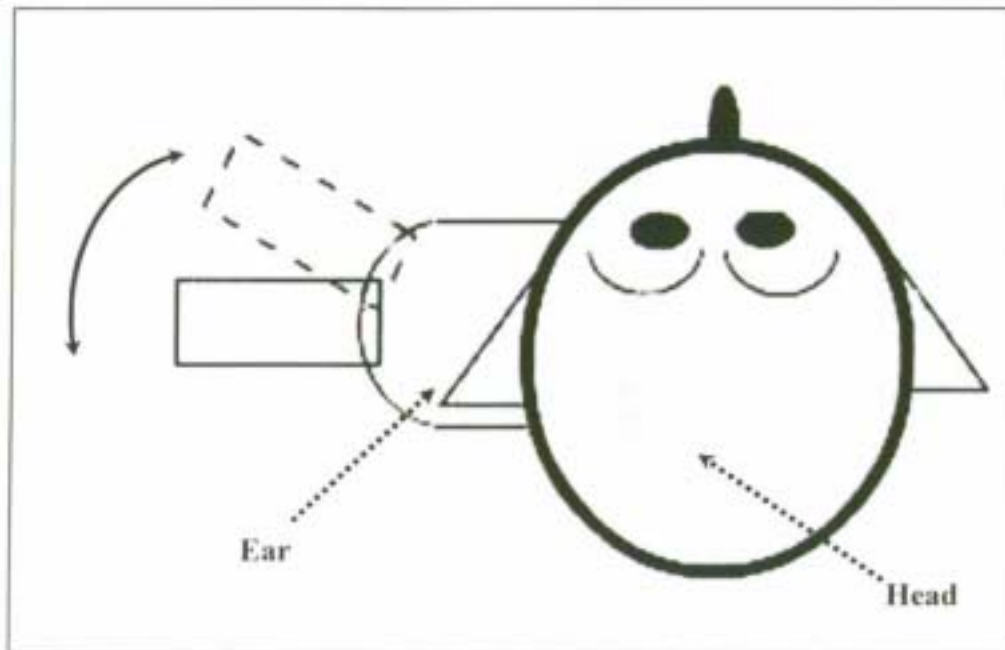
Fig. 6.4 Top view of a client using the device
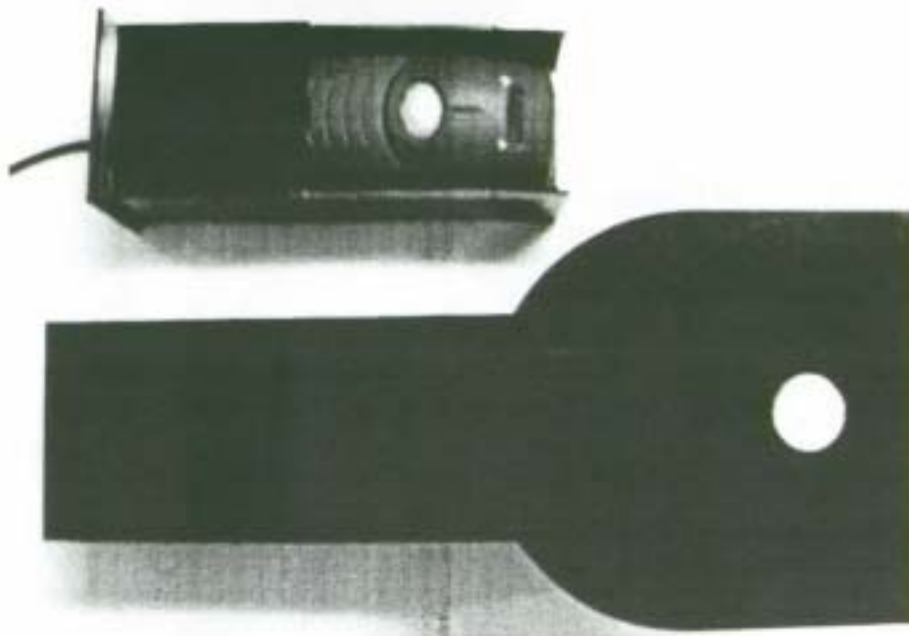
Fig. 6.5(a) The outlook of the device.
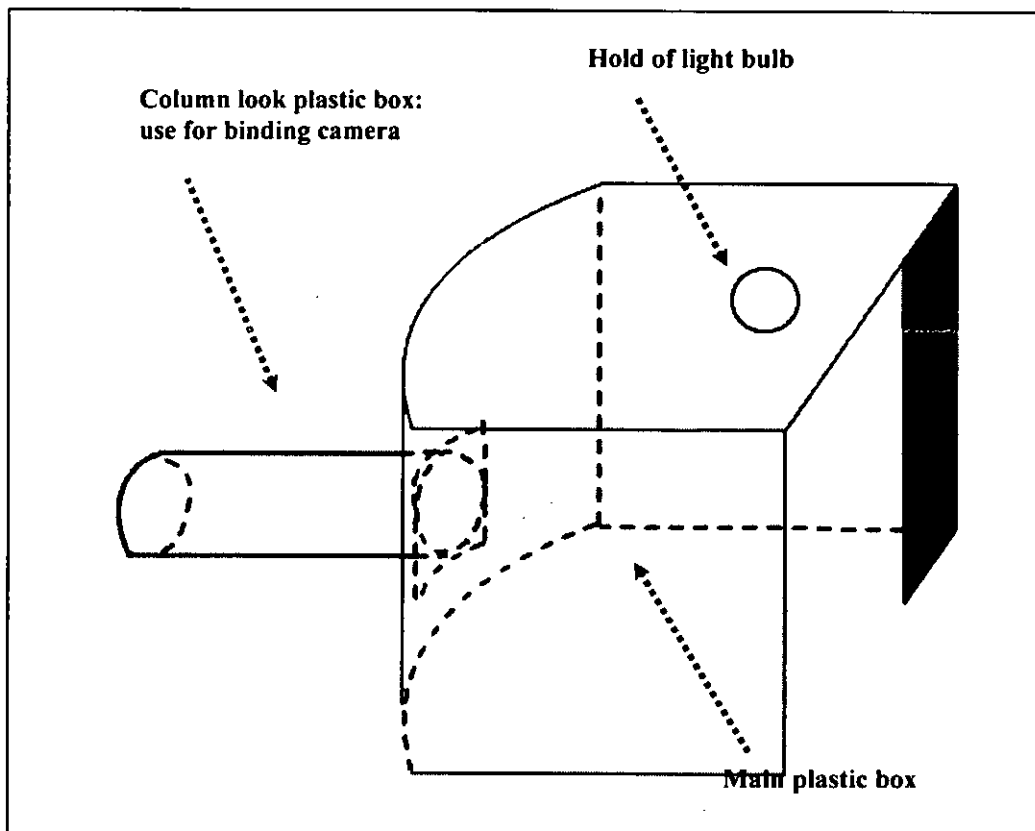
Fig. 6.5(b) Draft of the device design (used for capturing the left ear)

6.5   Image Selection

In this section, we propose a method to select the best image from the image sequence but we do not implement this idea in our program. For the steps from normalization to matching, we have implemented and tested them. The important points of our image selection are illustrated in Fig. 6.6. The steps of image selection are shown below:

Step 1   Outer boundary of the ear is detected by an active contour.

Step 2   Search the two points, (x_1, y_1) and (x_2, y_2), on the boundary with maximum distance. The two points form a major axis.

Step 3   Compute the reference point, O, which is the mid-point of (x_1, y_1) and (x_2, y_2).

Step 4   Compute the distance from the mid-point to the outer reference point.

Step 5   Select the image with maximum b_{max} for recognition.
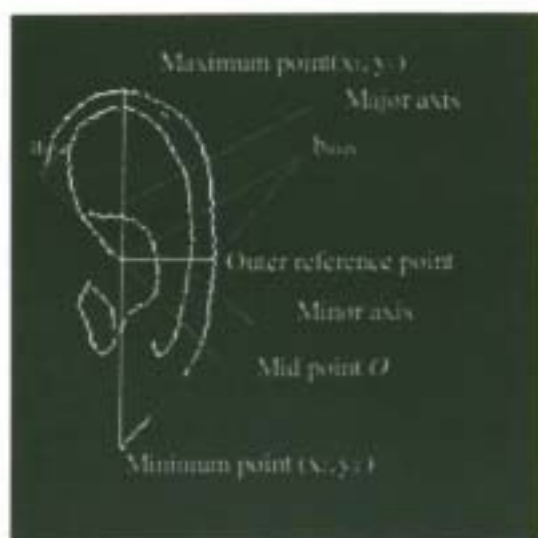
Fig. 6.6 Key points of our image selection process

6.6 Normalization

In order to provide a translation and rotational invariant matching, this step sets up a coordinate system to align two ear images. The midpoint, O, serves as the origin of the coordinate system. The major axis is formed by the maximum and minimum points; in addition, the minor axis is constituted by the mid-point and the outer reference point. The major and minor axes are shown in Fig. 6.6. In fact, this coordinate system is formed in the step of Image Selection.

6.7 Feature Extraction for Ear Recognition

6.7.1 Filtering

In our method, texture information in the ear image is captured by the real circularly symmetric Gabor filters which are defined as

$$G(x, y, \theta, u, \sigma) = \frac{1}{2\pi\sigma^2} \exp\left\{-\frac{x^2 + y^2}{2\sigma^2}\right\} \cos\{2\pi(ux\cos\theta + uy\sin\theta)\}, \qquad (5\text{-}1)$$

where u, θ and σ are defined in Section 2.3.3. The same set of the parameters as in Table 4.1 is applied to ear recognition.

92

6.7.2 Regional Decomposition

To compensate for the variation of the optical size of the ears in the image due to different distances between the camera and the users and the different zoom factors of the video camera, a convoluted ear image would be decomposed into many small areas where local features are extracted. Firstly, a convoluted ear image is decomposed into five elliptic rings and then each ring is separated into 12 regions. Based on the length of the major and minor axes, we employ linear interpolation to decompose the convoluted image. The ellipses can be computed by the following formulas,

$$\frac{x^2}{\left(a_{max} * \dfrac{i}{5}\right)^2} + \frac{y^2}{\left(b_{max} * \dfrac{i}{5}\right)^2} = 1 , \tag{5-2}$$

where a_{max} and b_{max} are illustrated in Fig. 6.6 and $i=1,2,3,4,5$. However, the left (right) lower part of the elliptic mask will not be used since it is not always covered by our right (left) ear. The effective area is shown in Fig. 6.7. The filled part will not be imposed for extracted feature.
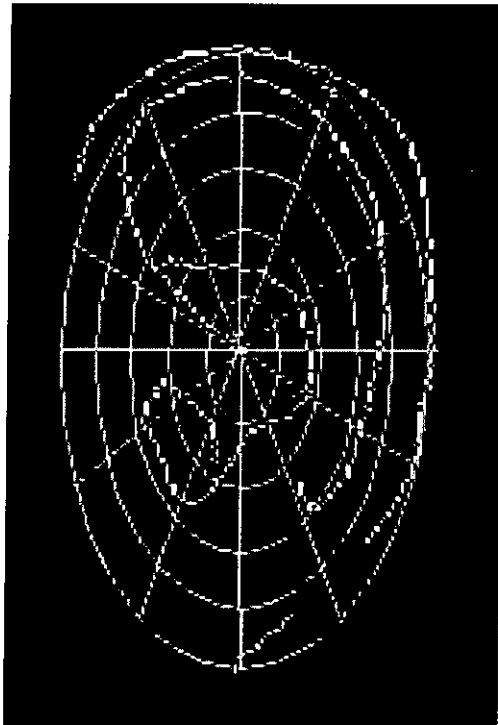
Fig. 6.7 Effective area for feature extraction in ear recognition

6.7.3 Feature Computation

Three statistical features 1) average energy, 2) variance and 3) average absolute deviation will be used for the following experiments. The computational formula of average energy is

$$E_R = \frac{\sum\limits_{(x,y)\in R} I_k[x,y]^2}{n_R},$$ (5-3)

where I_k is a convoluted image and R is a small region. Also, let n_R be the number of pixels in the region R. Variance can be obtained by the following equation,

$$V_R = \frac{\sum\limits_{(x,y)\in R} \left(I_k(x,y) - M_{kR}\right)^2}{n_R},$$ (5-4)

where M_{kR} is the mean of intensity in the region R of the filtered image I_k. In addition, the formula of average absolute deviation is shown below,

$$D_R = \frac{\sum\limits_{(x,y)\in R} \left|I_k(x,y) - M_R\right|}{n_R}.$$ (5-5)

6.8 Ears Matching

Since the coordinate system normalizing translation and rotation provides invariant matching, we use a sample vector norm to measure the similarity between two feature vectors. The matching score can be computed by,

$$S = \sum_{i=1}^{n} |x_i - y_i|,$$ (5-6)

where x and y represent two feature vectors and n is the length of the feature vector.

6.9 Experimental Results and Discussion

In this section, we apply the twelve filters to our database containing 60 images from 20 persons. The number of comparisons for imposter and genuine distributions are 459 and 54, respectively. Their equal error rates are shown in Table 6.1 and a graphical representation of the equal error rates is illustrated in Fig. 6.8. From these, we can discover that average absolute deviation is the best feature. The average difference between variance and average

absolute deviation is 4%. Based on the average absolute deviation, the minimum error is 9% generated by Filter 7.

Compared with the recognition rates of palmprint, iris and fingerprint, the recognition rate of ear is relatively low. In our experiment, our method uses a very simple classifier and one scale texture analysis. Using multiscale analysis and complex classifiers such as neural networks and support vector machine, will improve the recognition rate.

6.10   Conclusion

In this Chapter, we report ear recognition using texture information. Three kinds of features, energy and average absolute deviation are extracted from the filtered images and two features are measured by a simple vector norm. According to our experimental results, average absolute deviation provides the best result with a 9% equal error rate. We have also designed a device for ear recognition

Table 6.1 The Equal error rate of different features and different filters

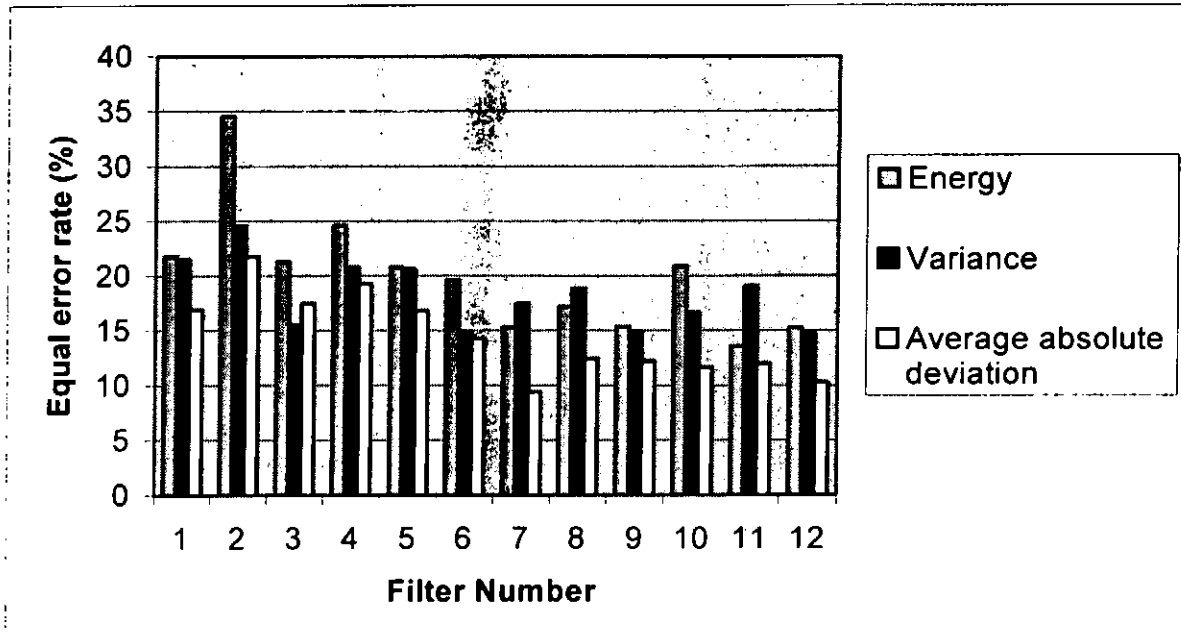| Filter No.	Energy	Variance	Average absolute deviation
1	22%	22%	17%
2	35%	25%	22%
3	21%	16%	17%
4	25%	21%	19%
5	21%	21%	17%
6	20%	15%	14%
7	15%	17%	9%
8	17%	19%	12%
9	15%	15%	12%
10	21%	17%	12%
11	14%	19%	12%
12	15%	15%	10%

Fig 6.8 A graphic representation of the equal error rates of our method

Chapter 7.

Conclusions and Further Research

7.1   Conclusions

In this study, we have applied texture analysis techniques including Gabor filters and wavelets to three different biometrics, iris, palmprint and ear. Through a series of experiments, we have attained different levels of achievement in these three biometrics technologies.

For the iris, we have proposed an eyelash and reflection model and evaluated Boles' approach by various 1-D wavelets. According to the experimental results, our detection model is effective in segmenting eyelashes and reflection; consequently, the accuracy rate of Boles' approach can be improved by our proposed model. The maximum improvement is 3% equal error rates. Various wavelets including Gabor, Haar, Shannon and normalized Mexican hat have also been applied to Boles' approach but none of them can provide as accurate a result as Daugman's approach, which is used in almost all iris recognition technologies in the market.

For the palmprint, we have developed a texture-based feature extraction technique. Using a 2-D Gabor filter on palmprints to obtain the phase information as feature vectors, we have proved through experimentation that the palmprint is an information density object, which contains more than 170 degrees-of-freedom that can be used for personal identification. From accuracy, user acceptance and hardware cost points of view, our proposed palmprint recognition method is better than, or at least comparable with, the iris and fingerprint approaches. We expect that palmprint will take over 3-D hand geometry in the market

because of its high accuracy and user acceptance. According to published or accepted papers on palmprint recognition, this method is the state of the art, and because of the result described in this thesis, some construction companies are considering using our palmprint system to solve their security problems.

For the ear, we were to design a capture device and to develop a feature extraction method for ear recognition. In Chapter 6, we have developed a special device for image acquisition. We have also proposed a novel feature extraction for ear recognition, which measures two ear features by l_1 norm. The experimental results show that ear recognition can provide middle level security.

7.2   Further Research

We have proposed several approaches that solve a range of problems in different biometric technologies. Some of them provide impressive results. Nevertheless, further research is still necessary to improve their accuracy and to ensure high user acceptance.

In the personal identification area, Daugman made great advances in iris recognition, and came close to solving all the technical problems. However, iris recognition still suffers from high cost and low user acceptance. Modifying the current capture device and image acquisition process is a further improvement that can be made. There are also many opportunities. For example, extraction of the structural features from the iris, and classification of structural features and feature description can be used to extend iris recognition to iris diagnosis.

Using palmprints for personal identification is one of the successful achievements in this study. However, it still needs some improvements: 1) Our CCD-based palmprint scanner is relatively large; to reduce the size is an advance for some applications. 2) To improve the accuracy of the system, we need to combine the texture energy or other texture features for coarse-level classification and the proposed texture representation.

Ear recognition is a new member of the biometric technology family. With just a classifier, vector norm and one scale analysis, the recognition rate only supports middle security. In order to improve its accuracy, multiscale analysis and a complex classifier,

including a support vector machine and neural networks, should be applied to the current ear recognition architecture.

Bibliographies:

[1]   G.S.K. Fung, R.W.H. Lau and J.N.K Liu, "A signature based password authentication method", in *Proceedings of IEEE International Conference on Systems, Man, and Cybernetics (SMC'97)*, Orlando, Florida, USA, pp. 631-636, October 12-15, 1997.

[2]   A. Jain, R. Bolle and S. Pankanti, *Biometrics: personal identification in networked society*, Kluwer Academic Publishers, 1999.

[3]   D. Zhang, *Automated biometrics – technologies and systems*, Kluwer Academic Publishers, 2000.

[4]   K. Wang, D. Zhang, B. Pang, Y. Li and X. Wu, "Biometrics based tongue diagnosis of TCM," *in Proceedings of First International Conference on Image and Graphics*, August 16-18, 2000 Tiangin, China, pp.206-209.

[5]   C.H. Li, P.C. Yuen, "Tongue image matching using color content", *Pattern Recognition*, (In press) 2001.

[6]   W.T. Jellema, B.P.M. Imholz, H, Oosting, K. H. Wesseling and J. J. van Lieshout, "Estimation of beat-to-beat" changes in stroke volume from arterial pressure: a comparison of two pressure wave analysis techniques during head-up tilt testing in young, healthy men," *Clinical Autonomic Research*, vol.9 pp. 185-192, 1999.

[8]   D. Zhang, "Biometrics technologies and applications" *in Proceedings of First International Conference on Image and Graphics*, Tiangin, China, pp.42-49, August 16-18, 2000.

[9]   R.B. Hill, "*Rotating beam ocular identification apparatus and method*", US Patent No. 4393366, 1983.

[10]   R.B. Hill, "*Fovea-centered eye fundus scanner,*" US Patent No. 4620318, 1986.

[11]   J.H. Arndt, "*Optical alignment System,*" US Patent No. 4923297, 1990

[12]   R.B. Hill, "*Apparatus and method for identifying individuals through their retinal vasculature patterns,*" US Patent No. 4109237, 1978.

[13]   Biometrics Consortium page: http://www.biometrics.org

[14]   J. Berry, "*The history and development of fingerprinting,*" in Advances in Fingerprint Technology, (H.C. Lee and R.E. Gaensslen, ed.s), CRC Press, Florida, 1994, pp. 1-39, 1994.

[15]   A.K. Jain and S. Pankanti, "*Automated Fingerprint Identification and Imaging Systems*", Advances in Fingerprint Technology, 2nd Ed. (H. C. Lee and R. E. Gaensslen), Elsevier Science, New York, 2001.

[16]   A.K. Jain, L. Hong and R. Bolle, "On-line fingerprint verification'", *IEEE Transactions on Pattern Analysis and Machine Intelligence*, vol. 19, no. 4, pp. 302-314, 1997.

[17]   N. Ratha, S. Chen, K. Karu and A.K. Jain, "A real-time matching system for large fingerprint databases", *IEEE Transactions on Pattern Analysis and Machine Intelligence*, vol. 18, no 8, pp. 799-813, 1996.

[18]   K. Karu and A.K. Jain, "Fingerprint classification", *Pattern Recognition*, vol. 29, no. 3, pp. 389-404, 1996.

[19]   R. Cappelli, A. Lumini, D. Maio and D, Maltoni, "Fingerprint classification by directional image partitioning", *IEEE Transactions on Pattern Analysis and Machine Intelligence*, vol. 21 no. 5, pp. 402-421, 1999

[20]   D. Maio and D. Maltoni, "Direct gray-scale minutiae detection in fingerprints", *IEEE Transactions on Pattern Analysis and Machine Intelligence*, vol. 19, no. 1, pp. 27-40, 1997

[21]   M. Burge and W. Burger, "Using ear biometrics for passive identification", *in Proceedings of the 14th Information Security (SEC'98)*, (Vienna, Austria), Austrian Computer Society , pp. 139-148, September 1998.

[22]   M. Burge and W. Burger, "Identification using ear biometrics," *in Proceedings of the 22th Workshop of the Austrian Association for Pattern Recognition*, Illmitz, Austria, Austrian Computer Society, pp. 195-204, 1998.

[23]   M. Burge and W. Burger, "Ear biometrics for machine vision", *in Proceedings of the 21th Workshop of the Austrian Association for Pattern Recognition*, Hallstatt, Austria, Austrian Computer Society, pp. 275-282, 1997.

[24]   D.J. Hurley, M.S. Nixon and J.N. Carter, "Automatic ear recognition by force field transformations", *IEE Colloquium on Visual Biometrics*, pp. 7/1-7/5, 2000

[25]   A. Iannarelli, "Ear identification", Forensic Identification Series, Paramont Publishing Company, Fremont, California, 1989.

[26]   S. Pankanti, R.M. Bolle and A. Jain, "Biometrics: the future of identification", *IEEE Computer*, vol. 33, no. 2, pp. 46-49, 2000.

[27]   International Biometrics Group page http://www.biometricgroup.com/

[28]   Flom and A. Safir, "Iris recognition system," U.S. Patent 4 641 349, 1987.

[29]   J. Daugman, "High confidence personal identification by rapid video analysis of iris texture", *in Proceeding of the IEEE International Carnahan Conference on Security Technology*, pp. 50-60, 1992.

[30]   J. Daugman, "High confidence visual recognition of persons by a test of statistical independence", *IEEE Transactions on Pattern Analysis and Machine Intelligence*, vol. 15, no. 11, pp. 1148-1161, 1993.

[31]   J. Daugman, "Biometric personal identification system based on iris analysis," U.S. Patent No 5,291,560, 1994.

[32]   J. Daugman, "High confidence recognition of persons by rapid video analysis of iris texture", *in Proceeding of the European Convention on Security and Detection*, pp. 244-251. 16-18 May 1995

[33]   J. Daugman, "Recognizing Persons by Their Iris Pattern," *in Biometric: Personal Identification in Networked Society*, 1998

[34]   J. Daugman, "Biometric decision landscapes." *Technical Report No. TR482, University of Cambridge Computer Laboratory*, 1999.

[35]   C. Seal, M. Gifford and D. McCartney, "Iris recognition for user validation", *British Telecommunications Engineering Journal*, vol. 16, pp. 113-117, July 1997.

[36]   M. Negin, T.A. Jr, M. Salganicoff, T.A. Camus, U.M. von Seelen, P.L. Venetianer and G.G. Zhang, *"An iris biometric system for public and personal use"*, Computer, vol. 33, no. 2 , pp. 70-75, 2000.

[37]   T. Camus, U.M. Cahn von Seelen, G.G. Zhang, P.L. Venetianer and M. Salganicoff, "Sensar ... secure^tm iris identification system," *in Proceedings of Fourth IEEE Workshop on Applications of Computer Vision*, pp. 254-255, 1998.

[38]   G.O. Williams, "Iris recognition", *IEEE Aerospace and Electronics Systems Magazine*, vol.12, no. 4, pp. 23-29, April 1997.

[39]   G.O. Williams, "Iris Recognition", *in Proceedings of the 30th Annual 1996 International Carnahan Conference on Security Technology*, pp. 46-59, 1995.

[40]   T. Camus, K. Hanna, R. Mandelbaum, D. Mishra, L. Wixson, and M. Salganicoff, "Real-time stereo and eye finding for an iris identification system," *in Demo Program of the IEEE Conference on Computer Vision and Pattern Recognition*, pp. 11, San Juan, Puerto Rico, pp. 17-19, June 1997.

[41]   M. DellaVecchia, T. Chmielewski, T. Camus, M. Salganicoff and M. Negin, "Methodology and apparatus for using the human iris as a robust biometric," *In ophthalmic Technologies VIII, SPIE Proceedings*, vol. 3246, San Jose, CA, pp. 24-30 Jan 1998.

[42]   K. Hanna, R. Mandelbaum, D. Mishra, V. Paragano, and L. Wixson, "A system for non-intrusive human iris acquisition and identification," *In Machine Vision Application*, Japan, Nov. 1996.

[43]   R. Wildes, J. Asmuth, G. Green, S. Hsu, R. Kolczynski, J. Matey and S. McBride, "A machine vision system for iris recognition," *Machine Vision and Applications* vol. 9, pp. 1-8, 1996.

[44]   R. Wildes, J.C. Asmuth, G.L. Green, S.C. Hsu, R.J. Kolczynski, J.R. Matey and S.E. McBride, "A system for automated iris recognition", *In Proceedings of the IEEE Workshop on Applications of Computer Vision*, pp. 121-128, 1994.

[45]   R. Wildes, "Iris recognition: an emerging biometric technology", *in Proceeding of the IEEE*, vol. 85, no. 9, pp. 1349-1363, 1997.

[46]   R.P Wildes, J. C Asmuth, S.C. Hsu, R.J. Kolczynski, J.R. Matey and S.E. McBride, "*Automated, noninvasive iris recognition system and method*," U.S. Paten 5,572,5956, 1996.

[47]   W.W. Boles and B. Boashash, "A human identification technique using images of the iris and wavelet transform", *IEEE Transactions on Signal Processing*, vol. 46, no. 4, pp. 1185-1188, 1998.

[48]   W.W. Boles, "A wavelet transform based technique for the recognition of the human iris", *in Proceedings of the International Symposium on Signal Processing and its Application, ISSPA, Gold Coast, Australia*, pp. 25-30, August, 1996.

[49]   Vision, Eye Disease and Treatment http://www.gansmart.com/medinfo.html

[50]   Y. Zhu, T. Tan and Y. Wang "Biometric personal identification based on iris pattern", *Proceeding of 15th International Conference on Pattern Recognition*, vol. 2, pp. 801-804, 2000

[51]   A.J. Bron, R.C. Tripathi and B.J. Tripathi, *Wolff's Anatomy of the Eye and Orbit* 8th ed. London: Chapman & Hall Medical, 1997.

[52]   P.V.C. Hough, "*Method and means for recognition complex patterns*", U.S. Patent 3 069 654, 1962.

[53]   J.R. Bergen, P. Anadan, K. Hanna and R. Hingorani, "Hierarchical model-based motion estimation," *in Proceeding Europe Conference Computer Vision*, Santa Margherita Ligure, Italy, 199, pp. 5-10

[54]   B. Jahne, *Digital Image Processing*, 2nd ed. Berlin: Springer-Verlag, 1993.

[55]   R.A. Fisher, "The use of multiple measurements in taxonomoc problems", Annals Eugenics, vol. 7 no. 2, pp.179-188, 1936.

[56]   J. Colton, *Iridology: health analysis and treatments from the iris of the eye*, Queensland: Element, 1996.

[57]   E. Groen, J.E. Bos, P.F.M. Nacken and B.D. Graaf, "Determination of ocular torsion by means of automatic pattern recognition", *IEEE Transactions on Biomedical Engineering*, vol. 43, no. 5, pp. 471-479, 1996.

[58]   X. Xie, R. Sudhakar, and H. Zhuang, "A cascaded scheme for eye tracking and head movement compensation", *IEEE Transactions on System, Man and Cybernetics — Part A: Systems and Humans*, vol. 28, no. 4, pp. 487-490, 1998.

[59]   S. Bernogger, L. Yin, A. Basu and A. Pinz, "Eye tracking and animation for MPEG-4 coding", *Proceedings of 14th ICPR*, vol. 2, pp. 1281-1284, 1998.

[60]   X. Xie, R. Sudhakar, and H. Zhuang, "Real-time eye feature tracking from a video image sequence using kalman filter", *IEEE Transactions on Systems, Man and Cybernetics*, vol. 25, no. 12, pp. 1568-1577, 1995.

[61]   R.V. Hogg and E.A. Tanis, Probability and statistical inference (fourth edition), New York: Maxwell Macmillan International, 1993.

[62]   D. Zhang and W. Shu, "Two novel characteristics in palm print verification: datum point invariance and line feature matching", *Pattern Recognition*, vol. 32, no. 4, pp. 691-702, 1999.

[63]   W. Shu and D. Zhang, "Automated personal identification by palm print," *Optical Engineering*, vol. 37, no. 8, pp.2, 659-2,362, 1998.

[64]   D. Gabor, "Theory of communications," *J. IEE*, vol. 93, pp. 429-457, 1946.

[65]   C.K. Chui, *An Introduction to Wavelets*, Academic Press, Boston, 1992

[66]   J.G. Daugman, "Two-dimensional spectral analysis of cortical receptive field profiles," *Vision Research*, vol. 20, pp. 847-856, 1980.

[67]   J. Daugman, "Uncertainty relation for resolution in space, spatial frequency and orientation optimized by two-dimensional visual cortical filters", *Journal of the Optical Society of America A*, vol. 2, pp. 1,160-1,169, 1985.

[68]   A. Jain and G. Healey, "A multiscale representation including opponent color features for texture recognition", *IEEE Transactions on Image Processing*, vol. 7, no. 1, pp. 124-128, 1998.

[69]   D. Dunn and W.E. Higgins, "Optimal Gabor filters for texture segmentation," *IEEE Transactions on Image Processing*, vol. 4, no. 4, pp. 947-964, 1995.

[70]   A.C. Bovik, M. Clark and W.S. Geisler, "Multichannel texture analysis using localized spatial filters", *IEEE Transactions on Pattern Analysis and Machine Intelligence*, vol. 12, no. 1, pp. 55-73, 1990.

[71]   A.K. Jain, S. Prabhakar, L. Hong and S. Pankanti, "Filterbank-based fingerprint matching", *IEEE Transactions on Image Processing*, vol. 9, no. 5, pp. 846-859, 2000.

[72]   L. Hong, Y. Wan and A. Jain, "Fingerprint image enhancement algorithm and performance evaluation", *IEEE Transactions on Pattern Analysis and Machine Intelligence*, vol. 20, no. 8, pp. 777-789, 1998.

[73]   C.J. Lee and S.D. Wang. "Fingerprint feature extraction using Gabor filters", *Electronic Letters*, vol. 35, no. 4, pp. 288-290, 1999.,

[74]   M.J. Lyons, J. Budynek and S. Akamatsu, "Automatic classification of single facial images", *IEEE Transactions on Pattern Analysis and Machine Intelligence*, vol. 21, no. 12, pp. 1,357-1,362, 1999.

[75]   B. Duc, S. Fischer and J. Bigun, "Face authentication with Gabor information on deformable graphs", *IEEE Transactions on Image Processing*, vol. 8, no. 4, pp. 504-516, 1999.

[76]   Y. Adini, Y. Moses and S. Ullman, "Face recognition: The problem of compensation for changes in illumination direction", *IEEE Transactions on Pattern Analysis and Machine Intelligence*, vol. 19, no. 7, pp. 721-732, 1997.

[77]   J.D. Williams, Statistical methods, Lanham, Md, University Press of America, c1996.

[78]   A. Iannarelli, *Ear identification*, Forensic Identification Series. Paramont Publishing Company, Fremont, California, 1989.

[79]   B. Julesz, "Textons, the elements of texture perception, and their interactions", *Nature*, no. 290, pp. 91-97, 1981.

[80]   R.H. Harakuck and L.G. Shapiro, "Computer and robot vision", vol. 1. Reading: Addison Wesley, 1992.

[81]   G.L. Gimel'farb, *Image textures and gibbs random field*, Kluwer Academic Publishers, London, 1999.

[82]   T.Y. Young and K.S. Fu, *Handbook pattern recognition and image processing*, Academic Press, London, 1986.

[83]   A. Rosenfed and E. Troy, Visual texture analysis, Technical Report. pp. 70-116, University of Maryland, Collage Park, Maryland, June 1970.

[84]   A. Rosenfed and M. Thurston, "Edge and cure detection for visual scene analysis", *IEEE Transactions on Computers*, vol. 20, no. 5 pp. 562-569, 1971.

[85]   R.C. Gonzalez, R.E. Woods, *Digital image processing*, New York, 1993.

[86]   R.S. Ledley, "Texture problems in biomedical pattern recognition", *Proceedings of the IEEE conference on Decision*, New Orleans.

[87]   O. Mitchell, C. Myers and W, Boyne, "A max-min measure for image texture analysis", *IEEE Transactions on Computers*, vol. 25, 408-414, 1977.

[88]   G. String and T. Nguyen, *Wavelets and filter banks*, Wellesley- Cambridge Press, 1997.

[89]   S. Mallat, *A wavelet tour of signal processing*, Academic Press, 1998.

[90]   A. Witkin. "Scale space filtering", in *Proceeding of Joint Conference of Artificial Intelligence*, Espoo, Finland, June, 1983.

[91]   C.W.J. Shih, N. Ling and T. Ogunfunmi, "Memory reduction by Haar wavelet transform for MPEG decoder", *IEEE Transaction on Consumer Electronics*, pp. 867-873, 1999.

[92]   C.W.J. Shih, N. Ling and T. Ogunfunmi, "Memory reduction by Haar wavelet transform for MPEG decoder", in *Proceeding. International Conference on Consumer Electronics*, pp. 116-117, 1999.

[93] J.T. Miller and C.C. Li, "Segmentation of object surfaces using Haar wavelet at multiple resolution", *in Proceeding of IEEE International conference on Image processing*, vol. 3, pp. 475-477, 1994.

[94] J. Rosiene, "Non-separable Haar wavelets and the clustering of magnetic resonance imagery", *in Proceeding of the 16th Annual International Conference of IEEE*, vol. 2, pp. 1210-1211, 1994.

[95] S.E. Taweel and A.M. Darwish, "Texture segmentation using Shanon wavelet", *in Proceeding of International Conference on Image Processing*, vol. 3, pp. 343-347, 1998.

[96] T. Randen and J. HusØy, "Filtering for texture classification: A comparative study", *IEEE Transactions on Pattern Analysis and Machine Intelligence*, vol. 21, no. 4, pp. 291-310, 1999.

[97] H.C. Hsin and C.C. Li, "An experiment on texture segmentation using modulated wavelets", *IEEE Transactions on Systems, Man, and Cybernetics — Path A: Systems and Humans*, vol. 28, no. 5, 1998.

[98] G. Van de Wouwer, P. Scheunders and D. Van Dyck, "Statistical texture characterization from discrete wavelet representation", *IEEE Transactions on Image Processing*, vol. 8, no. 4, pp. 592-598,1999.

[99] P.G. Stimson and C.A. Mertz. "Forensic dentistry", CRC Press, New York. 1997

[100] W.R. Posey, "Computer assisted postmortem identification via dental and other characteristics". USAIDR Information Bulletin, Vol.5, No. 1, Autumn, 1990

[101] "Swissair Flight 111 Investigation – Identification Process". Http://www3.ns.sympatico.ca/swissair/identoverview.htm

[102] R, Sanchez-Reillo and C. Sanchez-Acila, and A. Gonzalez-Marcos, "Biometric identification through hand geometry measurements", *IEEE Transactions on Pattern Analysis and Machine Intelligence*, vol. 22, no. 10 pp. 1168-1171, 2000.

[103] R, Sanchez-Reillo and C. Sanchez-Acila, "Access control system with hand geometry verification and smart cards", *IEEE Aerospace and Electronics Systems Magazine*, vol. 15, no. 2, pp. 45-48, 2000.

[104] P.S. Wu and M. Li "Pyramid edge detection based on stack filter", *Pattern Recognition Letters*, vol. 18, no. 4, pp. 329-248, 1997.

[105] N. Duta, A. K. Jain and K. V. Mardia, "Matching of palmprints", To appear in *Pattern Recognition Letters*, 2001.

[106] J. You, W. Li and D. Zhang, "Hierarchical palmprint identification via multiple feature extraction", To appear in *Pattern Recognition*, 2001.

[107] W. Li, D. Zhang and Z. Xu, "Palmprint identification by Fourier transform", To appear in *Pattern Recognition and Artificial Intelligence*.

[108]   "2000 market review", *Biometrics Technology Today*, pp. 9, January 2001.

[109]   "Belgium considers smart ID cards", Biometric Technology Today, pp. 1, January 2001.

[110]   Biometrics market size: http://www.axistech.com/biomarket.html

[111]   W. Shi, G. Rong, Z. Bain and D. Zhang, "Automatic palmprint verification", *International Journal of Image and Graphics*, vol. 1, no. 1, pp. 135-152, 2001.

[112]   J. Chen, C. Zhang and G. Rong, "Palmprint recognition using crease", *Proceedings of 2001 International Conference on Image Processing*, vol. 3, pp. 234-237, 2001.

[113]   W. Shu, "Research on automatic palmprint recognition", PHD thesis, Tsinghua University, 1999.

[114]   NEC automatic palmprint identification system: http://www.nectech.com/afis/download/PalmprintDtsht.q.pdf.

[115]   W. Shu and D. Zhang, "Palmprint verification: an implementation of biometric technology", *Proceedings of 14th International Conference on Pattern Recognition*, Brisbane Australia, pp. 219-221, 1998.

[116]   http://www.printrakinternational.com/omnitrak.htm

[117]   C.C. Han, H.L. Cheng, K.C. Fan and C.L. Lin, "Personal Authentication Using Palmprint Features", To appear in *Pattern Recognition*.

[118]   C.J. Liu and H. Wechsler, "A shape- and texture-based enhanced fisher classifier for face recognition", *IEEE Transactions on Image Processing*, vol. 10, no. 4, pp. 598-608, 2001.

[119]   L. Fan and K.K. Sung, "A combined feature-texture similarity measure for face alignment under varying pose", *Proceedings of IEEE Conference on Computer Vision and Pattern Recognition*, vol. 1, pp. 308-313, 2001.

[120]   A.K. Jain, A. Ross and S. Pankanti, "A prototype hand geometry-based verification system", *Proceedings of 2nd Int'l Conference on Audio- and Video-based Biometric Person Authentication, Washington D.C.*, pp. 166-171, March 22-24, 1999.

[121]   J. Daugman, "The importance of being random: statistical principles of iris recognition", To appear in *Pattern Recognition*.

[122]   A. K. Jain and N. Duta, "Deformable matching of hand shapes for verification", *Proceedings of IEEE International Conference on Image Processing*, October 25-28, Kobe, Japan, 1999.

[123]   D. Maio, D. Maltoni R. Cappelli, J.L. Wayman and A.K. Jain, "FVC 2000: Fingerprint verification competition", To appear in *IEEE Transactions on Pattern Analysis and Machine Intelligence*.

Brief Curriculum Vitae

Kong Wai-Kin, Adams is an Mphil student at the Department of Computing, The Hong Kong Polytechnic University. He received his B.Sc degree in Mathematical Science in 1998 from Hong Kong Baptist University with first class honors and a Scholastic Award. During his studies, he received a few awards and scholarships from both universities. Adams is a student member of IEEE since 1999.

Adams has published and submitted a few papers during his studies. In addition, he was awarded Two Tuition Scholarships for Research Postgraduate Studies by The Hong Kong Polytechnic University in 1999 and 2000.

Publications:

[1]   A.W.K. Kong and D. Zhang, "An effective coordinate system to solve tilting problem for iris recognition", *In Proceedings of First International Conference on Image and Graphics*, pp. 373-375, August 16-18, 2000

[2]   W.K. Kong and D. Zhang, "Eyelash detection model for accurate iris segmentation", *In Proceedings of ISCA 16th International Conference on Computers and their Applications*, pp. 204-207, March 28-30,2001,

[3]   W.K. Kong and D. Zhang, "Accurate iris segmentation based on novel reflection and eyelash detection model", *In Proceedings of International Symposium on Intelligent Multimedia, Video & Speech Processing*, pp. 263-266, May 2-4, 2001

[4]   W.K. Kong and D. Zhang, "Criteria-based eyelash detection model for accurate iris segmentation", (invited to submit to *Information: An International Journal*)

[5]   Wai-Kin Kong and D. Zhang, "Using Texture Information of Low-Resolution Palmprint Images for Personal Identification" *ACM post graduation day*, February 2, 2002, Hong Kong